FINITE ELEMENT MODELLING OF CONSTANT STRESS DRAINED DIRECT SIMPLE SHEAR TESTS ON SAND FOR MONOTONIC LOADING

by

© SUDIPTA BHOWMICK

A thesis submitted to the

School of Graduate Studies

in partial fulfillment of the requirements for the degree of

Master of Engineering (Civil)

Faculty of Engineering and Applied Science

Memorial University of Newfoundland

May 2023

St. John's Newfoundland and Labrador Canada

ABSTRACT

Simple shear loading is commonly observed in many practical geotechnical engineering problems, and is considerably different from that applied in commonly used geotechnical laboratory tests, such as direct shear and triaxial tests. The simple shear loading conditions in laboratory specimens could be created in several ways; among them, the direct simple shear (DSS) test is a popular one because of simplicity of specimen preparation and testing. However, the interpretation of the test results is challenging because the stress state in the specimens cannot be properly evaluated, as typical DSS apparatus allows the measurement of only normal and shear stresses at the top or bottom surface. DSS tests show some different response in some cases; for example, there is less pronounced strain-softening of dense sand compared to that in triaxial tests. Moreover, empirical equations have been proposed based on experimental results, which might be used to estimate soil parameters such as angle of internal friction. Examining the response of soil elements in DSS specimens using Finite Element Method (FEM), it becomes possible to evaluate the complete behavior observed in the laboratory tests.

In the present study, three-dimensional finite element (FE) simulation of DSS test is performed for stacked ring and Cambridge type apparatus. In the simulations, a normal stress is applied and then sheared monotonically by maintaining the same normal stress (constant stress test). Simulations are performed for medium and dense sands using the Mohr–Coulomb and a modified Mohr–Coulomb model that considers post-peak softening, respectively. FE results show that stresses are uniform in the central core of the specimen while considerable stress non-uniformity occurs near the boundaries. The stress state at the failure is neither on the point of stress obliquity nor on the maximum shear stress, which has been considered in some studies to calculate the friction angle. Interface resistance between soil and vertical surface(s) increase the stress ratio compared to smooth interface conditions.

ACKNOWLEDGEMENTS

First and foremost, I would like to express my deepest gratitude to my supervisor, Dr. Bipul Hawlader, Professor, Memorial University of Newfoundland (MUN), Newfoundland, Canada, for his unwavering support, encouragement, and guidance throughout the course of my research. I have been extremely lucky to have a supervisor like him. This thesis would not have been possible without his immense support and continuous guidance.

I would also like to extend my heartfelt thanks to Dr. Kshama Roy, Dr. Ripon Karmaker, Dr. Jin Chen, and Dr. Auchib Reza for their valuable feedback, suggestions, and constructive criticism. Their guidance and support have been instrumental in shaping my research and making it a success. I also gratefully acknowledge the previous and current students working under Dr. Bipul Hawlader for being cooperative in different difficulties and for their continuous encouragement and knowledge sharing.

I am also grateful to the Faculty of Engineering and Applied Science at MUN, for providing me with the necessary resources and support to conduct my research. I would also like to acknowledge the support of the Natural Sciences and Engineering Research Council of Canada (NSERC), Equinor, Petroleum Research Newfoundland and Labrador, and Mitacs, without which this research would not have been possible.

I express my heartfelt gratitude to my younger brother, Ashish Bhowmic, and my loving grandmother, Joshna Rani Chowdhury, as well as all of my family members, for their unwavering love, consistent encouragement, and spiritual support during my studies.

I would like to dedicate this thesis to my idol, Cristiano Ronaldo. His tireless work ethic, unwavering determination, and commitment to excellence have always motivated me to do my best. His dedication to his craft serves as a reminder that with hard work and perseverance, anything is possible. I am incredibly grateful for the inspiration he has provided me. This thesis is a token of my appreciation and gratitude.

Table of Contents

List of Figures

List of Tables

List of Symbols

TX	Triaxial
PS	Plane strain
DS	Direct shear
MC	Mohr-Coulomb model with constant ϕ and ψ
MMC	Modified Mohr-Coulomb model with mobilized ϕ and ψ as Fig. 3.2
ϕ	Angle of internal friction
ψ	Dilation angle
γ	Shear strain
γ_p^p	Octahedral plastic strain
γ^p	Deviatoric plastic shear strain
$\varepsilon_x, \varepsilon_y, \varepsilon_z, \varepsilon_a$	Axial strain
$\tau_{zx}, \ \tau_{xz}$	Shear stress
σ_z	Vertical normal stress/ initial consolidation stress
σ_x	Lateral normal stress
σ_1	Major principal stress
σ_3	Minor principal stress
H	Height of the soil
D	Diameter of the soil sample

L	Length of the soil specimen
W	Width of the soil specimen
E	Young's modulus of soil
ν_{soil}	Poisson's ratio of soil
γ_{soil}	Unit weight of the soil
ε_{ij}^{p}	Plastic strain component
I_R	Relative density index
K	Material constant
ϕ_{in}	Initial friction angle
ϕ_c	Critical state friction angle
ϕ_p	Peak friction angle
ϕ_m	Mobilized friction angle
ψ_p	Peak dilation angle
A_ψ	Slope of $(\phi_p - \phi_c)$ vs. I_R in Eq. (3.3)
k_ψ	Slope of $(\phi_p - \phi_c)$ vs. ψ_p in Eq. (3.4)
m,C_1,C_2	Soil parameter (Eqs. 3.5 and 3.6)
Q	Material constant (Bolton 1986)
R	Stress Ratio (= τ/σ_z)

k Material property (= $\sin\phi_c$)

θ Inclination of the major principal stress to the vertical

ϕ_μ Interface friction angle

Chapter 1: Introduction

1.1 General

Direct simple shear (DSS) tests provide a measure of shearing resistance that could be very useful in analyzing many practical geotechnical engineering problems. The DSS test is a special form of plane stain test that allows the rotation of principal stresses during shearing, as occurs in many practical problems. In such cases, the behaviour obtained from the DSS test could be more representative than that of other laboratory tests, such as triaxial tests. In many practical geotechnical engineering problems, the loading occurs in simple shear mode, such as in soil below a shallow foundation and around a friction pile, slope failure along a long horizontal plane, and potential sliding of retaining structures or a dike (Fig. 1.1). Plane strain and simple shear loading conditions can be created in several ways in the laboratory, such as through plane strain tests, DSS tests, and hollow cylinder tests. However, in comparison to DSS tests, fewer laboratories have the necessary facilities to conduct these types of tests.

In conventional DSS tests, the soil specimen is first consolidated one-dimensionally (K_0 condition) by applying a vertical stress, and then sheared by applying a horizontal displacement at the bottom boundary. Depending upon vertical stress and displacement during shearing, two types of DSS tests can be performed. Firstly, in a “constant stress” test, a vertical stress equal to the consolidation pressure is maintained during shearing. Secondly, in a “constant height” test, vertical displacement is not allowed (e.g., constant volume is maintained) during shearing. The constant height DSS test represents the undrained condition, as pore water pressure develops during shearing while maintaining a constant volume. In contrast, the constant stress DSS test represents the drained condition. The present study focuses on constant stress tests; therefore, constant height tests will not be discussed further.

Sample preparation for the DSS test is relatively simple compared to other plane strain tests (e.g. hollow cylinder). However, there exist some uncertainties in interpreting the DSS test results. The sources of such uncertainties are still not well understood. Experimental, analytical and numerical studies have been conducted to understand the sources and level of uncertainties (Roscoe 1953; Stroud 1971; Budhu 1984; Doherty and Fahey 2011; Dabeet 2014). It was found that such uncertainties might be related to non-uniform stress distribution within the specimen, confining pressure, shear strain level and strain localization during shearing.

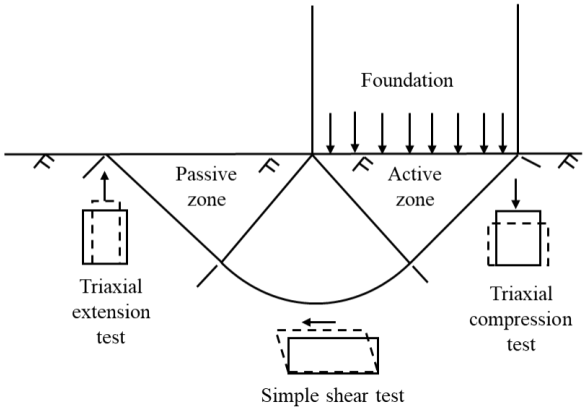

a) Failure surface under a shallow foundation (after Grimstad et al. 2011)

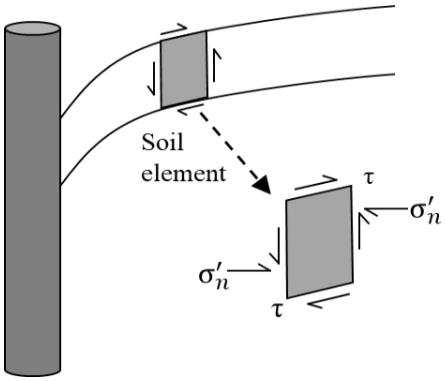

b) Soil around a friction pile (Randolph and Wroth 1981)

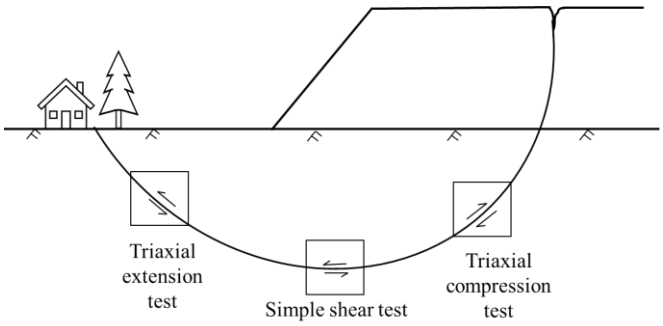

c) Slope stability (after Bjermm 1972)

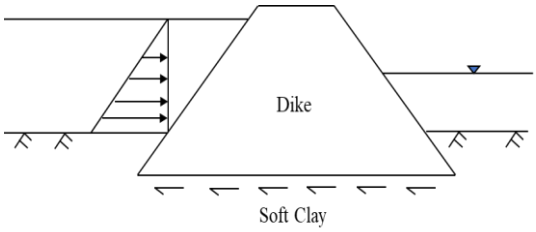

d) Sliding resistance under a dike (after Duncan 1969)

Figure 1.1: Simple shear loading conditions in the field

Proper estimation of soil parameters is the main objective of a laboratory test, including DSS tests. The stress–strain behaviour, shear strength parameters (e.g., angle of internal friction), and volume change (compression or dilation) depend on the stress level. In a soil element in the field, there could be six stress components (3 normal and 3 shear stresses). However, in a typical DSS test, only two stresses can be measured: the normal stress and shear stresses at the horizontal boundary (typically at the bottom of the specimen). The lateral deformation of the specimen is restrained by a wire-reinforced membrane, rigid stacked ring or rigid plates. The normal and shear stresses on the vertical plane(s) are not measured in DSS tests, unless there are some special modifications of the apparatus (Budhu 1985). As the required number of stress components are not known, some of the soil parameters (e.g., friction angle) cannot be calculated directly using the available stresses and therefore require some assumptions.

The main philosophy of the laboratory test setup is to mimic actual field loading conditions and obtain the response from the tested material. The underlying assumption is that the soil specimen represents a single point in a soil medium. Such assumptions are valid if the uniformity of stresses and strains within the soil specimen is maintained. Unfortunately, uniformity cannot be maintained in any laboratory test, although the effects of non-uniformity may not be significant in some tests. The non-uniformity within the soil specimen depends on the test configuration (e.g., boundary), strain level and soil type (Stroud 1971; Budhu and Britto 1987; Bernhardt et al. 2016; Wai 2019). Although widely used, the direct shear test only engages a small portion of the soil specimen in the shearing zone, while the soil outside the failure zone acts as a rigid body. In other words, significant strain non-uniformity occurs in a direct shear test. The DSS apparatus overcomes this limitation to a significant extent as it engages the whole soil sample in the shearing process. However, a downside of the DSS test is that it cannot apply complementary shear stress on the specimen's vertical faces, which induces some stress non-uniformity into the soil specimen. Previous studies show that,

although there are some non-uniformities of the stress distribution inside the DSS specimen, ~70% of the soil specimen remains in uniform stages, which is similar to the actual field loading conditions.

Numerical studies have been conducted in the past to understand the mechanisms involved during shearing, including the simulations using the Discrete Element Method (DEM) (Wijewickreme et al. 2013; Dabeet 2014; Bernhardt et al. 2016) and the Finite Element Method (FEM) (Doherty and Fahey 2011; Wu 2017). While the DEM provides some valuable information, defining some input parameters, such as interparticle frictional properties, is difficult. FE analyses have been performed assuming soil as an elastic or elasto-plastic material and showed that the response depends on the type of soil model (Finn et al. 1982; Budhu and Britto 1987).

1.2 Rationale

Over the last few decades, the use of DSS test apparatus has increased considerably, not only for research but also for industry practice. Monotonic and cyclic tests were performed on different sands for varying densities, such as loose, medium and dense. Monotonic loading is the focus of the present study. The behaviour of dense sand is very different from medium sand; the former shows a considerable post peak softening. Previous numerical studies show that stress non-uniformity is higher if the soil is modelled as elastic material than that obtained with an elasto-plastic soil model (e.g., Budhu and Britto 1987). Also, some studies strongly criticized the DSS device as it gives considerably lower shear strength and stiffness than other tests (Saada and Townsend 1981). On the other hand, some research justified its use, as there is no reason to have same shear strength as the stress paths are different in different tests (e.g., Budhu and Britto 1987). In terms of non-uniformity, a wide range of conclusions have been drawn (Lucks et al. 1972; DeGroot et al. 1994; Fu and Dafalias 2011). Also, considerable discussion on different types of DSS apparatus is available in the literature highlighting the

advantages and limitations of the available apparatus. Therefore, the key questions that need to be answered follow.

i) How significant is the stress non-uniformity, and how does it affect the soil parameters obtained from DSS tests?
ii) Can we obtain shear strength parameters (i.e., angle of internal friction) from DSS test results with reasonable accuracy?
iii) What kind of failure mechanisms are involved locally in the specimen, and do they affect the overall response obtained from the test?
iv) Are these factors different in medium and dense sands, and dependent on the type of apparatus?

The above questions are answered in the present study by conducting finite element analysis.

1.3 Objectives

This study aims to understand the mechanisms involved in direct simple shear tests on medium and dense sands. Finite element modelling techniques are developed to simulate the response of cylindrical (stacked ring type) and cuboidal (Cambridge type) soil specimens for constant stress conditions. The main objectives of this research are:

- Develop two and three-dimensional FE models for DSS tests;
- Implement appropriate soil models in the FE program, such as a model for dense sand that considers pre-peak hardening and post-peak softening during shearing;
- Simulate the response for monotonic loading, and compare numerical and experimental results; and
- Investigate the effect of non-uniformity on the overall stress–strain response and estimated soil parameters.

1.4 Outline of the thesis

The thesis consists of four chapters. The outline is as follows:

Chapter 1 highlights the background, rationale of the current study, and objectives of the research work.

Chapter 2 contains a literature review of DSS tests. The literature review covers the current understanding of sand behaviour under monotonic loading conditions. The findings from laboratory and numerical simulations are discussed. This chapter also provides an overview of the commonly used direct simple shear apparatus.

Chapter 3 presents two- and three-dimensional FE modelling of DSS tests. The stress–strain behaviour, stress non-uniformities and their effects on overall response are presented. A part of the work presented in Chapter 3 has been published as: Bhowmick, S. and Hawlader, B. (2022) "Numerical investigation of the stress and strain non-uniformities in direct simple shear sample and its effects on overall stress–strain behaviour," 75th Canadian Geotechnical Conference, Calgary, Alberta, Canada, paper ID-328 (Appendix A).

Chapter 4 summarizes the overall outcomes of the research. The limitations of the present study and recommendations for future research are also presented in this chapter.

Chapter 2: Literature Review

2.1 Introduction

The direct simple shear (DSS) test was initially developed to overcome significant stress non-uniformities induced in direct shear tests. Unlike direct shear tests, which only involve the soil between two halves of the shear box in the shearing process, the DSS test involves the entire specimen. DSS test became increasingly popular for characterizing soil behaviour as the rotation of the principal stresses occurs in many geotechnical problems (Wood and Budhu 1980; Finn et al. 1982; Wijewickreme et al. 2013). Due to its simplicity compared to other laboratory tests, such as the hollow cylindrical torsional shear test, and its ability to effectively simulate many field loading conditions (e.g., slope, piles, landslides and earthquakes), the DSS test has been widely used in many advanced geotechnical laboratories.

In DSS tests, a cylindrical or cuboidal soil sample is used. The cylindrical soil sample is enclosed within a reinforced rubber membrane in the Norwegian Geotechnical Institute type (NGI type) apparatus. This apparatus has been used in many laboratories although the insufficient lateral stiffness of the membrane, especially at large shear strains, has been questioned (Al Tarhouni 2020; Grognet 2011). Another commonly used DSS apparatus confines the cylindrical soil specimens using a set of frictionless stacked rings, known as "stacked ring type" apparatus (Budhu 1984). Cambridge University developed another type of DSS apparatus where a cuboidal soil specimen (square in plan) is enclosed within rigid platens linked together with hinges and sliders, which is known as the "Cambridge type" apparatus. In the present study, stacked ring and Cambridge type DSS apparatus are considered. The height of the soil specimen (H) should be small compared to the plan dimensions (diameter (D) or length (L)) to maintain uniform stress distribution throughout the sample (Vucetic and Lacasse 1982). Typical dimensions of the specimen are D = 70 mm and H = 20 mm for the stacked ring

type and L =100 mm and H = 20 mm for the Cambridge type, which give the aspect ratio (H/D or H/L) of 0.28 and 0.2, respectively.

2.2 Ideal Simple Shear and Direct Simple Shear

The direct simple shear (DSS) apparatus was designed to evaluate the stress–strain behaviour of soil under simple shear conditions. It allows the rotation of the axes of principal stresses during shearing. The objective of the laboratory test is to examine the behaviour of soil under actual field conditions and to identify the parameters that could be used to describe soil behaviour using constitutive equations. The behaviour obtained from a laboratory test specimen represents the behaviour of a single point in a soil medium. The validity of this hypothesis depends on the uniformity of stress and strain distributions within the soil sample (Saada and Townsend 1981, Zhang 2003). However, the DSS apparatus cannot impose uniform normal and shear stresses on the sample and thus deviates from the actual field condition. To understand the differences between ideal and real cases, a distinction between pure shear and simple shear states might be considered.

In pure shear, two principal stresses of equal magnitude but opposite in sign are applied (Fig. 2.1). This represents a state of plane strain condition, which consists of a uniform extension in the x-direction and a uniform contraction in the y-direction, in such a way that the volume remains unchanged (Fig. 2.1(b)). The term simple shear strictly refers to a state of strains, not the stresses. It is also a plane strain condition in which the points in the soil element displace in only one direction (parallel to the x-axis in Fig. 2.1(c)). Therefore, the simple shear can be viewed as a pure shear plus a rigid body rotation.

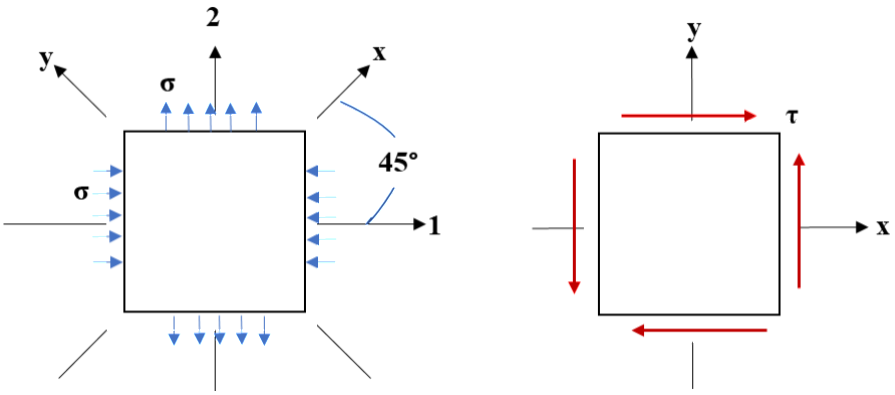

(a)

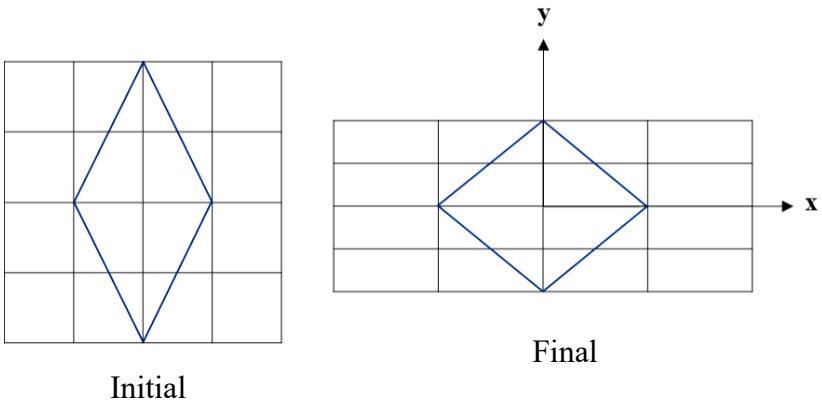

(b)

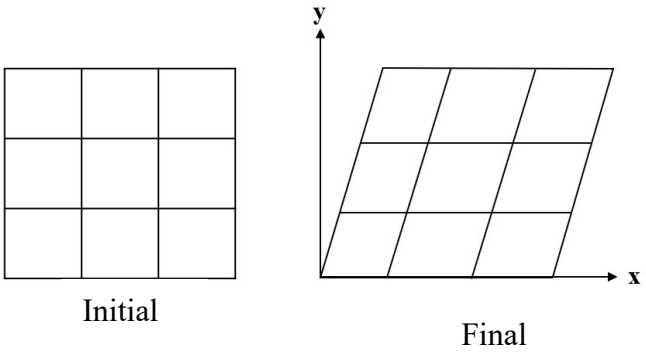

(c)

Figure 2.1: Comparison of pure shear and simple shear conditions: (a) pure shear stress conditions, (b) pure shear strain conditions, (c) simple shear stain conditions (after Saada and Townsend 1981)

Figure 2.2(a) shows the stresses in a soil element subjected to simple shear loading. The soil specimen is prevented from straining in the axial directions (i.e., $\varepsilon_x = \varepsilon_y = \varepsilon_z = 0$). In ideal simple shear conditions, a shear stress of equal magnitude must exist on the horizontal and on the left and right vertical faces. However in a typical DSS test, shear stresses are not applied or measured on the vertical faces. In fact, the vertical faces are tried to be made frictionless to maintain uniformity in vertical stress (Wai 2019). The absence of complementary shear stresses on these two vertical faces creates a non-uniform distribution of shear stress (Roscoe 1953; Saada and Townsend 1981). Therefore, the interpretation of DSS test results is difficult due to uncertainties with regard to the stress state of the soil specimen. However, from experimental and numerical studies, it was found that the sample core in the DSS test remains in a uniform stress state and represents a simple shear condition (Lucks et al. 1972). Unfortunately, the stresses in the sample core are not measured separately in typical DSS tests, although attempts have been made by some researchers with the Cambridge type DSS apparatus (Budhu 1985). Generally, in a DSS test, only the average normal and shear stresses on a horizontal boundary are measured, which are used for examining soil behaviour.

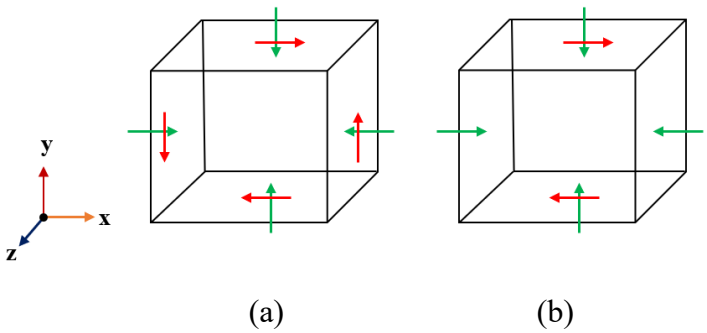

Figure 2.2: Simple shear stress state: (a) ideal simple shear, (b) direct simple shear

2.3 Typical behaviour of sand in monotonic DSS test

The DSS test on sand is the focus of the present study. A large number of studies investigated the response of sand under monotonic loading by conducting simple shear tests. These studies show contractive to dilative response during shearing with an increase in soil density. For

example, Vaid et al. (1981) conducted monotonic simple shear tests on Ottawa sand under 200 kPa normal stress for varying relative densities (27%–93%) and found that the dilative behaviour of sand increases with increasing relative density (Fig. 2.3).

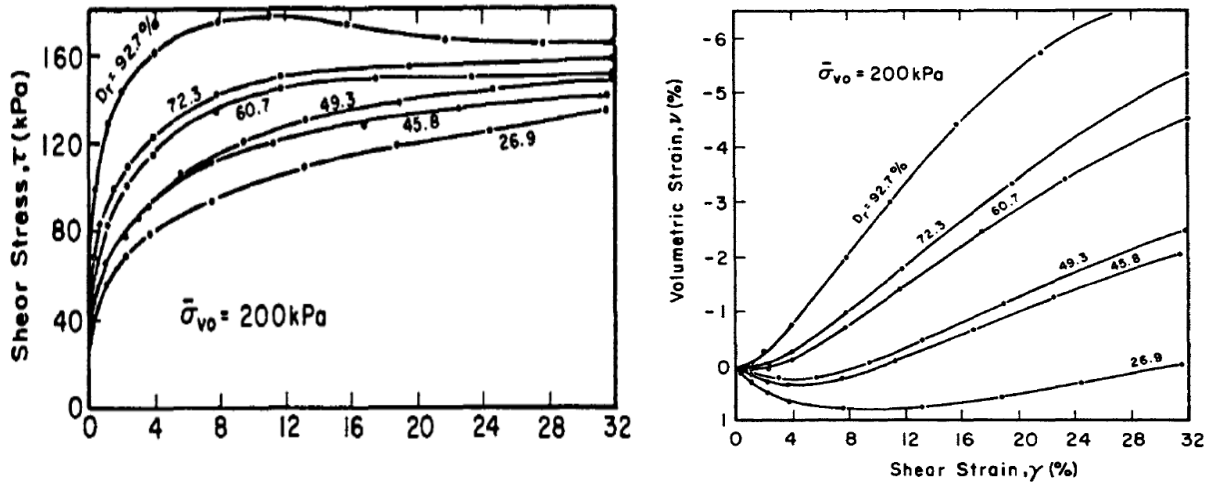

Figure 2.3: Drained simple shear tests on Ottawa sand: (a) stress–strain behaviour; (b) volume change behaviour (Vaid et al. 1981)

Al Tarhouni and Hawlader (2021) conducted a series of DSS tests on a dry dense fine silica sand (relative density, D_r = 87%) and showed that the stress–strain (Fig. 2.4(a)) and volume change (Fig. 2.4(b)) behaviour depend on the normal stress (σ_z) level. The tests under low-stress levels (e.g., σ_z = 50 kPa) give a stress ratio significantly higher than that of high-stress level tests.

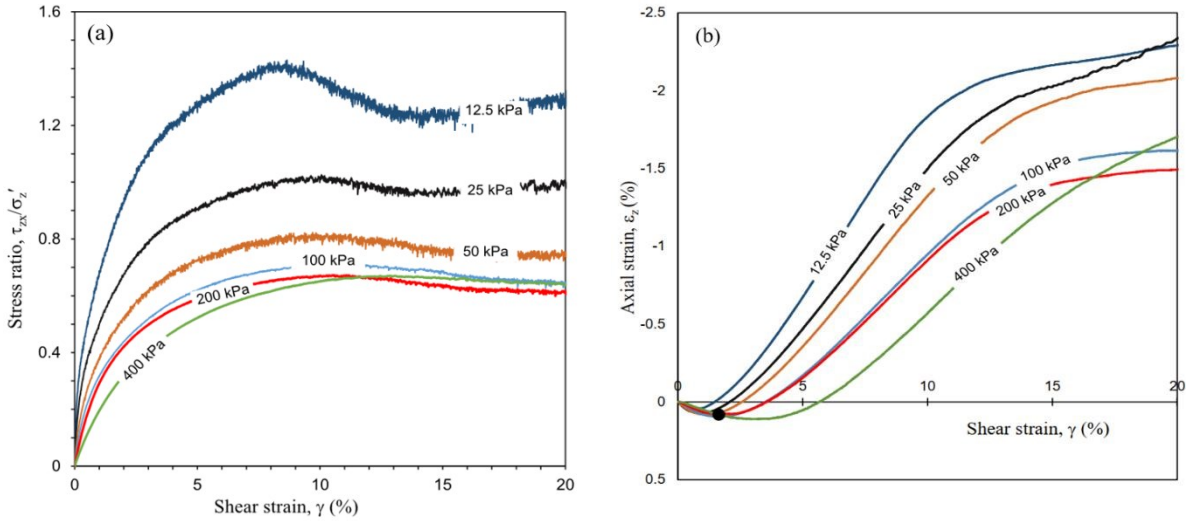

Figure 2.4: Effects of normal stress on DSS test results: (a) stress ratio; (b) volume change (Al Tarhouni and Hawlader 2021)

Triaxial compression tests were conducted on the same silica sand in saturated conditions having similar relative density (~85%), and the results are shown in Fig. 2.5 (Al Tarhouni et al. 2017). Compared to DSS test results (Fig. 2.4), triaxial tests give some different results: (*i*) considerably large post-peak softening occurs, especially in tests under low confining pressure (Fig. 2.5(a), and (*ii*) specimens dilate rapidly with axial strain and the dilation stops at an axial strain of ~8% (Fig. 2.5(b)).

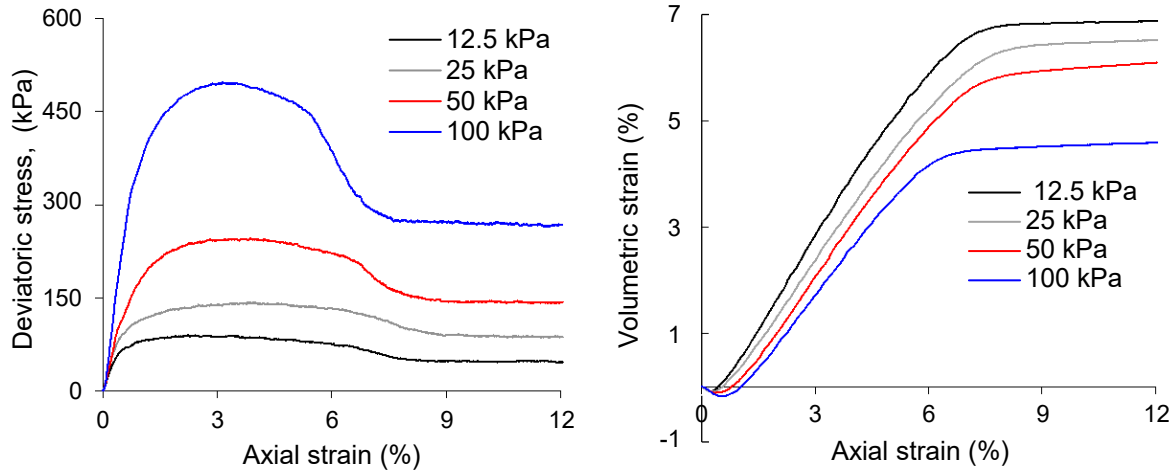

Figure 2.5: Triaxial test results on silica sand: (a) stress–strain behaviour; (b) volume change (Al Tarhouni et al. 2017)

Figure 2.6 shows the influence of relative density and normal stress on the dilation angle of Leighton Buzzard sand for simple shear loading conditions (Cole 1967). The soil becomes more dilative with an increase in relative density and a decrease in normal stress.

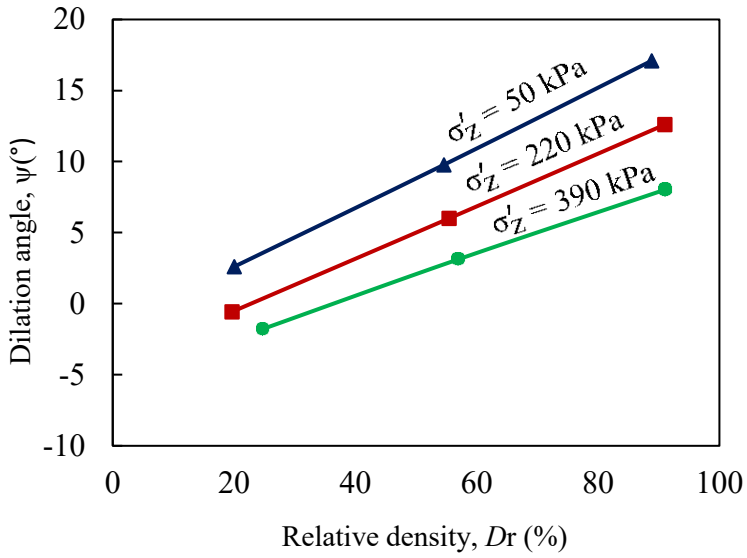

Figure 2.6: Dependence of dilation angle on relative density and stress level (Cole 1967)

Many studies focused primarily on the peak friction angle and maximum dilation angle. However, the relationship between the mobilized friction angle and mobilized dilation angle with shear strain can provide further insights. Significant changes in friction and dilation angles were reported for laboratory tests on dense sand (Toyota et al. 2004; Al Tarhouni et al. 2017). Under many field conditions, such as soil–pipeline interaction (Roy et al. 2018) and a shallow foundation on dense sand (Loukidis and Salgado 2011), a better understanding can be achieved by using the mobilized friction and dilation angles. The variation of the angle of internal friction (ϕ) and dilation angle (ψ) with plastic shear strain, loading conditions (triaxial or plane strain), density, and mean effective stress are important to capture the behaviour of sand (Hsu and Liao 1998; Guo and Stolle 2005; Roy et al. 2016). Different models have been proposed to describe the relationship between the mobilized ϕ and ψ and plastic shear strain. These models have also been calibrated against laboratory test data and have been utilized in numerical simulations to

model soil behaviour during the tests (Hsu and Liao 1998; Guo and Stolle 2005; Roy et al. 2016). The present study also uses a material model to capture the actual behaviour of dense sand, which will be discussed in detail in Chapter 3.

2.4 Stress and strain non-uniformities

As noted, the complementary shear stresses cannot be applied on the vertical sides of the specimen in a typical DSS apparatus. Therefore, the soil sample experiences a non-uniform distribution of shear stress at the top and bottom faces. A theoretical distribution of stresses in the middle of the specimen along the direction of shearing is shown in Fig. 2.7.

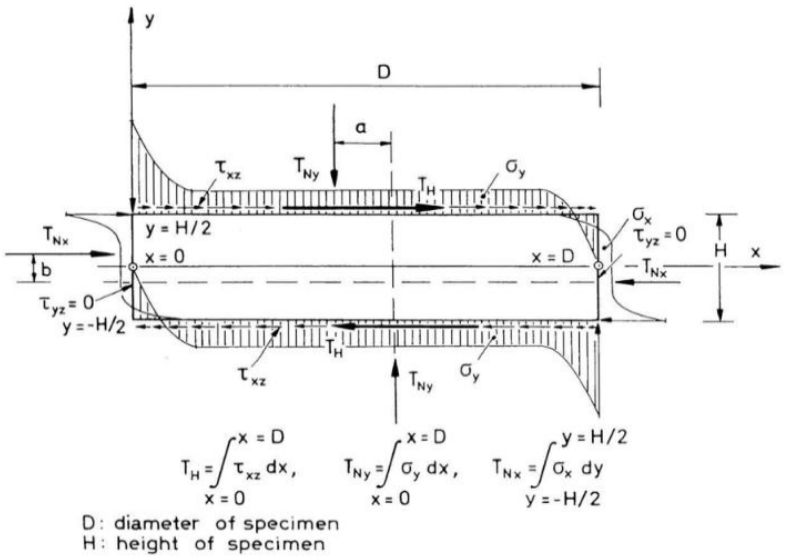

Figure 2.7: Stress distribution in middle of specimen and corresponding external forces (Vucetic and Lacasse 1982)

The effects of non-uniform shear stress are shown in Fig. 2.8 in a simplified way (Airey et al. 1985). As the complementary shear stress cannot be applied, the shear stress at the top and bottom boundaries distributes in such a way that it falls to zero at the end of the sample. The force couple resulting from non-uniform shear stress is balanced by the normal force at the top and bottom, which again cause non-uniform normal stress distribution.

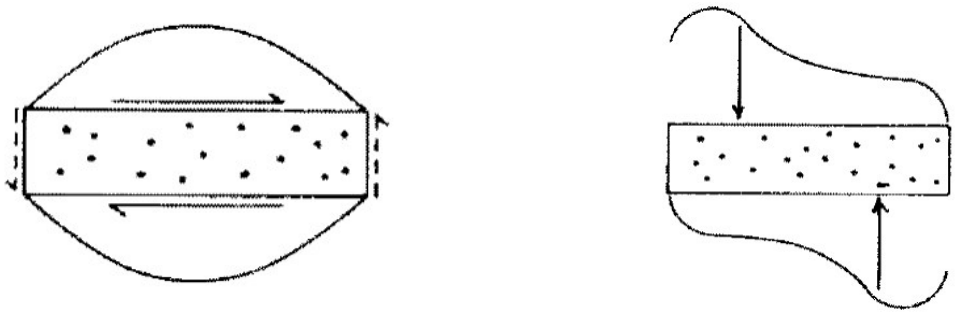

(a) (b)

Figure 2.8: (a) non-uniform distribution of shear stresses due to absence of complementary shear; (b) non-uniform distribution of normal stress to preserve moment equilibrium (after Airey et al. 1985)

Shen et al. (1978) used 3D finite element analysis to examine the effect of aspect ratio (H/D) on the cylindrical soil specimen. Shen et al. (1978) also showed that stress non-uniformity increases with an increase in aspect ratio (*H*/*D*, where *H* is the height and *D* is the diameter of the cylindrical specimen.

As shown above, the stress states of the soil sample are not in ideal simple shear conditions because of the lack of complementary shear stress on the vertical faces, although the core (middle third of the soil sample) remains in ideal simple shear conditions. Since only the shear stress and normal stress are measured from the horizontal boundary, it is useful to know the relationship between these stresses at the boundary and the stresses experienced by the soil elements in the sample core.

Roscoe (1953) carried out a mathematical analysis, assuming the soil as a linear elastic material, and showed significant stress non-uniformity at the end of DSS specimens, while it was uniform at central regions. Lucks et al. (1972) performed a 3D FE analysis, again assuming the soil as an elastic material, and showed stress non-uniformities near the boundaries; ~70% of the specimen in the middle was under a uniform stress condition. Budhu and Britto (1987)

conducted finite element analysis using the modified cam clay model and showed that the elastic analysis might significantly overestimate the non-uniformity at the end (Fig. 2.9).

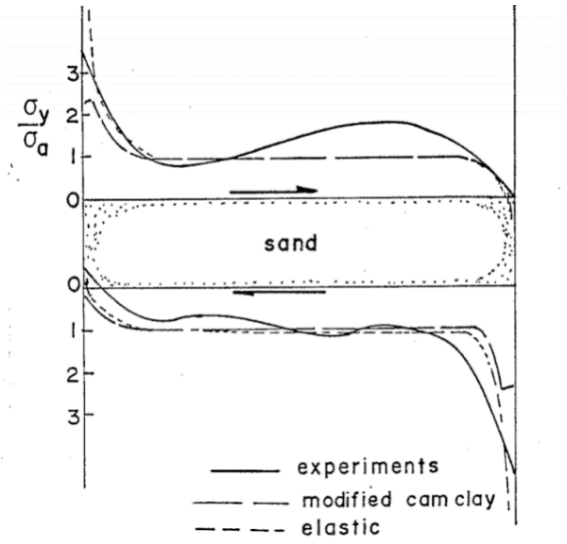

Figure 2.9. Vertical stress distribution in DSS test specimen for loose sand (Budhu and Britto 1987)

Doherty and Fahey (2011) conducted FE analysis for a single element and full 3D DSS specimen and compared the results for the ideal solution and the effects of non-uniformity on friction angle. The single-element simulation gives a maximum stress ratio of ~10% higher than that of the 3D model. Wijewickreme et al. (2013) conducted discrete element modelling (DEM) of DSS specimens. Investigating the simulation results at three "measurement spheres" at varying distances from the center, they showed considerably different volumetric strains at three different locations, which indicates non-uniform strain development within the specimen. Dabeet (2014) further examined DSS tests using DEM and found that, at high strain levels, additional force chains form at the leading and trailing end corners of the specimen (Fig. 2.10), which represents stress non-uniformity inside the soil specimen.

Figure 2.10. Images showing simulated particles and force chains at the central cross-section for 20% boundary shear strain (Dabeet 2014)

The response of soil in simple shear tests depends on several factors, such as apparatus type in the laboratory and single element versus full 3D simulations (Doherty and Fahey 2011). Budhu (1984) conducted experiments on identically prepared sand specimens using NGI type and Cambridge type DSS devices. The stress ratio measured from the horizontal boundary underestimated the stress ratio in the sample core by 6% in the NGI type and 12% in the Cambridge type DSS tests (Fig. 2.11). Airey et al. (1987) reported a 10% underestimation of shear strength measured from the horizontal boundary compared to that in the sample core for clay. Based on FE analysis, Doherty and Fahey (2011) calculated a friction angle of 4% smaller in 3D simulation than that of ideal simple shear simulation with a single element.

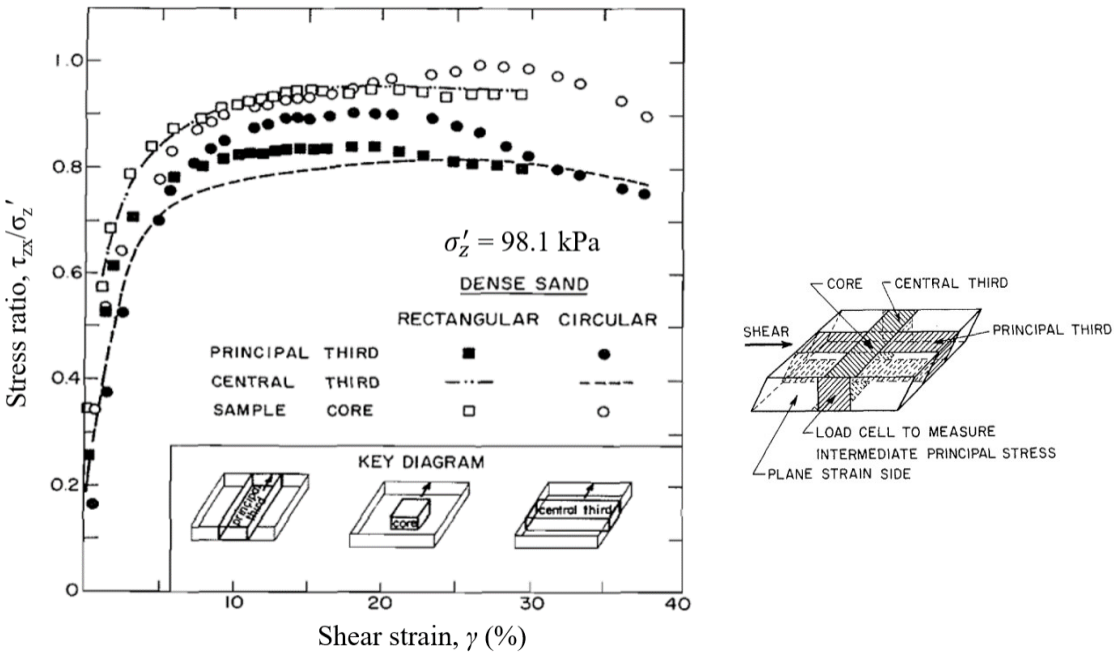

Figure 2.11: Development of stress ratios at three locations of the samples (Budhu 1984)

Previous research on DSS tests showed that stresses and strains are not uniformly distributed throughout the specimen. The degree of non-uniformity varies depending upon several factors such as the type of DSS apparatus, boundary conditions, material type, and aspect ratio of the sample. There is no consensus among previous researchers on the extent of non-uniformity and its effect on soil parameter estimation. Therefore, a comprehensive numerical analysis is performed in this study to evaluate non-uniformities and their impact on the overall response for both stacked ring and Cambridge type DSS tests on medium and dense sands.

A summary of previous studies on soil behaviour in DSS tests and more specifically, the non-uniformity of stress distribution in the specimen, is shown in Table 2.1. These studies include both experimental and numerical investigations.

Table 2.1: Summary of existing experimental and numerical studies

Reference	Method & Software	Material	Remarks
Roscoe (1953)	2D FE analysis	Linear elastic	Normal stress distribution is perfectly uniform at the end of the

			consolidation step. The distribution of shear stress is also uniform at the center.
Stroud (1971)	Experimental (Cambridge type)	Leighton Buzzard Sand	Non-uniformity is caused by weak interlocking contact between the sand particles and the top boundary. Non-uniformity is influenced by the rotation of the upper boundary.
Lucks et al. (1972)	3D FE analysis (NGI type)	Linear elastic	Uniform normal stress at the end of the consolidation. During the shearing, only two-thirds of the specimen experiences uniform stresses.
Prevost & Hoeg (1976)	2D FE	Linear elastic	Uniform normal stress at consolidation stage. More room for non-uniformity when slippage is allowed at the top and bottom rigid plates.
Shen et al. (1978)	3D FE (NGI type)	Linear elastic	Shear strain is not uniform during shearing, which is more evenly distributed in the thinner samples.
Wood & Budhu (1980)	Experimental (Cambridge type)	Leighton Buzzard sand	Overall response calculated from the specimen ends was similar to that of the core.

Saada & Townsend (1981)	Experimental	Epoxy material	Vertical consolidation stress was not applied in the study. The distribution of shear stress was not uniform even at the sample core.
Vucetic and Lacasse (1982)	Experimental (NGI type)	Medium-stiff clay	Aspect ratio of the soil sample does not have a significant influence on the overall stress–strain behaviour.
Finn et al. (1982)	2D FE	Linear anisotropic elastic	Anisotropic elastic analysis shows more uniform stresses. Increasing the width-to-height ratio of the specimen increases the uniformity of stresses.
Saada et al. (1983)	2D FE	Linear elastic	Non-uniformities arising during the consolidation stage can be as significant as those arising during shearing.
Amer et al. (1984)	Experimental (Cylindrical sample)	Silica sand	Stress uniformity increased with a decrease in sample height for a specific sample diameter and the effect of the sample size decreases at higher strain levels.
Budhu (1984)	Experimental (NGI & Cambridge type)	Leighton Buzzard sand	Distribution of shear stress is uniform at the low strain level. The non-uniformity of stresses increases with an increase in shear strain level.

Budhu and Britto (1987)	2D FE	Modified Cam-Clay	Normal stress is distributed evenly during the consolidation stage. The stress distribution is more uniform in the modified cam clay model than that in the elastic analysis.
Dounias and Potts (1993)	2D FE	Mohr–Coulomb model	The initial stiffness and peak simple shear strength are underestimated by about 20% in comparison to ideal simple shear conditions. The stresses become highly non-uniform at the high strain level.
DeGroot et al. (1994)	Experimental (Cambridge type)	Cohesive soil	Normal stress distribution is uniform during consolidation. The non-uniformity of stresses influences the stress–strain behaviour at large strains.
Wang et al. (2004)	2D FE	Multi-yield plasticity model	Normal stress distribution is uniform at the end of the consolidation. Constant stress tests give more uniform conditions than constant volume tests.
Doherty & Fahey (2011)	3D FE (NGI type)	Modified Cam-Clay	Normal stress is distributed evenly during the consolidation. Calculated simple shear friction angle is only 4%

			lower than that for the case of ideal simple shear conditions.
Fu & and Dafalias (2011)	2D DE M		The soil is consolidated isotopically. At large strain levels, significant non-uniformity occurs in the DSS test
Wijewickreme et al. (2013)	3D DEM		Uniform distribution of normal stress during the consolidation. Planes of maximum stress obliquity rotate with the development of shear strain. At large shear strains, the horizontal plane becomes a plane of maximum stress obliquity.
Chang et al. (2014)	3D DEM		Boundary effect is less intense for a smaller aspect ratio. The boundary effect difference between the Cambridge and NGI types of simple shear is insignificant.
Asadzadeh & Soroush (2018)	3D FE (NGI Type)		Uniform stress and strain distribution can be ensured by preventing slippage at the top and bottom plate soil interface.
Al Tarhouni and Hawlader (2021)	Experimental (stacked ring type)	Silica Sand	The initial consolidation stress has significant effects on the stress–strain behaviour. Lower consolidation

			stress provides a higher stress ratio and more dilative behaviour.
Wai et al. (2021)	3D FE (NGI Type)	SANISAND model	The normal stress distribution is uniform during consolidation for a smooth interface at the vertical wall(s). Higher contact friction allows better development of complementary shear stresses but may induce stress non-uniformities during the consolidation phase.
Liu et al. (2022)	Experimental (cylindrical soil sample)	Carbonate sand	The soil becomes highly non-uniform at large strains. The deformation becomes non-uniform due to the development of a shear band.

2.5 Summary

The DSS test is performed to characterize the soil behaviour when the rotation of the principal axis is important. It has become increasingly popular in determining the shear strength parameter of soil due to its simplicity and ability to impose realistic field loading conditions. Although sample preparation and test setup are relatively easier in DSS tests, interpretation of the test result is challenging due to uncertainties arising from imperfect boundary conditions. Many previous experimental and numerical studies have examined the impact of imperfect boundary conditions on the DSS test. However, a consensus has not yet been reached due to the uncertainties surrounding this issue.

Furthermore, the data collected from the laboratory DSS apparatus is inadequate to provide a thorough understanding of the DSS test. Also, the friction angle obtained from the average boundary measurement is not unique, due to several assumptions involved in its calculation. Numerical analyses can account for these imperfect boundary conditions and provide information that is difficult to obtain from experimental investigations. Therefore, to address these issues and provide a better understanding of the DSS test, this study focuses on a comprehensive numerical analysis of the DSS test.

Chapter 3: Finite Element Modelling of Direct Simple Shear Tests on Sand

Co-Authorship: Some parts of this chapter have been published in the 75th Canadian Geotechnical Conference, Calgary, Alberta, Canada, as: Bhowmick, S. and Hawlader, B. (2022) "Numerical investigation of the stress and strain non-uniformities in direct simple shear sample and its effects on overall stress–strain behaviour". Most of the research in this chapter has been conducted by the first author. He also prepared the draft manuscript. The other author mainly supervised the research and reviewed the manuscript.

3.1 General

The stress state in many geotechnical problems is similar to that of simple shear conditions. While direct shear and triaxial tests are commonly performed for practical engineering and research activities, direct simple shear (DSS) test facilities are available in some advanced laboratories. One of the limitations of the typical DSS test is that only the vertical normal and horizontal shear stresses at the boundaries are measured. The unknown shear stress on the vertical boundary makes the interpretation of the test results difficult. In addition, stress and strain non-uniformities might occur in the sample. In the present study, three-dimensional finite element (FE) modelling of the DSS test is performed for three different normal stresses to investigate possible non-uniformities during consolidation and shearing and their effects on the interpreted shear strength parameters. This study provides valuable insights into the potential limitations of the DSS test and highlights the importance of considering non-uniformities in stresses and strains when interpreting test results. A parametric study is also performed to show

the effects of soil–ring/sidewall interface friction and aspect ratios of the soil sample on the overall response of soil in DSS tests.

3.2 Introduction

Several devices are used in geotechnical laboratories to determine the shear strength parameters of soil, including commonly used direct shear (DS) and triaxial (TX) tests apparatus. Advanced systems, such as direct simple shear (DSS), plane strain, and hollow cylinder torsional shear test apparatus, were also developed to apply complex loadings that better represent the field behaviour. The simple shear condition is a loading condition that better represents many field conditions, such as slope failure along a riverbank or embankment, pipeline–soil and pile–soil interactions.

For simple shear loading, DSS device and hollow cylinder apparatus (HCA) are generally used. While a better measurement and control of the stresses can be performed in the HCA, the sample preparation is relatively difficult and time consuming. However, sample preparation and testing using a DSS device are relatively simple (Bernhardt et al. 2016). A variety of DSS devices have been developed over the last few decades. In the present study, simulations are performed for stacked ring and Cambridge type DSS tests.

Several researchers discussed the advantages and disadvantages of DSS devices (Shibuya and Hight 1987; Frydman and Talesnick 1991). DSS allows the rotation of the principal stresses during shearing, which cannot be done in a triaxial test. However, the missing information of the shear and normal stresses on the vertical plane of a DSS specimen makes the interpretation of test results difficult. Also, it is generally agreed that the core part of the DSS specimen is in simple shear condition, and the non-uniformity occurs mainly near the boundary. Unfortunately, no consensus has been reached on the degree of non-uniformity and its effect on the interpretation of results.

Measurement of stress and strain non-uniformities within the sample is difficult, if not impossible. Therefore, numerical simulations could be an alternative to enable further insights into the mechanisms involved locally and for the overall response. The Discrete Element Method (DEM) has been used in some studies to simulate DSS tests (Dabeet et al. 2015; Asadzadeh and Soroush 2016; Bernhardt et al. 2016; Guo et al. 2022). While DEM provides some valuable information, one of the challenges in DEM is defining the input parameters, such as interparticle frictional resistance. FE methods have also been used to simulate DSS tests (Potts et al. 1987; Doherty and Fahey 2011; Wu 2017; Wai et al. 2021). Wai et al. (2021) simulated monotonic DSS tests only for limited shear strain (γ) level ($\gamma < 4\%$).

This chapter is organized as follows. First, an FE model is developed in plane strain conditions and compared with the results of a previous study to show the effectiveness of the developed FE technique. Second, three-dimensional FE analyses are performed for stacked ring and Cambridge type DSS tests. Simulations are performed for varying normal stresses. Stress non-uniformity and interpretation of the results are discussed. Finally, a parametric study is performed to show the effects of some key factors that could affect the test results.

3.3 Finite element modelling

FE modelling was performed using Abaqus 6.19 FE software. The software adopted implicit and explicit schemes for time integration. The analyses are performed using Abaqus/Explicit; however, some simulations are performed using the implicit scheme in Abaqus/Standard for comparison. Three-dimensional (3-D) simulations are performed for DSS tests using stacked ring type and Cambridge type apparatus. In addition, a set of simulations is performed in two-dimensional (2-D) plane strain conditions, and the results are compared with a previous study (Dounias and Potts 1993) to show the effectiveness of the present FE modelling techniques.

3.3.1 2D DSS specimen

Figure 3.1(a) shows the typical FE mesh used in the 2-D simulations. A rectangular soil block of length (L) = 60 mm and height (H) = 20 mm is considered. The vertical walls are longer than the soil height, such that the volumetric expansion of the soil specimen during shearing can be accommodated. The length of the top and bottom plates is equal to the horizontal distance between two vertical walls. The soil block is discretized into a 0.5 mm × 0.5 mm 4-node bilinear plain strain quadrilateral element (CPE4R). The top and bottom plates, as well as the left and right boundary walls, are modelled as a rigid body, after discretizing them into 1 mm × 1 mm elements.

The bottom plate is restricted from any vertical displacement and rotation; however, it can displace laterally during shearing. The model dimensions and boundary conditions used in this set of analysis are the same as those used in the 2D DSS test simulation by Dounias and Potts (1993). No-slip conditions are used for the interfaces between soil and top and bottom plates to apply the stain more uniformly (Prevost and Hoeg 1976). Frictionless interface conditions are used for the vertical walls.

3.3.2 Stacked ring type DSS specimen

In this three-dimensional simulation, a cylindrical soil specimen of diameter D = 70 mm and height H = 20 mm is sheared up to 20% shear strain. Taking advantage of symmetry, only half of the specimen is modeled (Fig. 3.1(b)). A structured mesh is created by zoning the soil. An adaptive mesh domain with Lagrangian type boundary regions is used to improve the aspect ratio of the elements.

The top cap and bottom pedestal are modelled as 2-mm thick rigid plates. Twenty-five rigid stacked rings of an internal diameter of 70 mm, a width of 2 mm and a thickness of 1 mm (each) are used to provide lateral restraint. The diameter of the top plate is 70 mm, which is the same as the internal diameter of the stacked rings and the diameter of the soil sample, such that

the top plate can move vertically during loading. The diameter of the bottom plate is 74 mm (i.e., same as the outer diameter of the stacked ring). Mesh convergence analysis has been performed for this study. The detailed analysis shown in this paper has an approximate element size of 1.0 mm, and the total number of elements for the analysis is 43000.

The soil specimen is discretized by eight-node linear brick elements having reduced integration and hourglass control. The interface between the soil and the inner surface of the stacked rings is frictionless. Similar to 2D analyses, no-slip conditions are used for the interfaces between the soil and the top and bottom plates. Also, the top and bottom plates are not allowed to rotate.

3.3.3 Cambridge type DSS specimen

In this 3-D analysis, a soil specimen of length, L = 100 mm, width, W = 50 mm (half of the specimen) and a height of H = 20 mm is sheared up to 20% shear strain (Fig. 3.1(c)). Again, taking advantage of symmetry, only half of the soil sample is modelled. The top, bottom, left and right boundaries are modelled by 1-mm thick rigid plates. The interface between the soil and the inner surface of the side walls is frictionless. Rigid frictional interface conditions are used for the interfaces between soil and the top and bottom plates. For this study, a mesh convergence analysis has been performed. The approximate element size of the analysis presented in this paper is 1.0 mm, and the total number of elements for the analysis is 100000. Other conditions, including interface resistance, are the same as those used for stacked ring type DSS test simulations.

3.3.4 Loading and boundary conditions

Each simulation is performed in two steps. In the first step, the specimen is consolidated under K_0 condition by a applying vertical load on the top plate. As the simulations are performed for dry sand, the term consolidation in this study represents vertical one-dimensional compression without modelling pore pressure dissipation. In the shearing stage, keeping the top plate fixed to horizontal movements, the bottom plate is displaced leftward along the x-direction at a rate

of 0.004 m/s without rotation and vertical displacement, maintaining quasi-static loading conditions. The vertical displacement of the top plate provides the volume change of the specimen. The method of simulation described above represents the process followed by Al Tarhouni and Hawlader (2021) to conduct DSS tests using the stacked ring type apparatus at Memorial University of Newfoundland. The Cambridge type DSS test simulation is performed following the process described in previous studies (Stroud 1971; Budhu 1984). All the simulations are performed for constant stress conditions where the σ_z applied in the consolidation stage remains constant in the shearing stage.

3.4 Modelling of soil

Analyses are performed using two soil models: (*i*) elastic perfectly plastic Mohr–Coulomb (MC) model for medium sand, and (*ii*) modified Mohr–Coulomb (MMC) model with strain softening at large strains (Roy et al. 2016) for dense sand. The MC model is a widely used soil model and is a built-in model in the software. Table 3.1 shows the parameters used in the analyses with the MC model.

Table 3.1: Geotechnical parameters used for medium sand using Mohr–Coulomb model

Parameters	2D	3D
Young's modulus, E (MPa)	26	10
Poisson's ratio, ν	0.3	0.3
Angle of internal friction, ϕ (°)	35	38
Dilation angle, ψ (°)	0, 35*	8
Unit weight, γ_{soil} (kN/m^3)	16.9	16.9

*Two dilation angles are used in 2D analysis to compare the results of Dounias and Potts (1993) with the same soil parameters

The MMC model is not available in Abaqus; therefore, a brief description of the model and its implementation in the software is presented in the following sections.

Roy et al. (2016) proposed a MMC model to capture the effects of pre-peak hardening, post-peak softening, density, and confining pressure on the mobilized friction angle (ϕ) and dilation angle (ψ) for dense sand. A detailed discussion of the model, including the selection of model parameters by calibrating against laboratory tests' data, implementation in Abaqus FE software using a subroutine, and mesh sensitivity are available in previous studies (Roy et al. 2016, 2018(a–c)). ϕ and ψ of the MMC model changes with mean effective stress (p) and octahedral plastic strain (γ_p^p).

$$\gamma_p^p = \frac{2}{3}\sqrt{(\varepsilon_{11}^p - \varepsilon_{22}^p)^2 + (\varepsilon_{22}^p - \varepsilon_{33}^p)^2 + (\varepsilon_{11}^p - \varepsilon_{33}^p)^2 + 6 \times [(\varepsilon_{12}^p)^2 + (\varepsilon_{13}^p)^2 + (\varepsilon_{23}^p)^2]} \quad (3.1)$$

where ε_{ij}^p (i, j = 1–3) represents the components of plastic strains. Eq. (3.1) becomes the engineering shear strain, which was used by Roy et al. (2016) for plane strain simulation of pipeline–soil interaction.

Table 3.2: Equations for modified Mohr–Coulomb Model (MMC) (summarized from Roy et al. 2016)

Description	Eq. #	Constitutive Equations
Relative density index	(3.2)	$I_R = I_D(Q - lnp) - R$ where $I_D = D_r$ (%)/100
Peak friction angle	(3.3)	$\phi_p - \phi_c = A_\psi I_R$
Peak dilation angle	(3.4)	$\psi_p = \frac{\phi_p - \phi_c}{k_\psi}$
Strain-softening parameter	(3.5)	$\gamma_c^p = C_1 - C_2 I_D$
Plastic shear strain at ϕ_p	(3.6)	$\gamma_p^p = \gamma_c^p \left(\frac{p}{p_a}\right)^m$

Mobilized friction angle in Zone-II	(3.7)	$\phi = \phi_{in} + \sin^{-1}\left[\left(\frac{2\sqrt{\gamma^p \gamma_p^p}}{\gamma^p + \gamma_p^p}\right) \sin(\phi_p - \phi_{in})\right]$
Mobilized dilation angle in Zone-II	(3.8)	$\psi = \sin^{-1}\left[\left(\frac{2\sqrt{\gamma^p \gamma_p^p}}{\gamma^p + \gamma_p^p}\right) \sin(\psi_p)\right]$
Mobilized friction angle in Zone-III	(3.9)	$\phi = \phi_c + (\phi_p - \phi_c) \exp\left[-\left(\frac{\gamma^p - \gamma_p^p}{\gamma_c^p}\right)^2\right]$
Mobilized dilation angle in Zone-III	(3.10)	$\psi = \psi_p \exp\left[-\left(\frac{\gamma^p - \gamma_p^p}{\gamma_c^p}\right)^2\right]$
Young's modulus	(3.11)	$E = K p_a \left(\frac{p}{p_a}\right)^n$

In the MMC model, the stress–strain behaviour of dense sand is divided into three zones, i.e., the elastic zone, pre-peak hardening zone and post-peak softening zone. The elastic zone is defined by elastic properties such as Young's modulus (E) and Poisson's ratio (ν). Eq. (3.11) is used to calculate E as a function of mean effective stress (p), where p_a is the atmospheric pressure (Janbu 1963; Hardin and Black 1966).

In the pre-peak hardening, ϕ and ψ increase from ϕ_{in} and ψ_{in} to the peak values ϕ_p and ψ_p. Interparticle friction and soil fabric are the main contributors to ϕ_{in}. The values of ϕ_p and ψ_p are calculated using Eqs. (3.3) and (3.4), respectively. A simple shear test is a form of plane strain test (Randolph 1981); therefore, ϕ_p and ψ_p are calculated as $A_\psi = 5$ and $k_\psi = 0.8$, which represent the values for plane strain conditions (Bolton 1986). Previous studies show that the critical state friction angle (ϕ_c) could be 3 to 5° higher in plane strain conditions than in triaxial compression (Bishop 1961; Cornforth 1964). $\phi_c = 35°$ is used in this study. Table 3.3 shows

the soil parameters used to model dense sand using the MMC model. Figure 3.2 shows the variation of ϕ and ψ with plastic shear strain for three mean stresses.

Table 3.3: Soil parameters used for modified Mohr–Coulomb model for dense sand

Parameter	Value
K	150
n	0.5
v	0.2
A_ψ	5
k_ψ	0.8
ϕ_{in} (°)	29
C_1	0.22
C_2	0.11
m	0.25
Critical state friction angle, ϕ_c (°)	35
Atmospheric pressure, p_a (kN/m^2)	100
Relative density, D_r (%)	80
Unit weight, γ_{soil} (kN/m^3)	16.9

The MMC model is implemented in Abaqus/Explicit via a user defined subroutine VUSDFLD written in FORTRAN. In the subroutine, the stress and strain components are called to calculate the mean effective stress (p) and deviatoric plastic shear strain (γ^p), which are then defined as two field variables. The values of the field variables for each time increment are transferred to the Abaqus input file, which are then used to define the mobilized ϕ and ψ.

3.5 2D FE simulation results

In the following sections, the overall response is explained using the average shear stress (τ), and the average normal stress (σ_z) on the top/bottom surface of the specimen. During shearing,

the lateral and vertical forces at the reference point of the bottom plate are obtained and then, dividing these forces by the horizontal cross-sectional area, τ and σ_z are obtained. As the simulations are performed for single phase material, without modelling pore water pressure, all the normal stresses (e.g., σ_z) represent the effective stress. Similarly, the lateral displacement of the bottom plate (δ) and vertical displacement (v) of the soil specimen are obtained, which are divided by the height of the specimen to calculate shear strain (γ) and axial strain (ε_a).

First, a 2D simple shear loading in plane strain conditions is simulated using implicit and explicit time integration algorithms available in the software. All the conditions (e.g., loading and boundary conditions) are the same in these simulations, as discussed above. A very small difference in calculated stress ratio, R ($= \tau/\sigma_z$) is found, up to ~ 5% shear strain. The implicit simulation stopped at $\gamma \sim 6\%$ because of numerical issues related to mesh distortion; however, the explicit analysis is continued until $\gamma = 20\%$ without numerical issues. This implies that a considerably large deformation could be modelled using the explicit technique. Therefore, all the simulations presented in the following sections are conducted using Abaqus/Explicit.

Figure 3.3 shows a comparison of the results using the present FE modelling technique and those reported by Dounias and Potts (1993). The simulations are performed for two conditions: (*i*) associated ($\phi = \psi = 35°$), and (*ii*) zero dilation ($\psi = 0$). It can be seen that the current analysis matches perfectly with the previous study. The distribution of deviatoric plastic strain shown in Fig. 3.4(a) also compares well with the work of Dounias and Potts (1993) (Fig. 3.4(b)).

3.6 3D FE simulation results

In the following sections, the discussion is mainly focused on the variation of shear stress (τ) and shear stress ratio ($R = \tau/\sigma_z$) with shear strain (γ).

3.6.1 Stress-strain behaviour of medium sand with Mohr–Coulomb model

Figures 3.5(a) & (b) show the variation of shear stress and shear stress ratio, respectively, for stacked ring and Cambridge type DSS tests under three normal stresses. A very similar stress–strain response is found for these two types of tests. The shear stress reaches a maximum value at ~10% strain level and remains almost constant at higher strain levels.

The Young's modulus of sand (E) generally increases with confining pressure, as mentioned above; however, a stress-independent constant value of E is used in this set of simulations using the MC model. Therefore, the initial part of the stress–strain curve in Fig. 3.5(a) is almost linear and normal stress independent. Stress–strain behaviour is nonlinear before τ reaches the maximum value because the soil elements in the specimen are at different stress and strain levels for a given γ at the boundary. Figure 3.5(b) shows that the stress ratio R is normal stress dependent (as τ is normalized by σ_z); R increases rapidly for a low σ_z. However, at large strains, R is closer (= 0.64–0.69). This variation is due to non-uniform distribution of stresses and strains in the soil specimens, which also depends on the applied normal stresses.

3.6.2 Stress-strain behaviour of dense sand with modified Mohr–Coulomb model

Figure 3.6 shows the simulated results for dense sand with the modified Mohr–Coulomb model described in the previous sections. The symbols in Fig. 3.6 shows the results of DSS tests conducted by Al Tarhouni and Hawlader (2022) using a stacked ring type apparatus on dry dense silica sand. To show the importance of post-peak softening, one simulation is performed using the Mohr–Coulomb model with the critical state parameters ($\phi_c = 35°$ & $\psi = 0°$) for a normal stress of 100 kPa. For clarity, the results obtained from this simulation are also shown in Fig. 3.6(b). The following are the key observations in these simulations:

i. Both types of DSS apparatus give similar stress–strain and volume change behaviour and are comparable to the laboratory test results. The stress ratio decreases with an increase in normal stress. For σ_z = 50 kPa, the maximum stress ratio is 0.82, whereas it is 0.72 and

0.65 for normal stress levels of 100 kPa and 200 kPa, respectively. A similar trend of decreasing stress ratio with σ_z has also been reported in many previous studies. For example, Al Tarhouni and Hawlader (2021) used a stacked ring type device on silica sand and showed a maximum stress ratio of 0.84 at σ_z = 50 kPa and 0.67 at σ_z = 200 kPa. Similarly, Stroud (1971) showed a decrease in the stress ratio from ~1.0 at σ_z = 13.8 kPa to ~0.9 at σ_z = 172 kPa for dense sand.

ii. While ϕ and ψ decrease significantly with plastic shear strain after the peak (see Fig. 3.2), the post-peak reduction of shear stress and overall stress ratio is relatively small (Fig. 3.6(a) and 3.6(b))

iii. Calculated shear stress with the critical state soil parameters is considerably smaller than that in the MMC model even at large displacement, which implies that the critical state does not reach even at shear strain level of 20%. (Potential reasons are discussed further in later sections).

iv. A close examination of the simulation results shows that the stacked rings might move independently and shear strain localization might occur, especially at large γ and near the boundaries, which causes numerical issues, and the solution stops at ~ γ = 15% for stacked ring type simulations in Fig. 3.6, while the simulations could be continued for the Cambridge type as the loadings from rigid boundaries maintain the simple shear conditions without strain localization even at large strains (Budhu 1979). In numerical simulations, localized shear band formation near the top/bottom boundary affects the volume change behaviour for the stacked ring type DSS test at large strain (Fig. 3.6(c)), as discussed further in the later sections.

v. The stress ratio at large strain (e.g., γ = 20%), is not unique and has values of 0.71, 0.66, and 0.61 at σ_z = 50, 100, and 200 kPa, respectively. The critical state friction angle increases as the initial consolidation stress decreases. This suggests that the unique critical

state friction angle, a basic characteristic of soil, cannot be reached using these constant stress DSS tests. Lings and Dietz (2004) observed a similar pattern of stress ratio on coarse-grained Leighton Buzzard sand in the direct shear test. Rousé (2018) also showed that the critical state friction angle of sand increases as normal stress decreases. This variation of the stress ratio at large strain can come from two different sources, i.e., the magnitude of consolidation stress and lateral stress. Stroud (1971) and Lade and Nelson (1984) also showed that the critical state friction angle varies depending on the stress level, density, and test procedure. The second reason for the increased stress ratio at low stress levels is due to the increased lateral stress caused by the stacked rings/side walls and the rotation of principal stresses. Atkinson et al. (1991) showed that the lateral to vertical stress ratio affects the critical state of the simple shear test.

vi. Both types of apparatus give similar volume change behaviour up to $\gamma \sim 12\%$, which is comparable to the laboratory test data from a stacked ring type apparatus (Fig. 3.6(c)). However, at larger shear strains, the Cambridge type gives higher dilations, which might be due to localized displacement of rings at large strains.

3.6.3 Estimation of stresses to construct Mohr's circle

In a conventional DSS tests, only σ_z and τ (= τ_{zx}) are known. The location of σ_z and τ_{zx} is shown in Fig. 3.7. Unfortunately, these two stresses are not sufficient to construct a Mohr's circle and determine shear strength parameters. Several empirical approaches were proposed in the past to overcome these issues (e.g., Oda and Konishi 1974; Oda 1975a, b; Ochiai et al. 1983; Frydman and Talesnick 1991). Among them, the performance is shown for the following two approaches: (*i*) estimation of principal stresses (σ_1 and σ_2) (Ochiai et al. 1983), and (*ii*) estimation of lateral stress (σ_x) (Frydman and Talesnick 1991).

3.6.3.1 Estimation of principal stresses

The rotation of principal stress directions with shearing in a simple shear test was examined in several studies, and the following relationships have been proposed (e.g., Oda and Konishi 1974; Oda 1975 a, b; Ochiai et al. 1983).

$$R = k\tan\theta \tag{3.12}$$

$$k = \sin\phi_c \tag{3.13}$$

where, θ is the inclination of the major principal stress to the vertical, and k is a material property. The value of θ is zero at the beginning and increases with shearing. The value of R also changes with shear strain (e.g., Fig. 3.6(b)). Experimental results show k remains almost constant irrespective of applied normal stress, initial void ratio, stress path, and initial fabric (Cole 1967).

Ochiai et al. (1983) carried out a series of simple shear experiments and proposed the following empirical relation for θ as a function of stress ratio R.

$$\theta = 1.82R - 0.75R^2 \text{ (in rad.)} \tag{3.14}$$

Now, for a given R (known in DSS tests or simulations), θ is calculated using Eq. (3.14), which is then used to calculate "tanθ" and plotted against R in Fig. 3.8. The slope of this R vs tanθ line represents k (Eq. (3.12)). Figure 3.8 also shows R–tanθ line with $k = \sin\phi_c$ (Eq. (3.13)) where $\phi_c = 32°$ or 35°, as used in the present FE simulations. There is no significant difference between the two lines in Fig. 3.8; therefore, $k = \sin\phi_c$ is used in the following sections.

From geometric relationships of stresses on Mohr's circle, Ochiai et al. (1983) showed that the major and minor principal stresses (σ_1 and σ_3) in a simple shear specimen are related to measured normal and shear stresses and the parameter k as:

$$\sigma_1 = (k\sigma_z^2 + \tau_{zx}^2)/k\sigma_z \tag{3.15}$$

$$\sigma_3 = (1-k)\sigma_z \tag{3.16}$$

3.6.3.2 Estimation of lateral stress

Using the same relationships in Eqs. (3.12) and (3.13) and Mohr's circle for stresses, Frydman and Talesnick (1991) showed that the lateral stress (σ_x) in a simple shear specimen can be estimated as:

$$\sigma_x = [1 - k + R^2/k]\,\sigma_z \tag{3.17}$$

The applicability of Eq. (3.17) is evaluated using the present FE simulation results. For each time increment, the stress ratio R is known. Now, inserting R and k (= $\sin\phi_c$), the value of σ_x is calculated using Eq. (3.17).

As shown in later sections, non-uniform stress occurs primarily near boundaries. The average of lateral stresses (σ_x) for all soil elements in a central core is calculated. For the cylindrical soil specimen, the central core has a thickness of 6 mm and a diameter of 36 mm in the middle of the specimen, while for the rectangular soil specimen, the central core has a thickness of 6 mm, a width of 20 mm (as half of the specimen is modelled), and a length of 40 mm.

Figure 3.9 shows the comparison of calculated lateral stress using Eq. (3.17) and average lateral stress in the soil elements in the central core for MC analysis. No significant difference is found between the calculated σ_x, which implies that Eq. (3.17) can be used for a reasonable estimation of σ_x.

Figure 3.10 shows the variation of calculated lateral stress using above empirical approach and the average lateral stress of the soil elements in the central core for dense sand using the MMC model. Again, the average lateral stress in the central core is similar to the calculated lateral stress up to a shear strain level of 10%. After that, the FE calculated lateral stress in the central core is greater than that obtained from the empirical approach, and the difference is more pronounced in higher normal stress cases.

3.6.4 Mobilized friction angle

The full stress state of the DSS specimen is not known, as the stresses on the lateral boundary are not generally measured. Therefore, the question is whether the friction angle can be reasonably estimated using the stresses measured. The measured stresses give only one stress point X(σ_z,τ_{zx}), which is not sufficient to construct a Mohr's circle. The following assumptions are made to construct Mohr's circle (Fig. 3.11) to calculate the approximate friction angle (Roscoe et al. 1967; Stroud 1971)

a) If the horizontal plane is assumed to be the plane of maximum shear stress, the Mohr's circle I in Fig. 3.11 can be constructed. A tangent on this Mohr's circle from the origin represents an approximate friction angle, which is denoted as α.

$$\alpha = \sin^{-1}(\tau_{zx}/\sigma_z) \tag{3.18}$$

b) If the horizontal plane is assumed to be the plane of maximum stress obliquity, the Mohr's circle II in Fig. 3.11 can be drawn, which gives an approximate friction angle (β).

$$\beta = \tan^{-1}(\tau_{zx}/\sigma_z) \tag{3.19}$$

In reality, the stress point X(σ_z,τ_{zx}) is neither on the point of maximum stress obliquity nor on the maximum shear, but in between these two, as shown by the Mohr's circle III in Fig. 3.11. To construct Mohr's circle III, the principal stresses (σ_1 & σ_3) are calculated using Eqs. (3.13), (3.15) and (3.16) based on FE calculated normal and shear stresses at the boundary (σ_z,τ_{zx}). From Mohr's circle III, the mobilized friction angle (ϕ_m) is calculated as:

$$\phi_m = \sin^{-1}\left(\frac{\sigma_1 - \sigma_3}{\sigma_1 + \sigma_3}\right) \tag{3.20}$$

In this section the reliability of the estimated friction angle (α and β) are evaluated by comparing them with the mobilized friction angle (ϕ_m).

Figures 3.12 and 3.13 show the variation of α and β for stacked ring and Cambridge type DSS test simulation results, respectively. Simulations are performed for varying normal stresses (σ_z = 50, 100 and 200 kPa) using the Mohr–Coulomb and modified Mohr–Coulomb models for medium and dense sands, respectively. As the plastic strain develops after some elastic deformation (e.g., Fig. 3.6), the variation of α and β is shown for $\gamma > 2\%$. The following are the key findings:

a) For all cases, α is greater than β, irrespective of normal stress and shear strain levels. The difference between these two angles is relatively small at a lower strain level; however, they are considerably different at larger strains. For example, $\alpha = 39.4°$ and $\beta = 55°$ at 10% shear strain in Fig. 3.13.

b) α, β and ϕ_m for medium sand with the Mohr–Coulomb model increases with shear strain and then either remains almost constant or drops in some cases (e.g., Figs. 3.12(a, b)). A similar trend in α, β and ϕ_m variation is found for dense sand with the modified Mohr–Coulomb model; however, the decrease in α is higher in some cases (e.g., Fig. 3.13(d)). Note that, for the same variation in stress ratio (τ_{zx}/σ_z), the variation of α is more pronounced than β and ϕ_m (e.g., Fig. 3.13(d)), which indicates that interpretation of DSS test results using $\sin^{-1}$ or $\tan^{-1}$ might give considerably different friction angles in some cases.

c) None of these angles (α, β and ϕ_m) is equal to the critical state friction angle, even at large strains.

d) α, β and ϕ_m depends not only on shear strain but also on normal stress.

The insets of Figs. 3.12 and 3.13 show the Mohr's circle type III in Fig. 3.11 for four shear strains (γ = 5%, 10%, 12% and 15%). At these strains, the specimen reaches the failure state after considerable plastic deformation. Shearing starts from the initial principal stresses of σ_z

and $K_0\sigma_z$, where K_0 is the coefficient of earth pressure at rest. As the simulations are performed for constant normal stress, the minor principal stress remains the same with shearing for constant k (= $\sin\phi_c$) (Eqs. 3.13 and 3.16). However, the major principal stress increases with shearing and the Mohr's circle enlarges. Note that the Mohr's circle shrinks slightly in some cases at large strains (e.g., for 3.13(d)); however, it is not shown in the insets to maintain clarity. The insets of Figs. 3.12 and 3.13 show that, with increase in shear strain, the current stress points (circles) simply move vertically while the maximum shear stress points (rectangles) shift in an inclined direction. The current stress is neither the maximum shear stress nor the point of maximum stress obliquity, regardless of the specimen type (stacked ring or Cambridge type). The initial consolidation stress also plays a significant role in determining the location of the current stress point measured at the top/bottom cap on Mohr's circle. At low consolidation stress (e.g., σ_z = 50 kPa), the measured stresses are closer to the point of maximum stress obliquity. However, for higher consolidation stresses (100 kPa & 200 kPa) and larger strains, the measured stresses are closer to the point of maximum shear stress than to the point of maximum stress obliquity.

Based on simulations of Discrete Element Method (DEM), Wijewickreme et al. (2013) suggested that ϕ_m is closer to α at a low strain level, and closer to β at a high strain level (γ = 15–20%). The present study also shows a very similar pattern for low stress level (σ_z = 50 kPa). However, for high stress levels ($\geq$ 200 kPa), Wijewickreme et al. (2013) found a more conservative pattern than what is found in the present study.

Figures 3.14(a) and 3.14(b) show the comparison of friction angles (α, β and ϕ_m) in stacked ring and Cambridge type DSS test simulations at three strain levels (γ = 5%, 10%, & 15%). For medium sand (Fig. 3.14(a)), all the data points are close to the 1:1 line, which indicates that both types of tests give similar friction angle. However, for dense sand, the data points are

slightly above the 1:1 line (< 3°), which indicates that the MMC model gives slightly higher friction angles in Cambridge type DSS tests in some cases.

3.6.5 Mobilized friction angle for MC analysis

As discussed in Section 3.6.3, the Mohr's circle could be constructed by estimating principal stresses (Eqs. (3.12)–(3.16)) or lateral stress (Eq. 3.17)). In section 3.6.4, the friction angle is calculated based on the former approach. If the lateral stress (σ_x) is known from Eq. (3.17), a Mohr's circle can be constructed with (σ_z, τ_{zx}) and (σ_x, τ_{xz}) can be constructed, and the mobilized friction angle (ϕ_m) can be obtained by drawing a tangent from the origin. To show some comparison, ϕ_m is calculated for γ = 15% for medium sand and γ = 10% for dense sand. A lower value of γ is considered for dense sand, as estimated σ_x does not match well after γ ~ 10% for the Cambridge type test (Fig. 3.10(b)).

Table 3.3 shows that, for medium sand, the calculated friction angle (0.9°–3.2°) is lower than the input parameter (ϕ = 38°), and the difference increases with an increase in normal stress. For dense sand, the mobilized friction angle at γ = 10% is considerably lower than the peak value (Fig. 3.2) and 3°–7° higher than the critical state friction angle (ϕ_c = 35°) used in the analysis, and the difference is higher for lower normal stresses.

Table 3.3: Mobilized friction angle based on estimated values of non-measured stresses

	Test type	Mobilized friction angle (°)		
		50 kPa	100 kPa	200 kPa
Based on principal stresses	stacked ring	37.1 (41.1)	35.9 (39.8)	35.3 (38.6)
	Cambridge	37.4 (42.2)	37.2 (41.8)	36.9 (39.4)
	stacked ring	36.8 (38.8)	35.6 (38.4)	34.8 (37.3)

Based on lateral stress	Cambridge	36.0 (39.0°)	35.5 (37.9°)	35.0 (36.8)

Note: Numbers in parenthesis for dense sand with MMC model and at γ = 10%

3.7 Stress non-uniformities

Stress non-uniformity is one of the limitations of the DSS test. Non-uniformity occurs not only near the cylindrical vertical face (Wu 2017; Wai et al. 2022) but also near the top and bottom surfaces of the soil specimen (DeGroot et al. 1994; Wu 2017; Wai et al. 2022). The non-uniformity of stresses coupled with unknown normal and shear stresses on the vertical surface cause the interpretation of the test results to be challenging; for example, a Mohr's circle cannot be drawn as in the triaxial test. Several studies have assessed the degree of non-uniformity and its effects on boundary stresses (DeGroot et al. 1994; Wijewickreme et al. 2013; Asadzadeh and Soroush 2016; Bernhardt et al. 2016; Wai et al. 2022). In the following sections, the non-uniformities of stresses are investigated using the simulation results for σ_z = 100 kPa.

3.7.1 Stress distribution paths for stacked ring type DSS test

Five paths are created to show the variation of stresses (Fig. 3.15). Path 1 and 2 is along the x-axis and 1.0-mm inside the soil specimen from the top and bottom plates, respectively. Path 4 and 5 are along the z-axis and again 1.0-mm inside the soil from the left and right vertical surfaces, respectively. Finally, path 3 is a circular line at a radial distance of 25 mm from the centre and 1.0 mm inside the soil from the top.

3.7.1.1 Distribution of shear stresses along the paths

Figure 3.16 shows that the distribution of shear stress (τ_{zx}) along path 1 and 2 are not uniform. The shear stress drops to a small value in the upper right and lower-left corners of the soil sample (see points c and a in the inset of Fig. 3.16(a)). However, τ_{zx} in the middle two-thirds

is almost uniform throughout the test. Modelling the soil as an elastic material, Roscoe (1953) also showed a similar pattern of shear stress distribution along the horizontal boundaries.

The distribution of shear stress (τ_{xz}) along path 4 and 5 is shown in Fig. 3.17. Concentration of shear stress occurs at the top-left and bottom-right corners of the soil sample (see points d and b in the inset of Fig. 3.17(a)). However, τ_{xz} is relatively smaller in the other two corners. At lower strain level (γ = 0–5%), the distribution of shear stress is almost uniform. With an increase in γ (e.g., γ = 15%), non-uniformity of shear stress also increases. The shear stress distribution for MMC is more uniform than for MC analysis. Non-uniformity is overestimated when using the MC material model. Budhu and Britto (1987) showed that modified cam clay analysis leads to more uniform stress distribution in clayey soil than elastic analysis. Vucetic and Lacasse (1982) also showed that linear elastic material predicts a large zone of non-uniformity. Adding plasticity to the material model increases uniformity of stresses during DSS tests, which is consistent with the current study.

3.7.1.2 Distribution of vertical normal stresses along the paths

Figure 3.18 shows the vertical normal stress (σ_z) distribution along path 1 and 2 for MC and MMC analysis, respectively. As no wall friction is considered at the vertical boundary, the normal stress distribution at the end of consolidation (i.e., the beginning of shearing, γ = 0) is uniform. With shearing, σ_z becomes non-uniform, although the total force applied from the top plate remains the same. σ_z is considerably higher than 100 kPa within ~5 mm in the top left corner (point d in the inset of Fig. 3.18(a)) and bottom right corner (point b in the inset of Fig. 3.18(a)). On the other hand σ_z is considerably lower than 100 kPa in the soil elements near the top right corner (point c in the inset of Fig. 3.18(a)) and bottom left corner (point a in the inset of Fig. 3.18(a)). A similar trend has also been shown in previous studies (e.g., Lucks et al. 1972; Budhu and Britto 1987; Wu 2017; Wai et al. 2022). However, Fig. 3.18 shows that the

vertical stress remains almost constant at the targeted value (100 kPa) in the middle two-thirds of the soil specimen for the entire range of shear strain simulated in this study.

Figures 3.19(a) and (b) present the distribution of vertical normal stress along the radial path 3 for the MC and MMC analysis, respectively. The radial distance from the center represents the value of σ_z at a particular point on path 3 at an angle θ to the horizontal, as shown in Fig. 3.15(a). At the beginning of shearing, σ_z uniform and symmetric, as shown in Fig. 3.19. However, with an increase in shear strain, stress non-uniformity becomes apparent, and the curves become non-symmetric. The soil elements near the top cap experience higher σ_z on the left half of the specimen compared to the right half, while the opposite pattern is observed for the soil elements near the bottom pedestal. In comparison to the MC analysis, the distribution of normal stress in the MMC analysis is more uniform, as previously discussed.

3.7.2 Stress distribution paths for Cambridge type DSS test

Four paths have been created to capture the distribution of normal and shear stress within the soil sample, as illustrated in Fig. 3.20. The paths consist of two horizontal and two vertical stress paths, each selected 1 mm inside their respective boundary. Path 6 and 7 are located along the x-axis, while path 8 and 9 are located along the z-axis.

3.7.2.1 Distribution of shear stresses along the paths

Figure 3.21 shows the distribution of shear stress along path 6 and 7. The shear stress is similar to that of a cylindrical type soil sample, but decreases in the upper right and lower left corners (see points c and a in the inset of Fig. 3.21(a)). The shear stress at the middle two-third of the soil sample remains uniform. Geometrically, the soil sample moves freely and encounters less resistance at corners a and c (in the inset of Fig. 3.21(a)), compared to the opposite corner. This contributes to the abrupt decrease in shear stress observed in the upper right and lower left corners of the soil sample.

Figure 3.22 shows the shear stress distribution along vertical paths. The distribution is uniform up to 5% strain, then deviates. At high strain levels, shear stress concentrates at the top right and bottom left of the soil sample, similar to the cylindrical type soil sample. Wai et al. (2022) also showed a similar type of shear stress distribution along the vertical plane.

3.7.2.2 Distribution of normal stresses along the paths

Figure 3.23 shows the normal stress distribution along path 6 and 7. Similar to the stacked ring type DSS test, the normal stress is uniform at the end of consolidation because no friction is considered along the vertical boundary. However, as shearing progresses, the normal stress concentrates at the upper right and lower left corners of the soil sample. The middle third remains mostly uniform. This distribution was also observed by Finn (1985) and Dabeet et al. (2015) in their studies of the DSS test. The difference between stacked ring and Cambridge DSS tests is that the normal stress distribution in Cambridge is more uniform across the length of the specimen. The shear stress along the soil sample, as shown in Fig. 3.22, is not uniform and varies along the boundary, creating unbalanced moments within the soil sample. To achieve moment equilibrium, the normal stress must counteract these unbalanced moments by distributing in such a way that σ_z generates an opposite moment. This results in the normal stress distribution deviating from a uniform stress state, as seen at the corners of the soil sample. This pattern is also observed in the stacked ring type DSS test. The introduction of plasticity also improves the normal stress distribution along the soil sample, resulting in a pattern similar to that of cylindrical type soil samples.

3.8 Distribution of deviatoric plastic strain with shearing

Figures 3.24 and 3.25 show the development of deviatoric plastic shear strain (γ^p) with loading for the cylindrical type of soil sample. After a certain level of shearing, plastic shear strain accumulation occurs locally, and failure planes form. To show the plastic shear strains and

failure planes, the front view (left column of Figs 3.24 and 3.25) and rear view (right column of Figs. 3.24 and 3.25) are shown. The plastic shear strain is small and almost homogeneous throughout the specimen during the early stage of shearing, especially in the central area. At γ = 2–3%, a shear band (zone of large plastic shear strain) develops in the middle of the soil specimen. As the simulation progresses, this diagonal shear band extends toward the boundary and separates the specimen into two parts (Fig. 3.25 (c– f)). A similar pattern of the rupture zone was reported by Budhu (1984 and 1988) in cylindrical soil specimens in laboratory tests using the radiographic technique. In addition, considerably large plastic shear strain developed in the soil elements near the top and bottom plates, which can affect the stress distribution, such as the lateral stress on the rings and stress non-uniformity.

Figures 3.26 and 3.27 demonstrate the progression of deviatoric plastic shear strain (γ^p) with loading for Cambridge type DSS tests. As the test progresses, plastic shear strain begins to develop at 5% shear strain, similar to the cylindrical type soil sample. However, the plastic shear strain development initiates from the end of the sample and then spreads to the middle. The generated shear strains are more evenly distributed throughout the sample. At higher strain levels, shear bands form and extend towards the boundary, which is similar to the stacked ring type DSS tests (Figs. 3.26 and 3.27). The distribution of plastic shear strain is largely consistent on the front and back sides of the soil specimen, and no accumulation of plastic strain is observed near the top and bottom plates. The generated shear strains are more evenly distributed throughout the sample. Additionally, the deviatoric plastic strain (γ^p) at the lateral boundaries is nearly zero and two elastic zones develop near the left and right vertical boundaries due to the lack of friction between the soil and these boundaries, potentially leading to strain non-uniformity and progressive failure of the soil specimen. The shear band formation in dense sand is clearer, as strain-softening occurs, than that in medium sand.

3.9 Effects of vertical wall friction

The ideal DSS test condition does not allow any wall friction on the vertical boundary of the soil sample. The main goal of the frictionless interface between the wall and the soil sample is to give a uniform distribution of normal stresses during the consolidation stage. Even though modern devices use a thin membrane between the wall and the soil sample to reduce friction, there can still be some frictional resistance between them during the laboratory test. Given the possibility of wall friction in the laboratory test, the effects of vertical wall friction on the overall stress-strain behaviour are examined in this section.

The interface between rigid vertical walls/rings and soil is simulated using the Coulomb friction model by defining the friction coefficient (μ) as $\mu = \tan(\phi_\mu)$, where ϕ_μ is the interface friction angle. The simulations are performed for $\phi_\mu = 0$ (frictionless), 5°, 10° and 20°.

Figures 3.28 and 3.29 show a trend of increasing stress ratio with increase in ϕ_μ for Cambridge type tests. However, ϕ_μ has less effects on stress ratio in stacked ring type tests for both medium and dense sands (left column of Figs. 3.28 and 3.29).

For a better comparison, consider the simulations for the frictionless case as the ideal case. The increase in stress ratio with respect to the ideal case at $\gamma \sim 15\%$ is shown in Fig. 3.30. The stress ratio increase is less than 5% and 8% for medium and dense sands, respectively, for the simulated cases ($\phi_\mu \leq 20°$) in the stacked ring type test (Figs. 3.30(a and c)). However, in Cambridge type tests, the stress ratio might increase up to 18% at $\gamma \sim 15\%$ when $\phi_\mu = 20°$ is used (Figs. 3.30(b and d)). In other words, the interface friction significantly affects the stress ratio in Cambridge type tests.

The vertical stress at the bottom of the specimen could be considerably lower than the applied stress at the top surface for higher ϕ_μ (Fig. 3.31). For example, the vertical stress at the bottom of the specimen is ~12.5% smaller than that of the top in stacked ring type test on dense sand for $\phi_\mu = 20°$ (Fig. 3.31(a)). This effect is smaller in Cambridge type tests (compare Figs. 3.31(a)

and (b)), which is because of the lower aspect ratio. Very similar normal stress change, as in Fig. 3.31, is found for medium sand. Note that, the normal stress at the bottom of the specimen increases when horizontal shear displacement is applied at the bottom because of dilation of the soil. In summary, considerable vertical stress non-uniformity might develop for higher ϕ_μ, which could affect the overall stress–strain response during shearing.

3.10 Effect of aspect ratio

To investigate the effects of aspect ratio (= H/D for stacked ring and H/L for Cambridge), FE simulations are performed for dense sand for four specimen heights (H = 15 mm, 20 mm, 25 mm, and 30 mm). In these simulations, the diameter of the cylindrical specimens is 70 mm, and the length of the cuboidal specimen is 100 mm. All other conditions, including soil properties, boundary and loading conditions are the same as those described in previous sections for modeling dense sand with the MMC model.

Figure 3.32 shows that the higher the aspect ratio, the lower the stress ratio, and the effect is higher in stacked ring type tests. The Cambridge type DSS apparatus guarantees a simple shear configuration due to its rigid boundaries, while the stacked ring type does not provide such guarantees (Budhu 1979). For this reason, at high aspect ratio, the horizontal displacement of the rings does not change linearly from bottom to top. This leads to a more non-uniform vertical boundary for a higher aspect ratio, which affects the overall distribution of stresses within the specimen.

Figures 3.33 and 3.34 show the deviatoric plastic strain (γ^p) at γ = 12% for various aspect ratios. As shown, non-uniform strains generate within all soil specimens. For higher aspect ratios, multiple shear bands form within the soil specimens.

3.11 Summary

The direct simple shear test is an advanced method of geotechnical testing, as it simulates many field loading conditions. However, several studies have pointed out some limitations of the DSS test, such as non-uniform stress distribution within the soil specimen and the difficulties in estimating shear strength parameters.

To understand soil behaviour in DSS tests, the present study utilizes the FE method to simulate DSS tests on dry sand. The FE models used in this study include a simple elastic perfectly plastic Mohr–Coulomb model for medium sand and a modified Mohr–Coulomb model for dense sand. FE results show that the existing empirical relations could be used to estimate the unknown lateral stress and principal stresses, which can then be used to draw a Mohr's circle and determine the shear strength parameter from the DSS test. The calculated angle of internal friction, based on the developed Mohr's circle, is slightly lower than the input value of the friction angle given for the Mohr-Coulomb model.

The research also found that the stress state measured from the bottom pedestal can be used to determine the mobilized friction angle with reasonable accuracy. For dense sand with high consolidation stresses, the shear stress measured from the bottom pedestal is close to the point of maximum shear stress. At low consolidation stresses, it is close to the point of maximum stress obliquity.

For medium sand, both the stacked ring and Cambridge type DSS tests give similar mobilized friction angles, whereas for dense sand, the mobilized friction angle calculated from the Cambridge type DSS test is slightly greater than that from the stacked ring type DSS test.

Non-uniformities developed near the boundaries, especially near the vertical surfaces, due to the lack of complementary shear stress. At large strain level, plastic shear strain develops with shearing and shear bands form, which separates the soil specimen into blocks. The formation of shear bands affects the stress development and non-uniformities at large strains.

Higher interface resistance between soil and side wall/ring causes non-uniform distribution of normal stress during the consolidation, which can affect the overall stress–strain response during the shearing stage. Also, the higher the interface resistance, the higher the stress ratio at large displacements.

The specimen dimensions have a notable effect on the overall response and the stress distribution of the DSS test. Specifically, the higher the aspect ratio, the lower the stress ratio, and this relationship is likely due to increased non-uniformity of the stress distribution across the specimen.

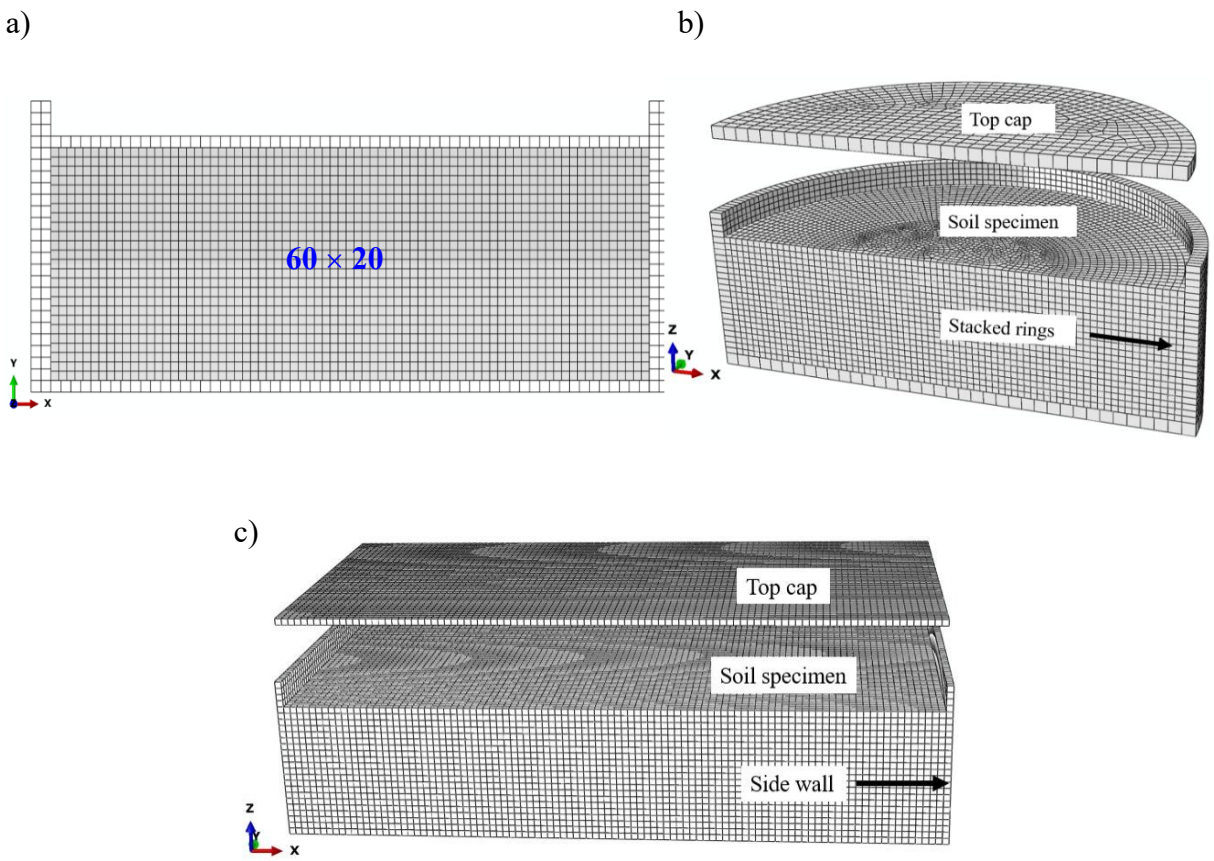

Figure 3.1: Typical finite element mesh prior to loading: (a) plane strain condition (2D); (b) stacked ring type; (c) Cambridge type

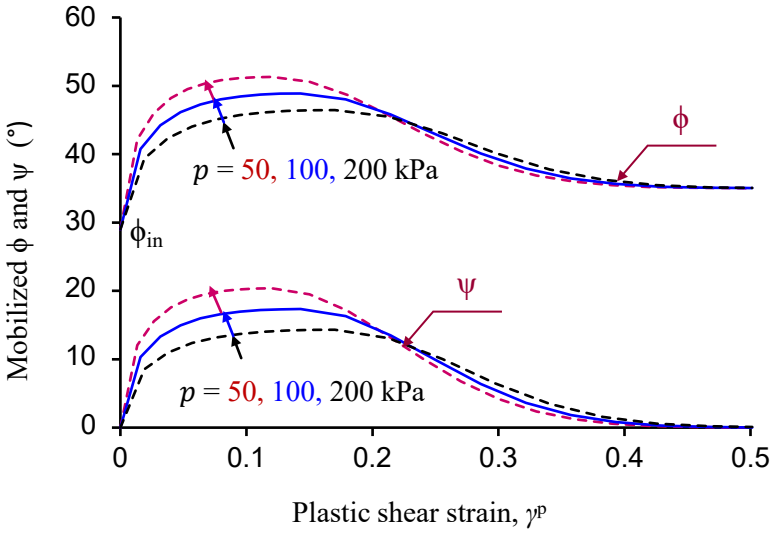

Figure 3.2: Variation of mobilized friction and dilation angles

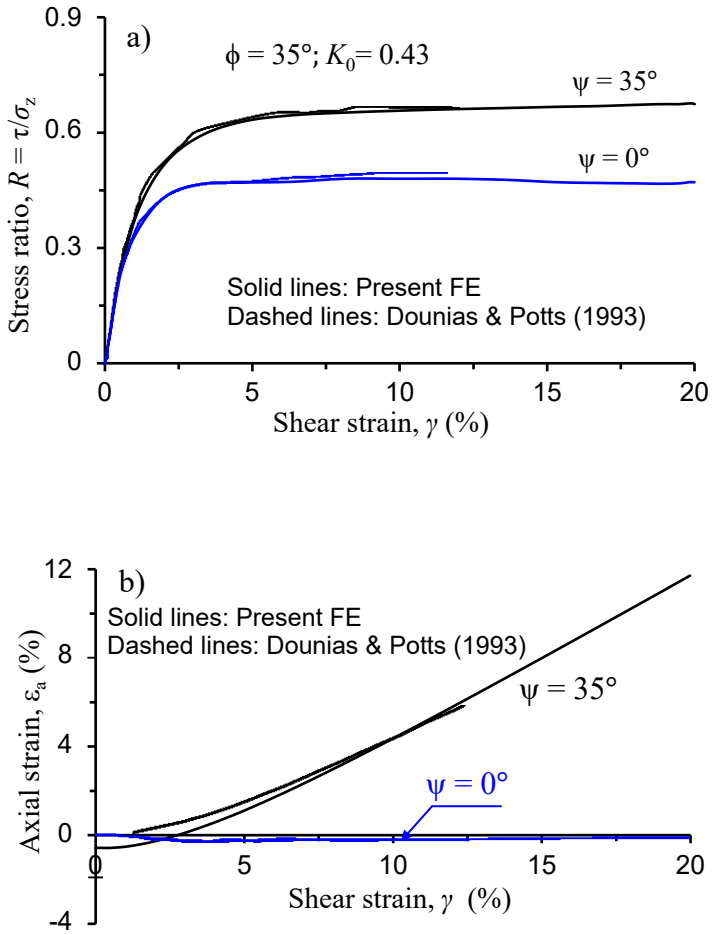

Figure 3.3: Comparison of present FE analysis with a previous FE analysis with Mohr–Coulomb model and ϕ = 35° and K_0 = 0.43: (a) stress–strain behaviour ; (b) volume change

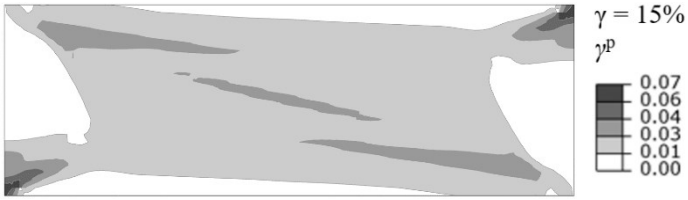

a) Present study

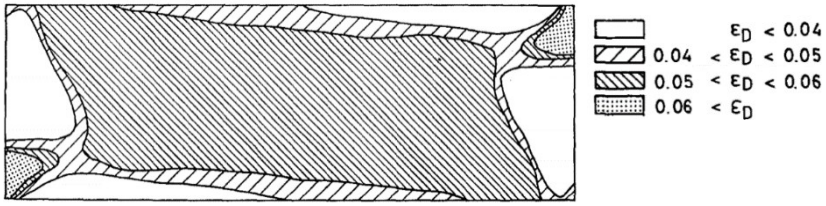

b) Dounias & Potts (1993)

Figure 3.4: Comparison of plastic zone obtained from present FE analysis with a previous FE analysis with Mohr–Coulomb model for $\phi = 35°$ and $K_0 = 0.43$ at shear strain of 15%: (a) Present study; (b) Dounias and Potts (1983)

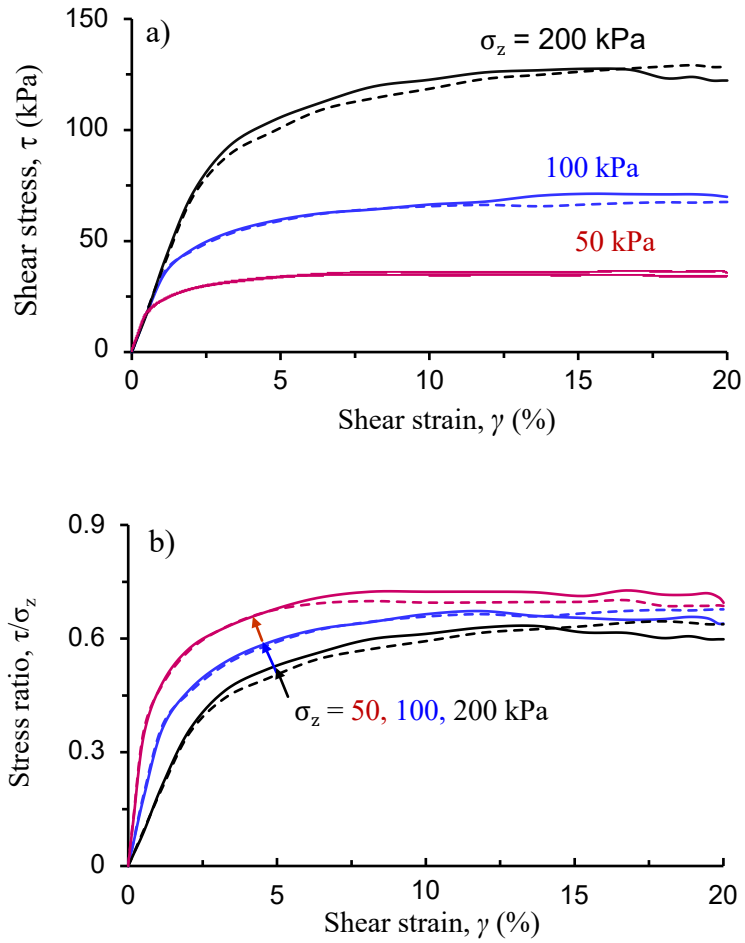

Figure 3.5: Simulations with Mohr–Coulomb model: (a) stress–strain response; (b) variation of stress ratio (solid lines for stacked ring type and dashed lines for Cambridge type)

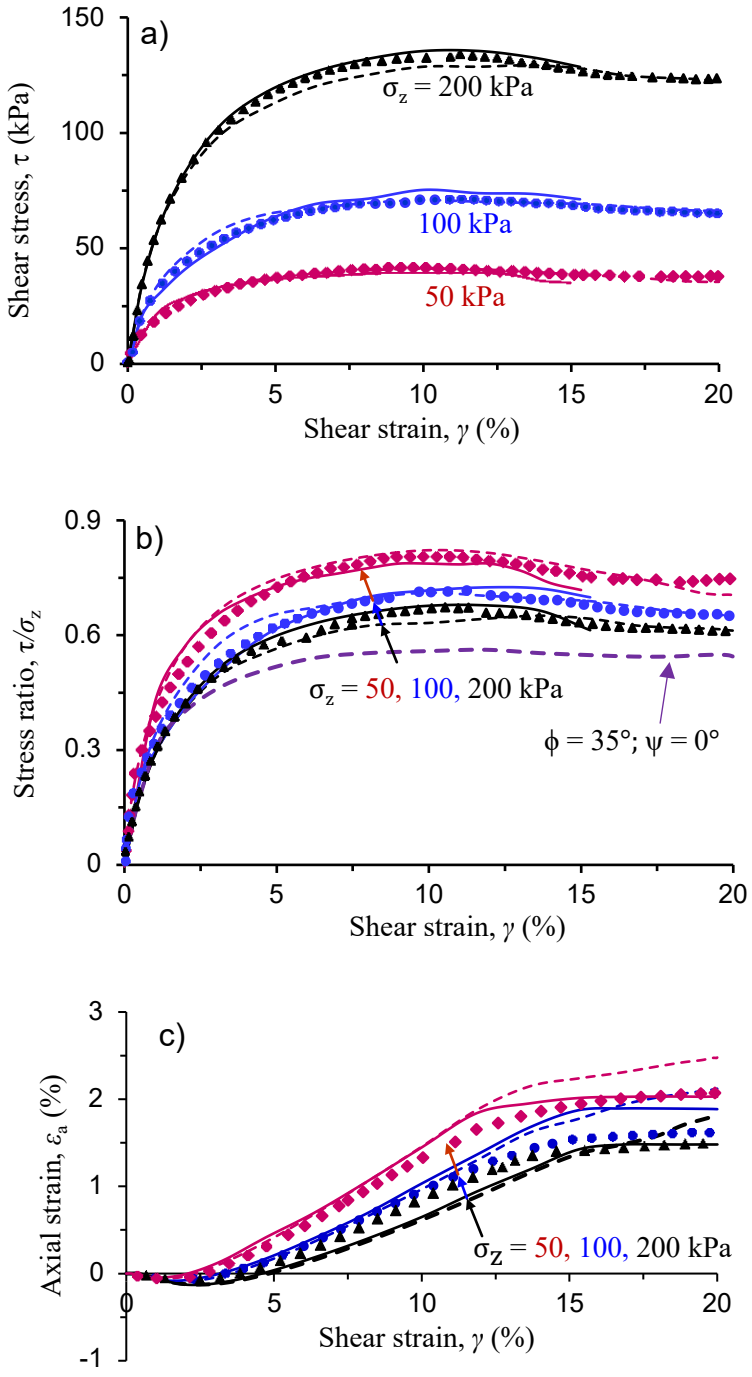

Figure 3.6: Simulations with Modified Mohr–Coulomb model: (a) stress–strain response; (b) variation of stress ratio; (c) volume change (solid lines for stacked ring type, dashed lines for Cambridge type, and symbols for laboratory test (Al Tarhouni and Hawlader 2021))

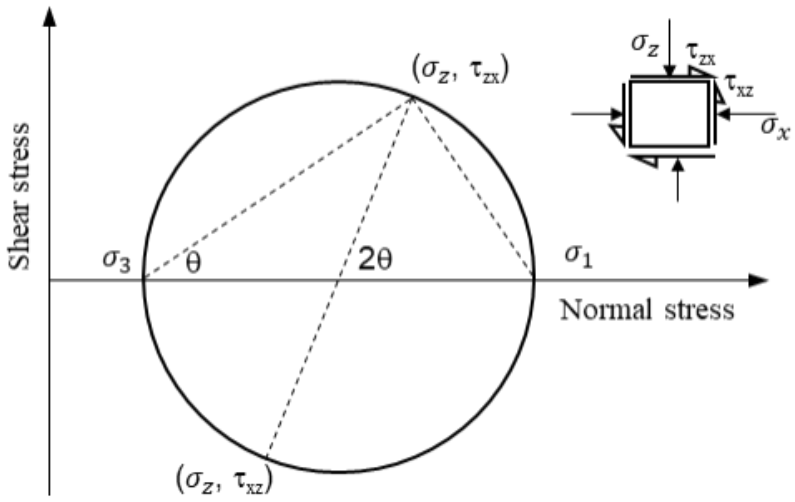

Figure 3.7: Estimation of stresses from DSS test results

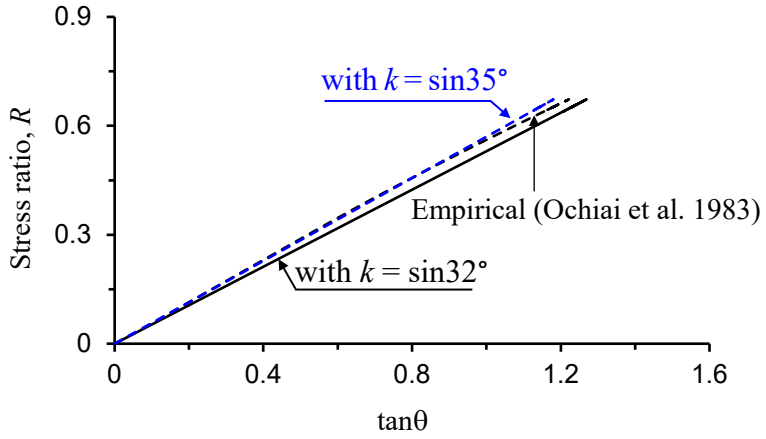

Figure 3.8: Variation of k with shear stress increase and rotation of principal stress

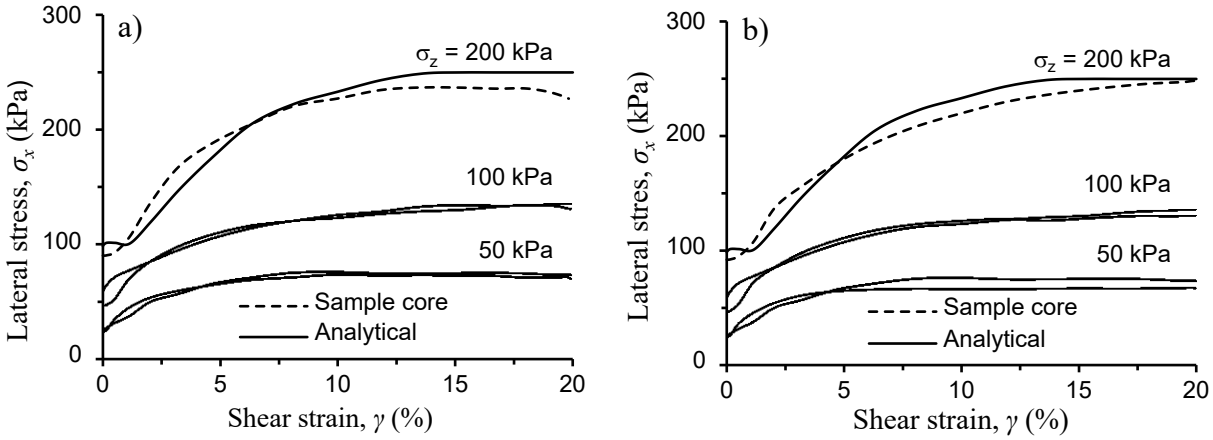

Figure 3.9: Estimation of lateral stress in medium sand specimen using MC model: (a) stacked ring type; (b) Cambridge type

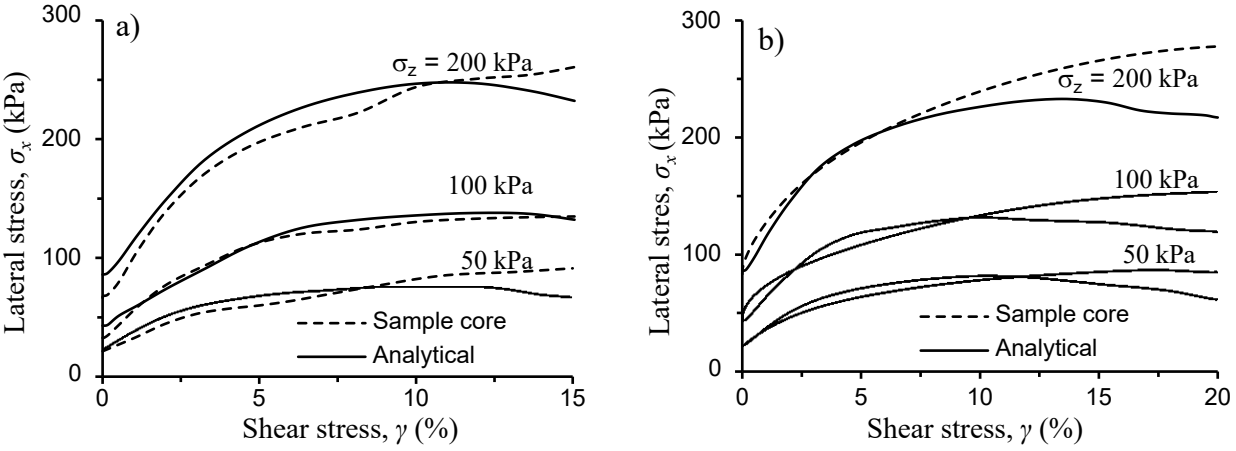

Figure 3.10: Estimation of lateral stress in dense sand using MMC model: (a) stacked ring type; (b) Cambridge type

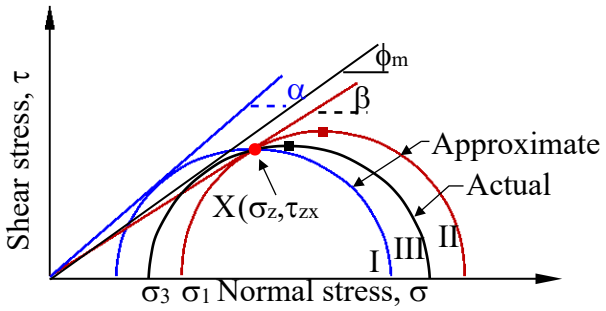

Figure 3.11: Construction of Mohr's circle from stresses measured in DSS test to calculate friction angle

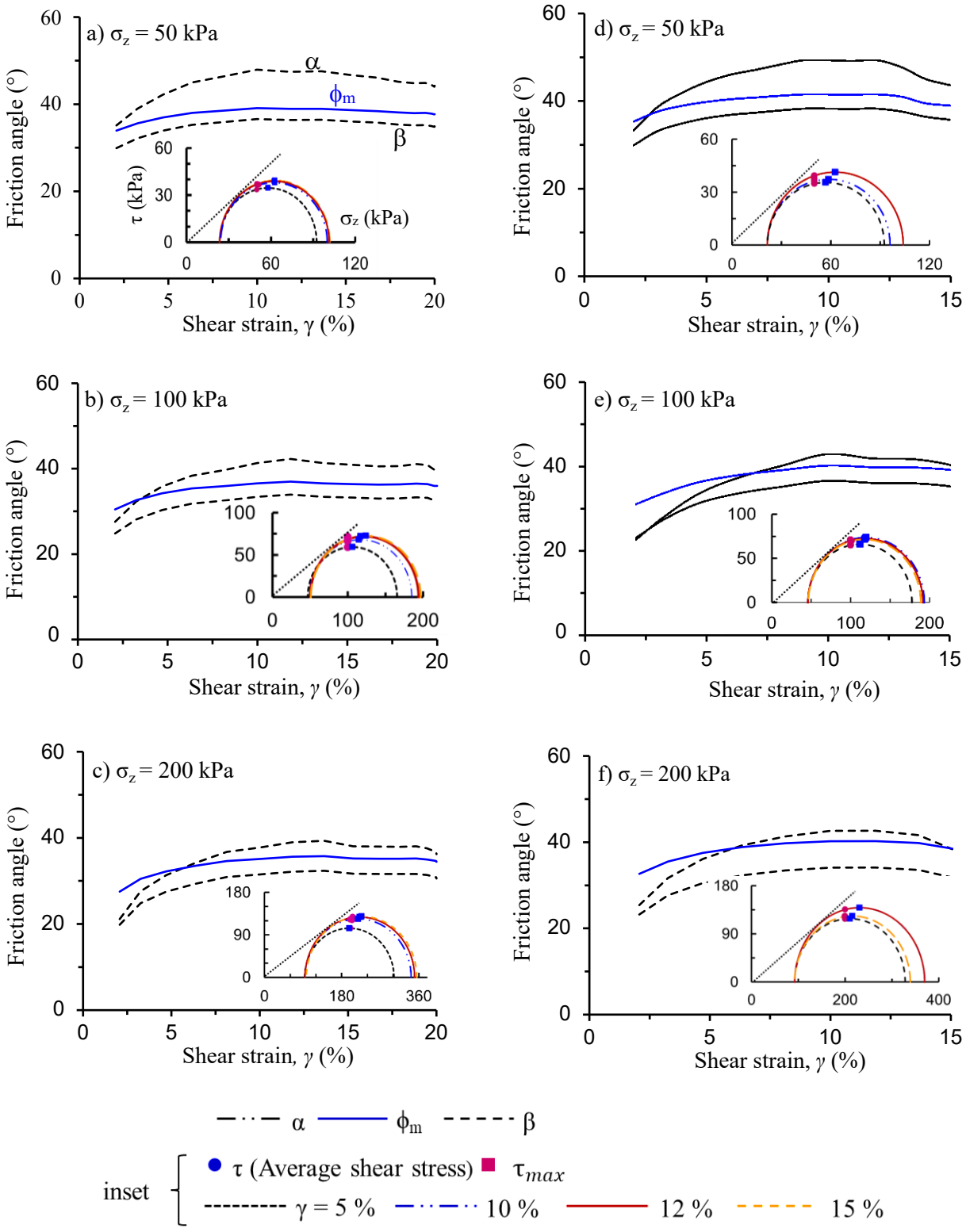

Figure 3.12: Comparison of approximate friction angle (α and β) with mobilized friction angle (ϕ_m) for stacked ring type test: (a–c) using MC model; (d–f) using MMC model

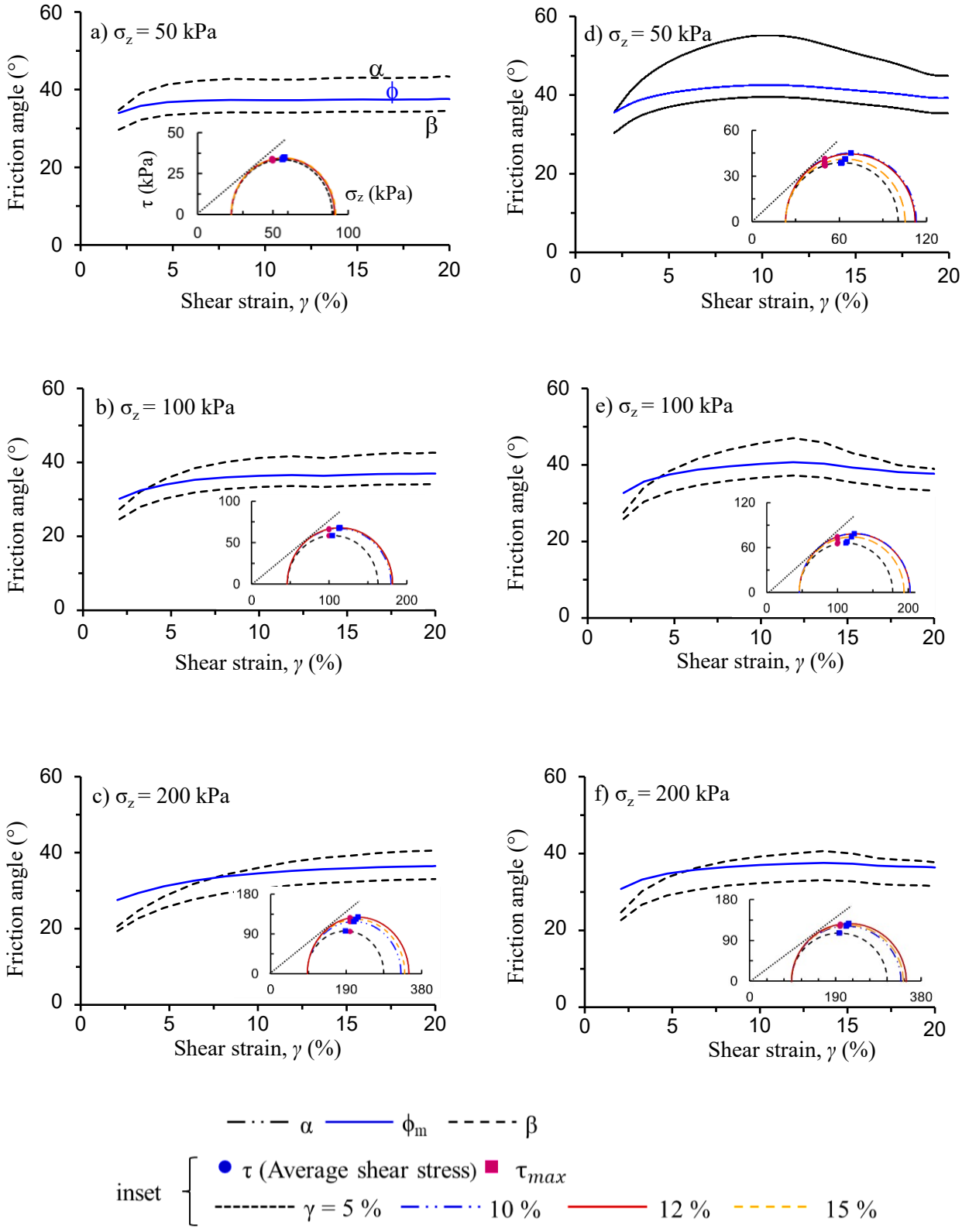

Figure 3.13: Comparison of approximate friction angle (α and β) with mobilized friction angle (ϕ_m) for Cambridge type test: (a–c) using MC model; (d–f) using MMC model

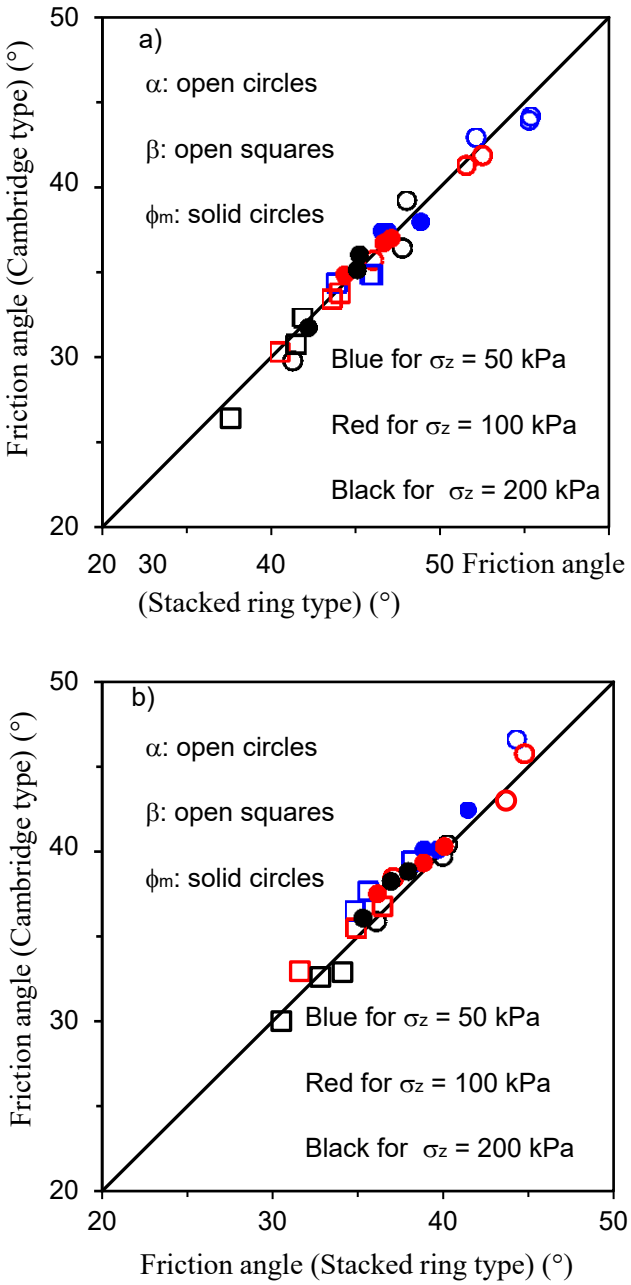

Figure 3.14: Comparison of mobilized friction angles in stacked ring and Cambridge type DSS tests: (a) medium dense sand with MC model; (b) dense sand with MMC model using MMC model

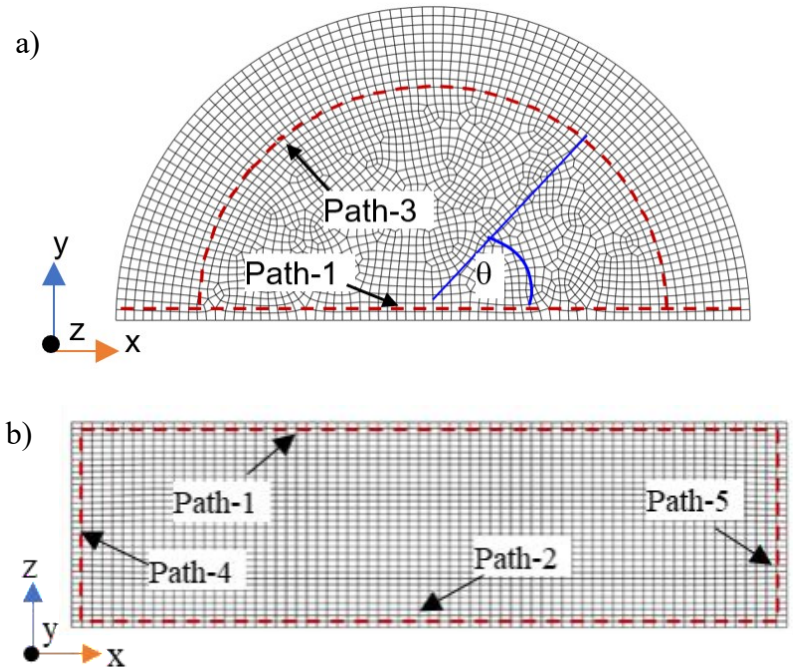

Figure 3.15: Three-dimensional FEM model for stacked ring type simple shear tests with stress paths: (a) mesh in viewpoint of x-y space, (b) mesh in viewpoint of x-z space

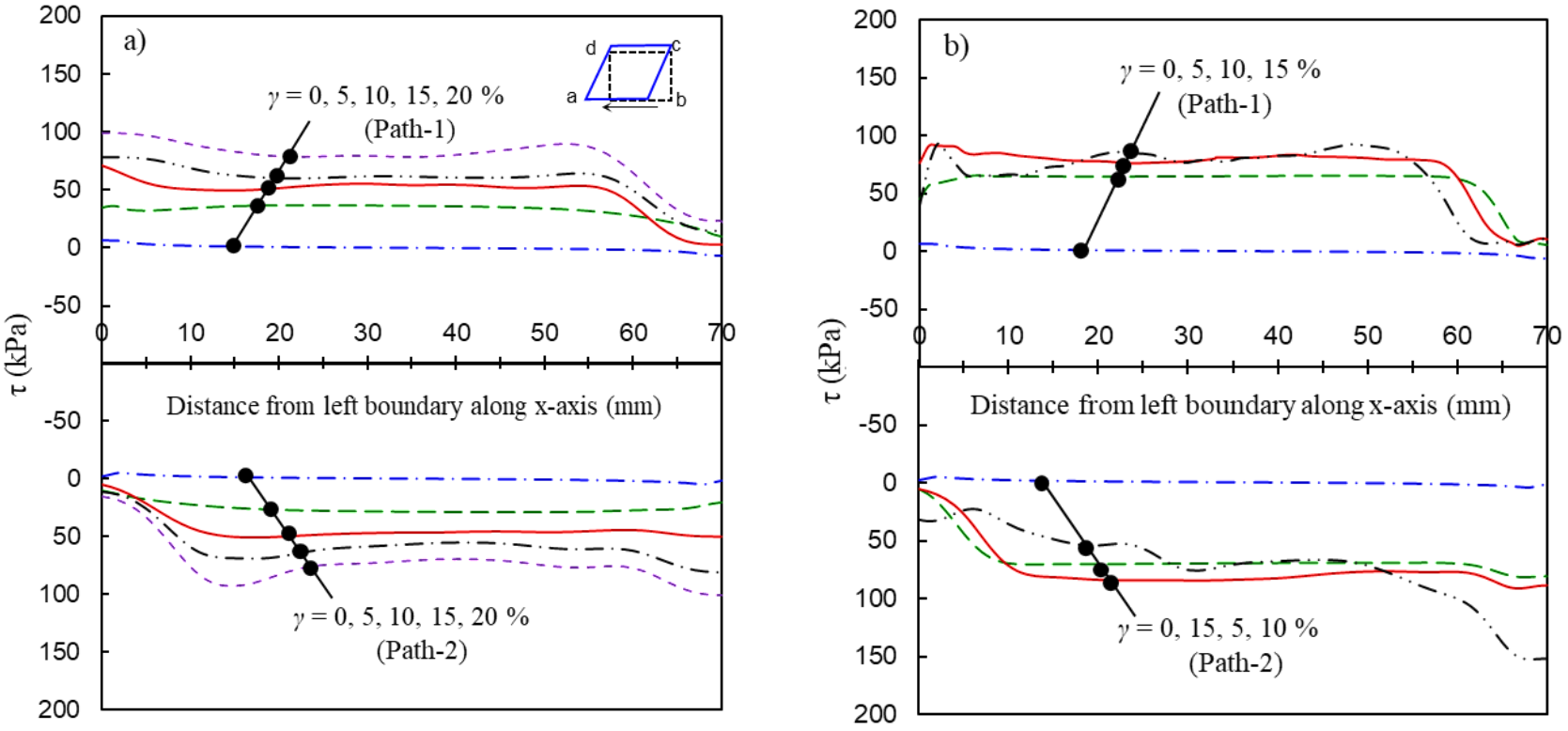

Figure 3.16: Distribution of shear stresses (τ) along path 1 and 2 for stacked ring type DSS test under σ_z = 100 kPa: (a) MC model; (b) MMC model

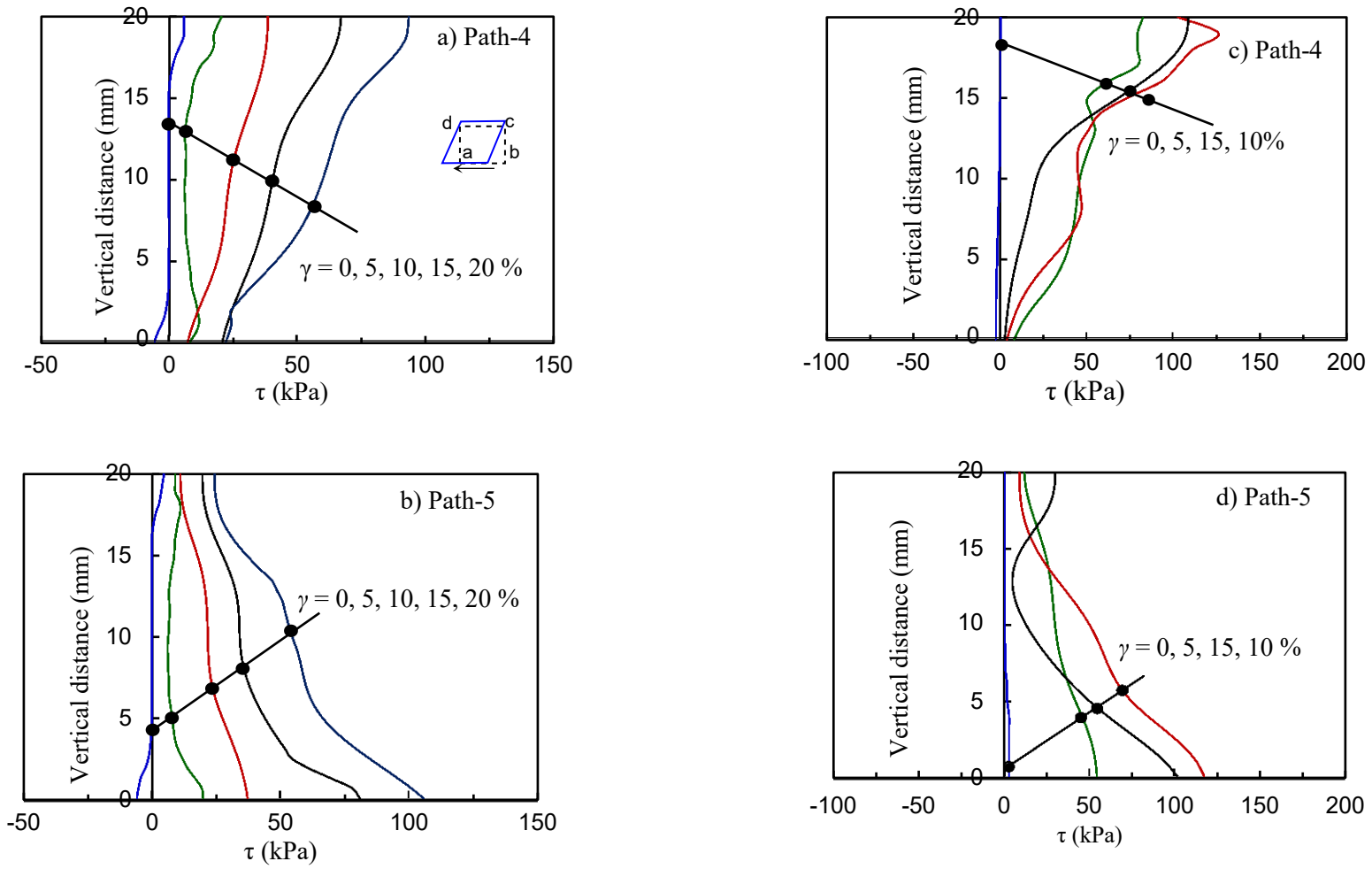

Figure 3.17: Distribution of shear stresses (τ) along path 4 and 5 for stacked ring type DSS test under σ_z = 100 kPa: MC model (a–b) (left column), MMC model (c-d) (right column)

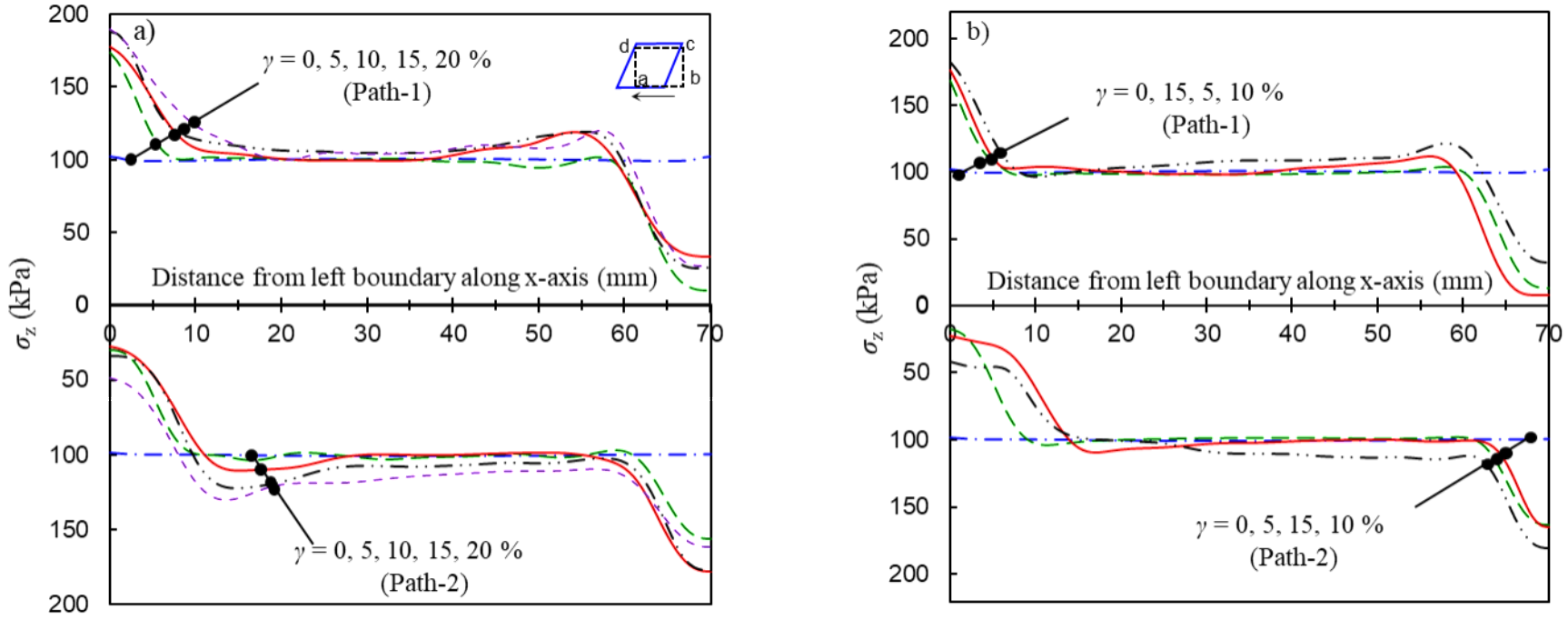

Figure 3.18: Distribution of normal stresses (σ_z) along path 1 and 2 for stacked ring type DSS test under σ_z = 100 kPa: (a) MC model; (b) MMC model

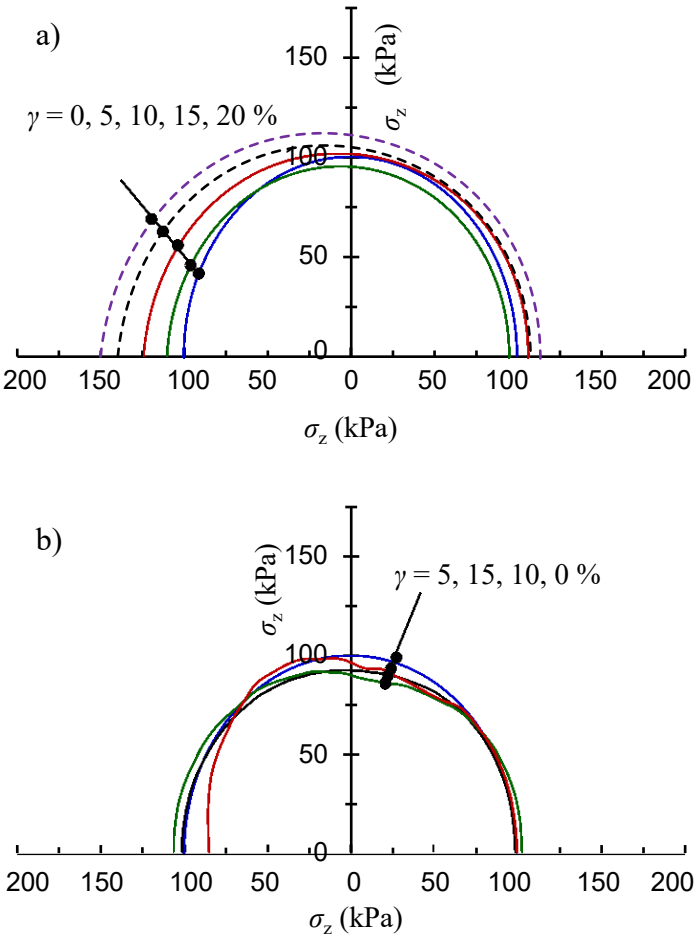

Figure 3.19: Distribution of vertical normal stress (σ_z) along path 3 for stacked ring type DSS test using: (a) MC model; (b) MMC model

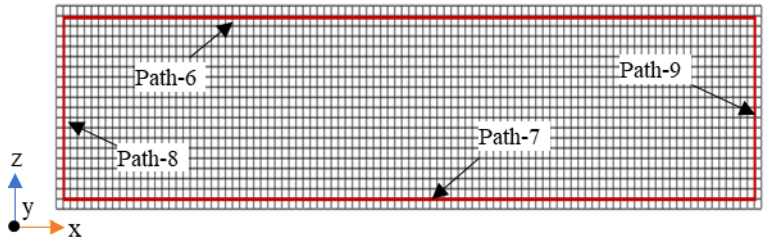

Figure 3.20: Three-dimensional FEM model for Cambridge type simple shear tests with stress paths mesh in viewpoint of x-z space.

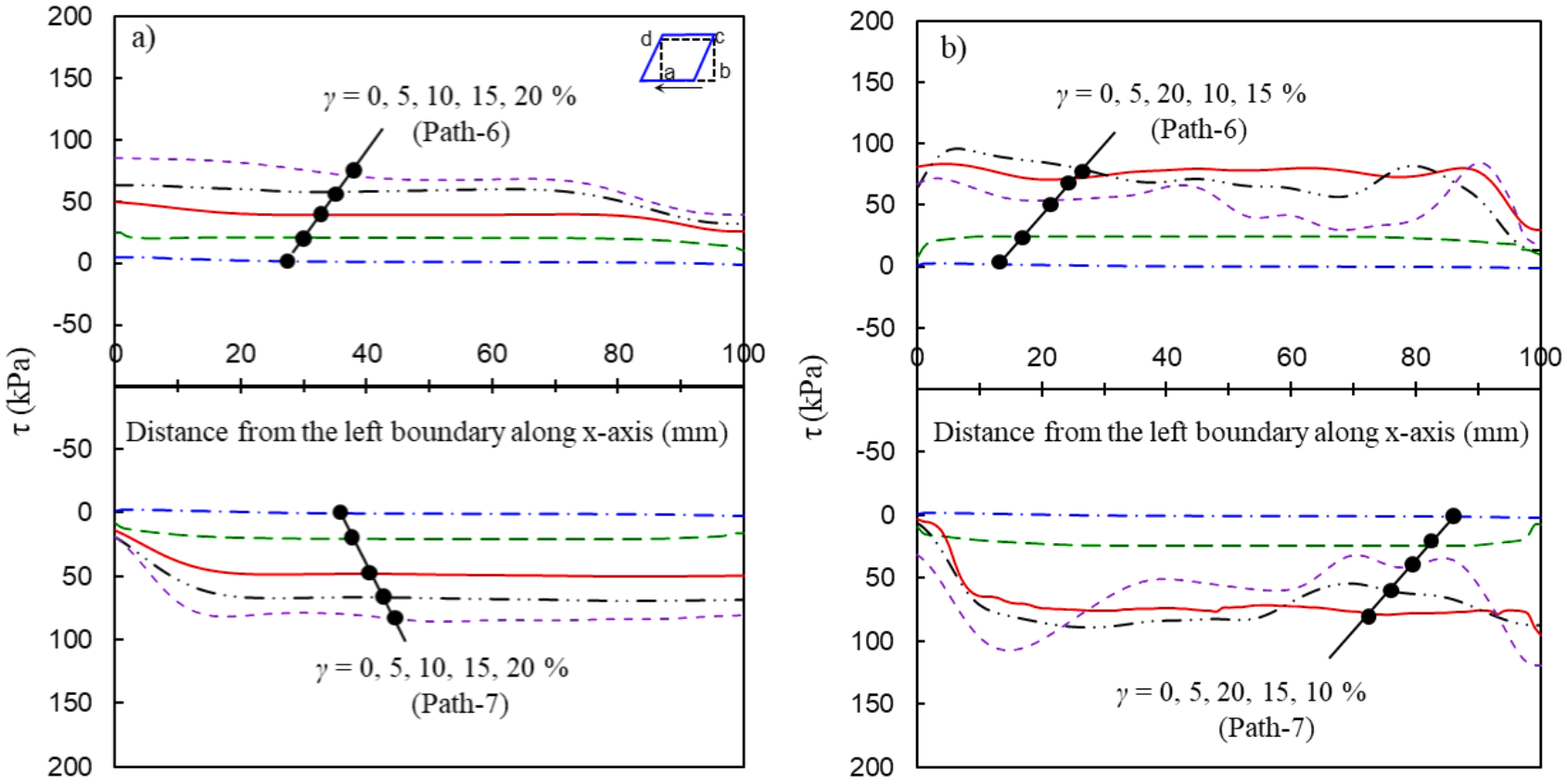

Figure 3.21: Distribution of shear stresses along path 6 and 7 for Cambridge type DSS test under σ_z = 100 kPa: (a) MC model; (b) MMC model

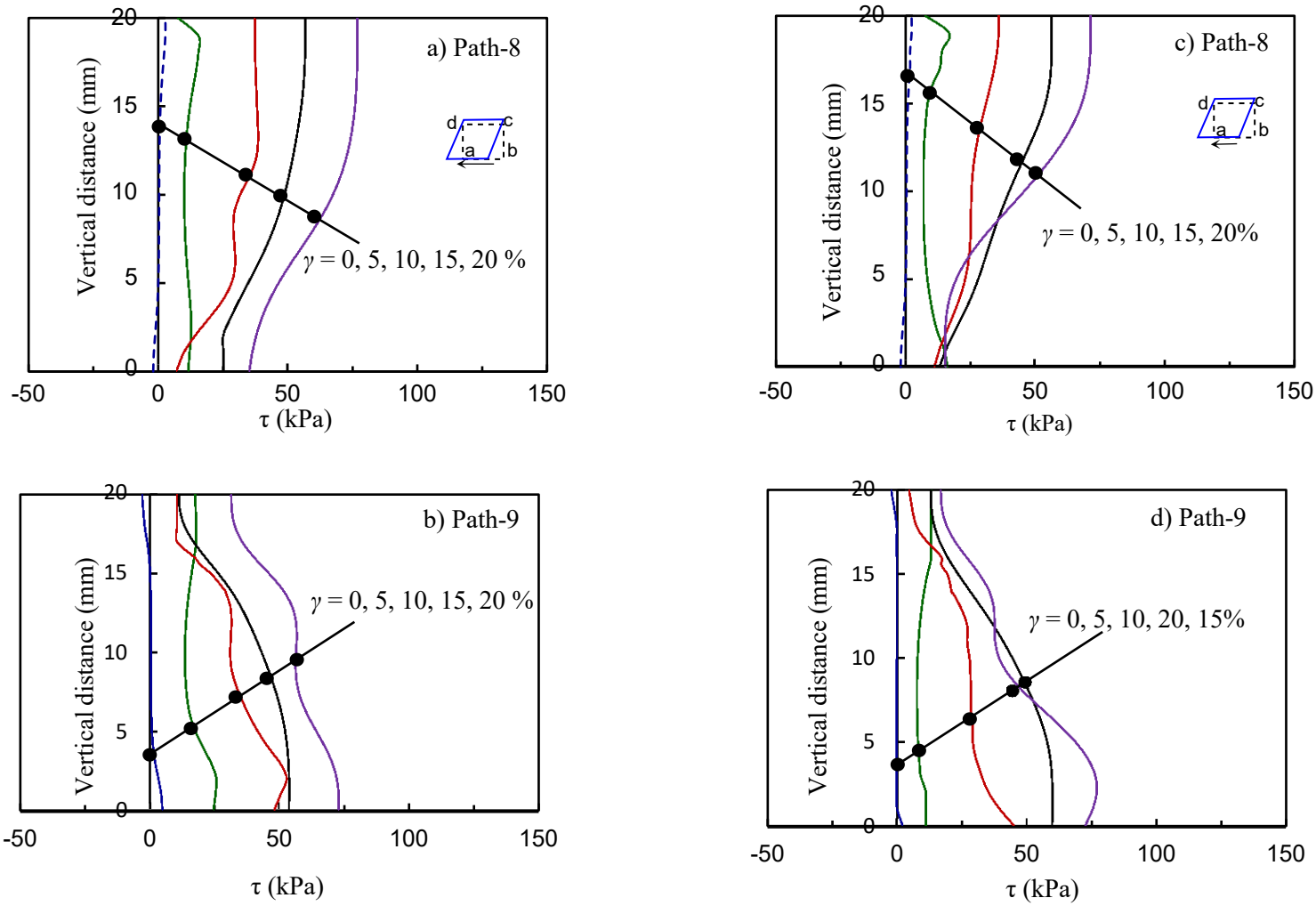

Figure 3.22: Distribution of shear stresses (τ) along path 8 and 9 for Cambridge type DSS test under σ_z = 100 kPa: MC model (a–b) (left column), MMC model (c-d) (right column)

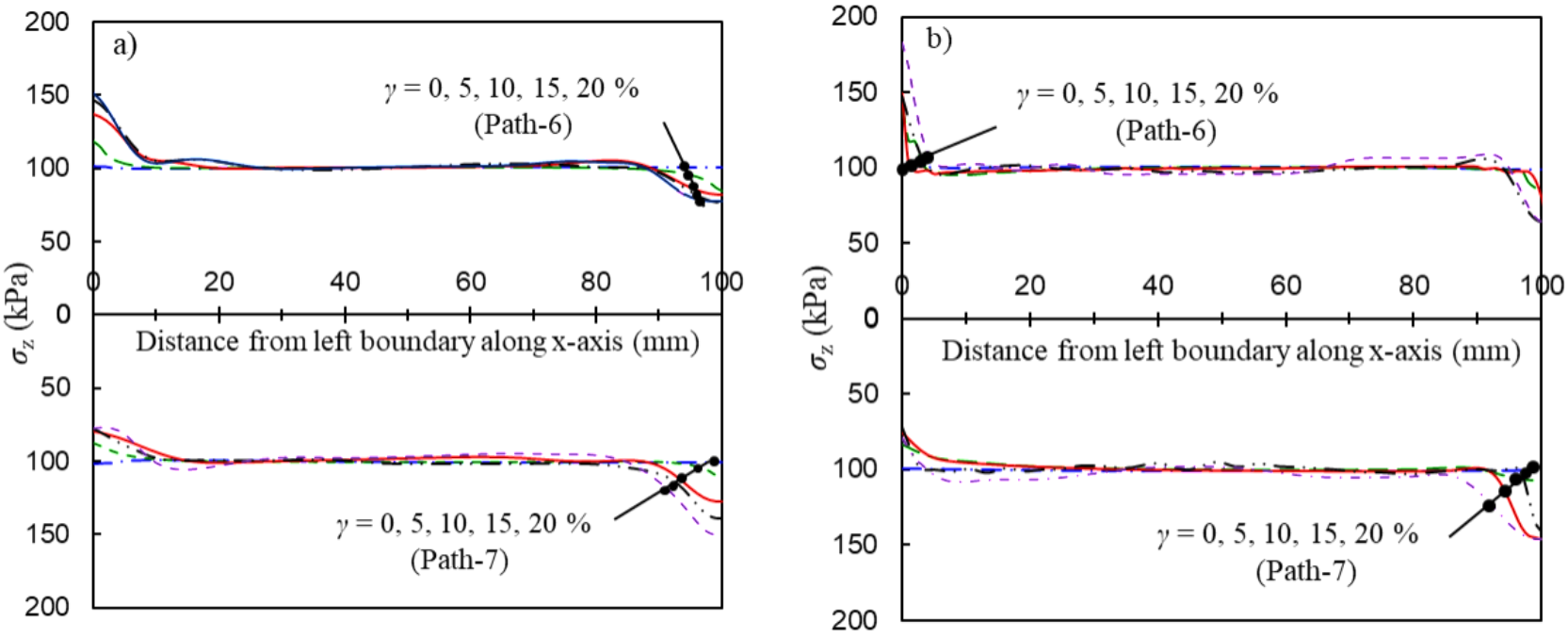

Figure 3.23: Distribution of normal stresses (σ_z) along path 6 and 7 for Cambridge type DSS test under σ_z = 100 kPa: (a) MC model; (b) MMC model

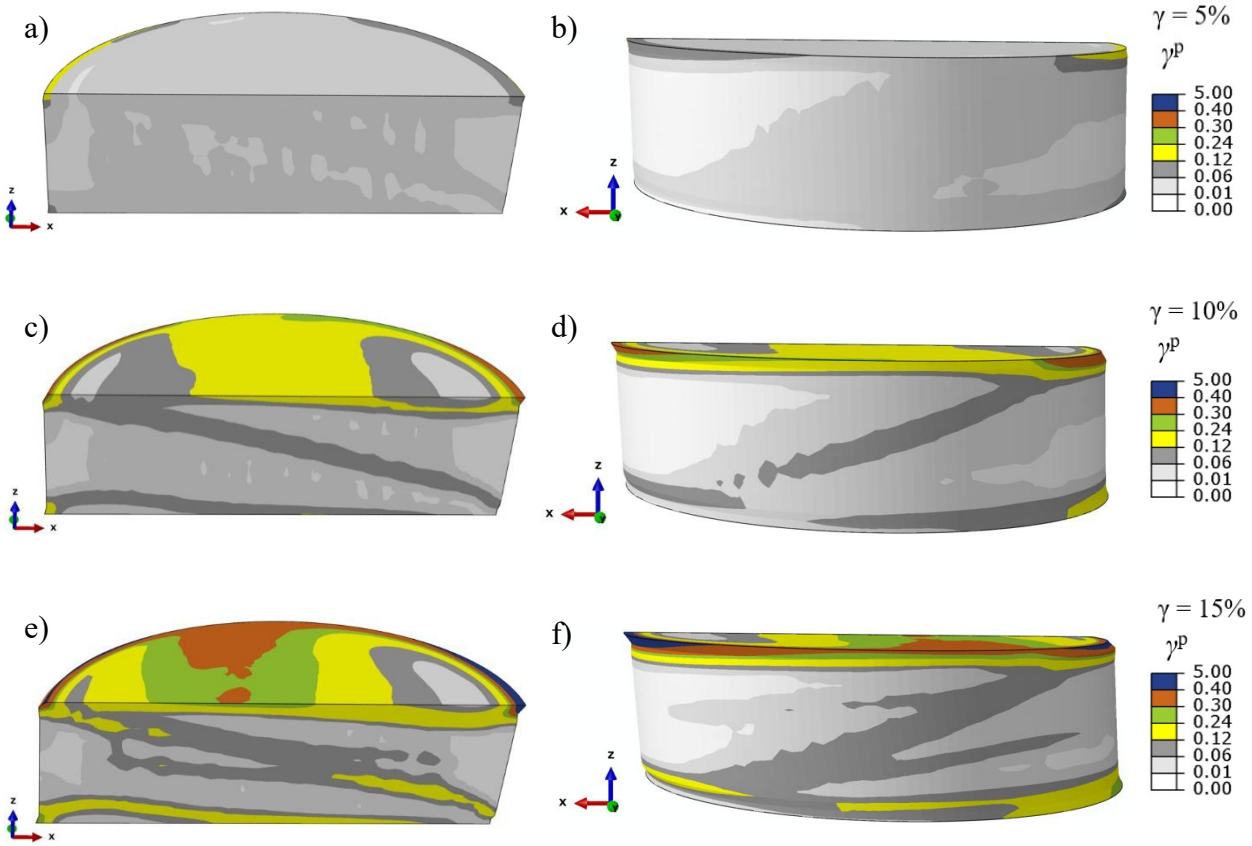

Figure 3.24: Deviatoric plastic shear strain (γ^p) for 100 kPa vertical normal stress: left column front view and right column rear view for stacked ring type DSS test using MC material model

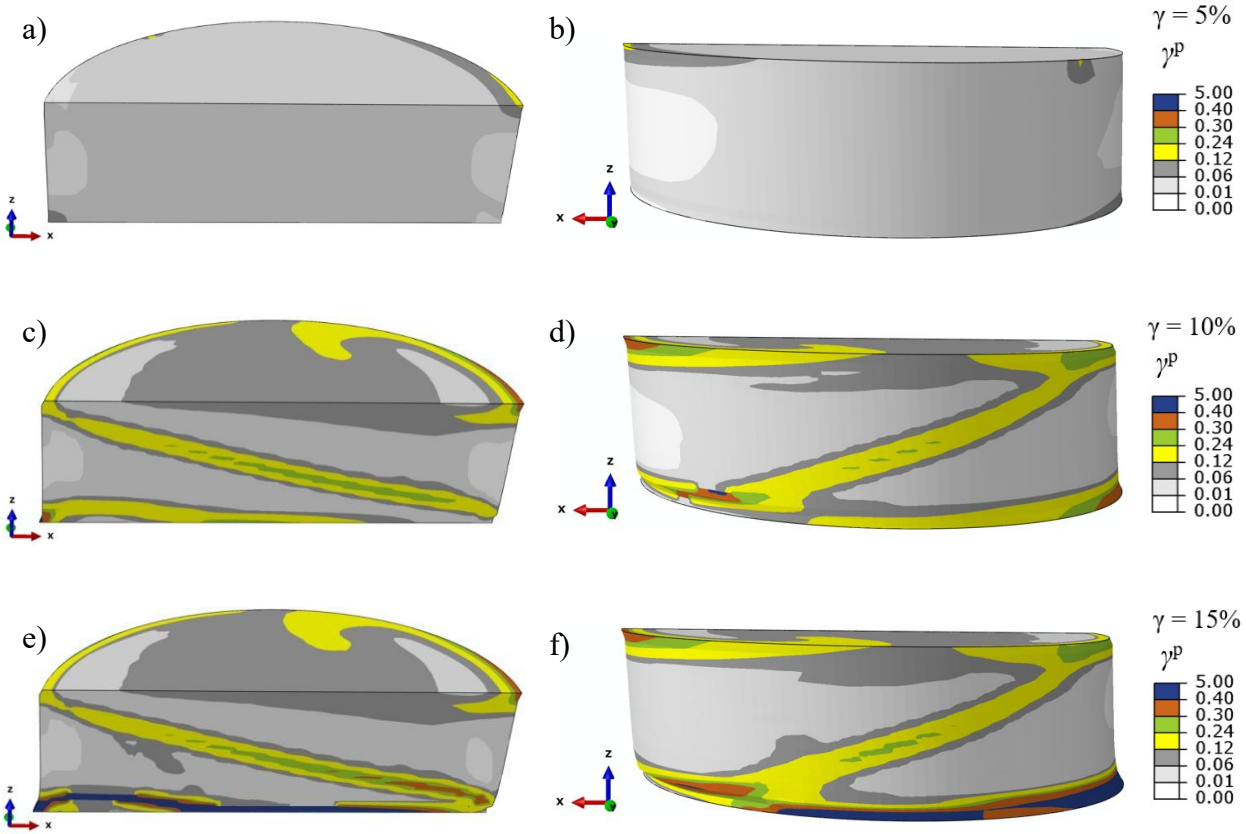

Figure 3.25: Deviatoric plastic shear strain (γ^p) for 100 kPa vertical normal stress: left column front view and right column rear view for stacked ring type DSS test using MMC material model

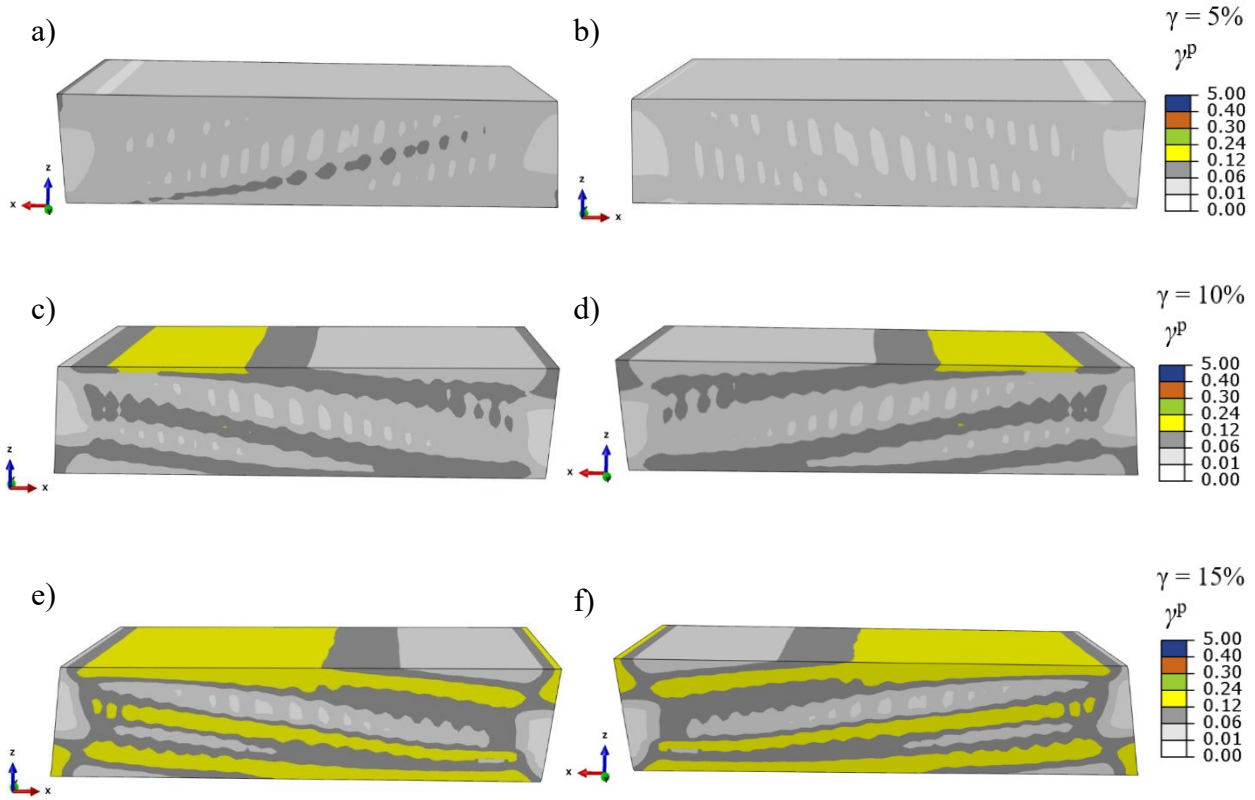

Figure 3.26: Deviatoric plastic shear strain (γ^p) for 100 kPa vertical normal stress: left column front view and right column rear view for Cambridge type DSS test using MC material model

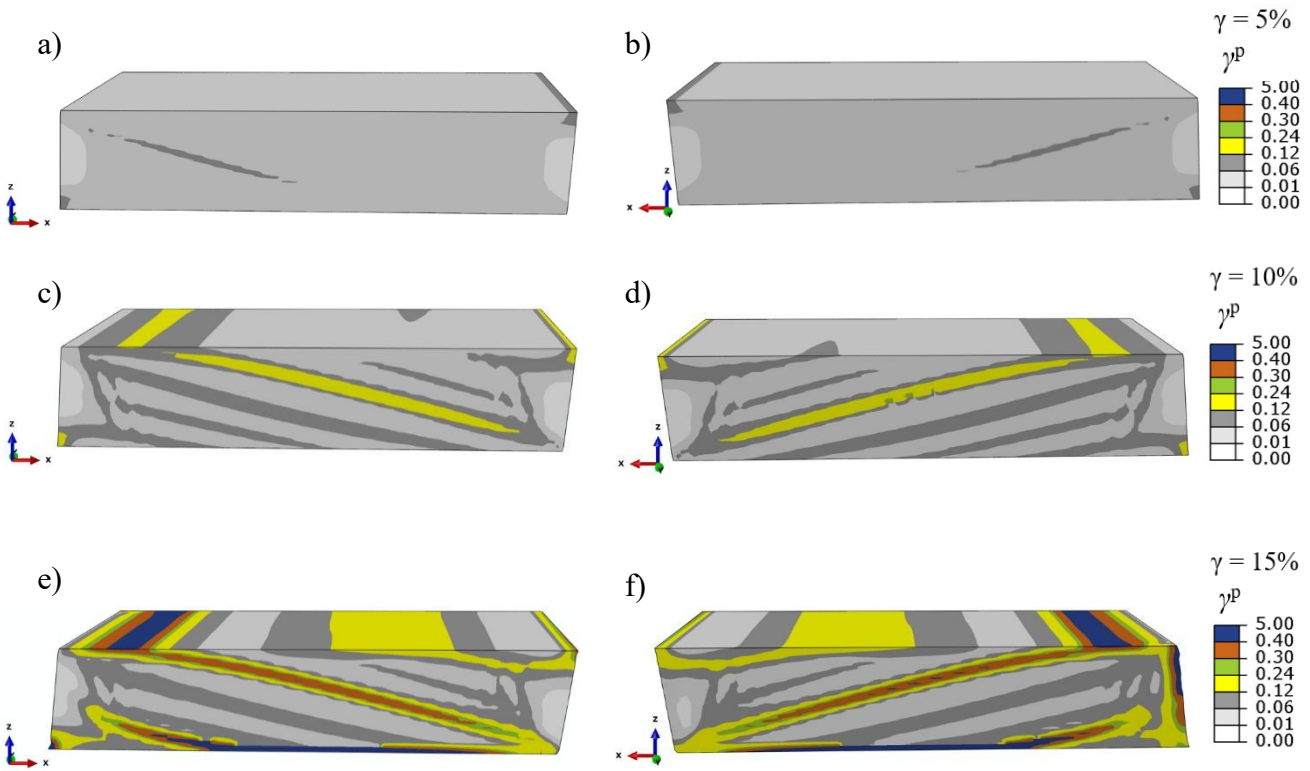

Figure 3.27: Deviatoric plastic shear strain (γ^p) for 100 kPa vertical normal stress: left column front view and right column rear view for Cambridge type DSS test using MMC material model

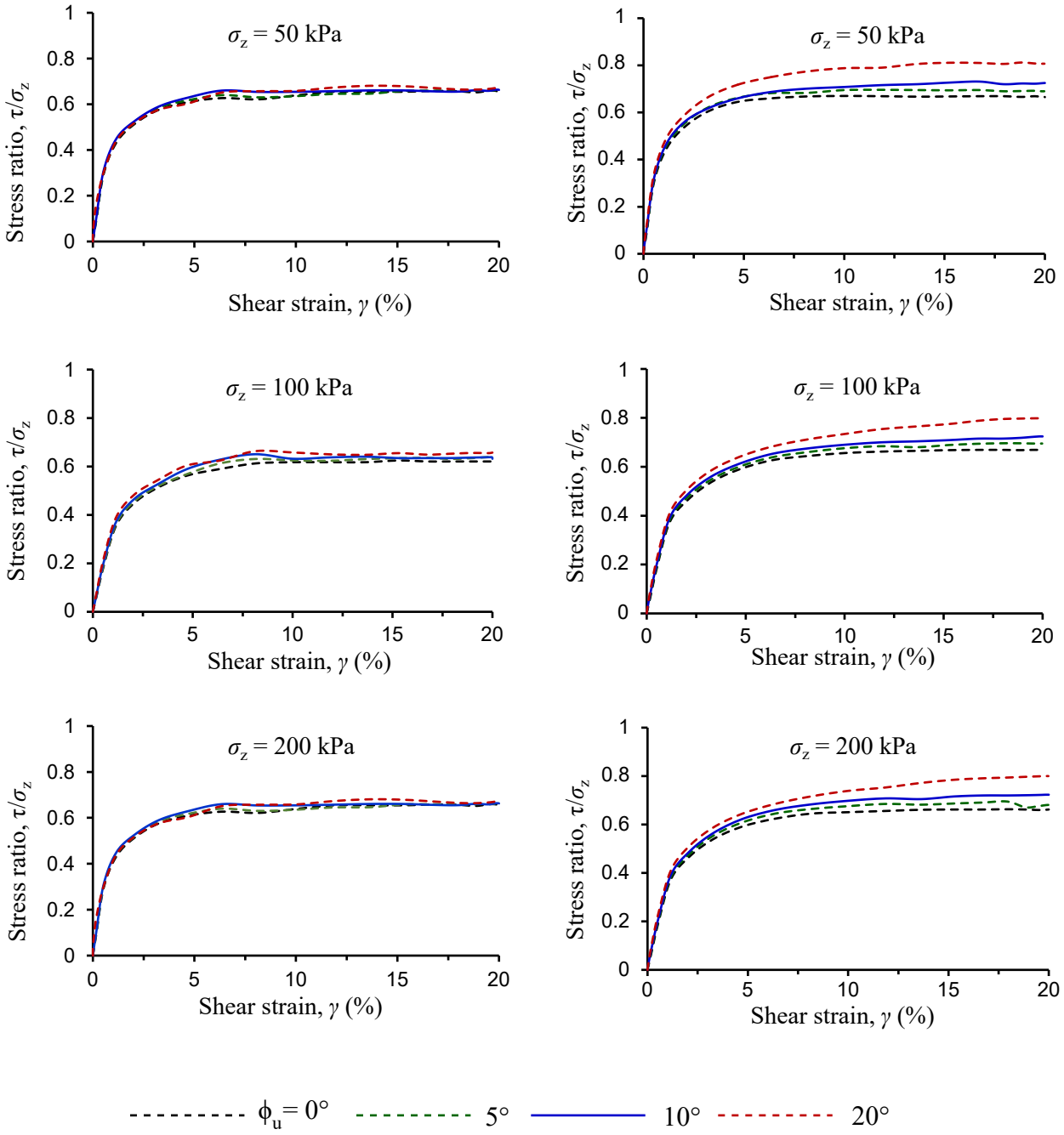

Figure 3.28: Effects of interface friction angle on stress ratio for medium sand with MC model: stacked ring type (left column); (b) Cambridge type (right column)

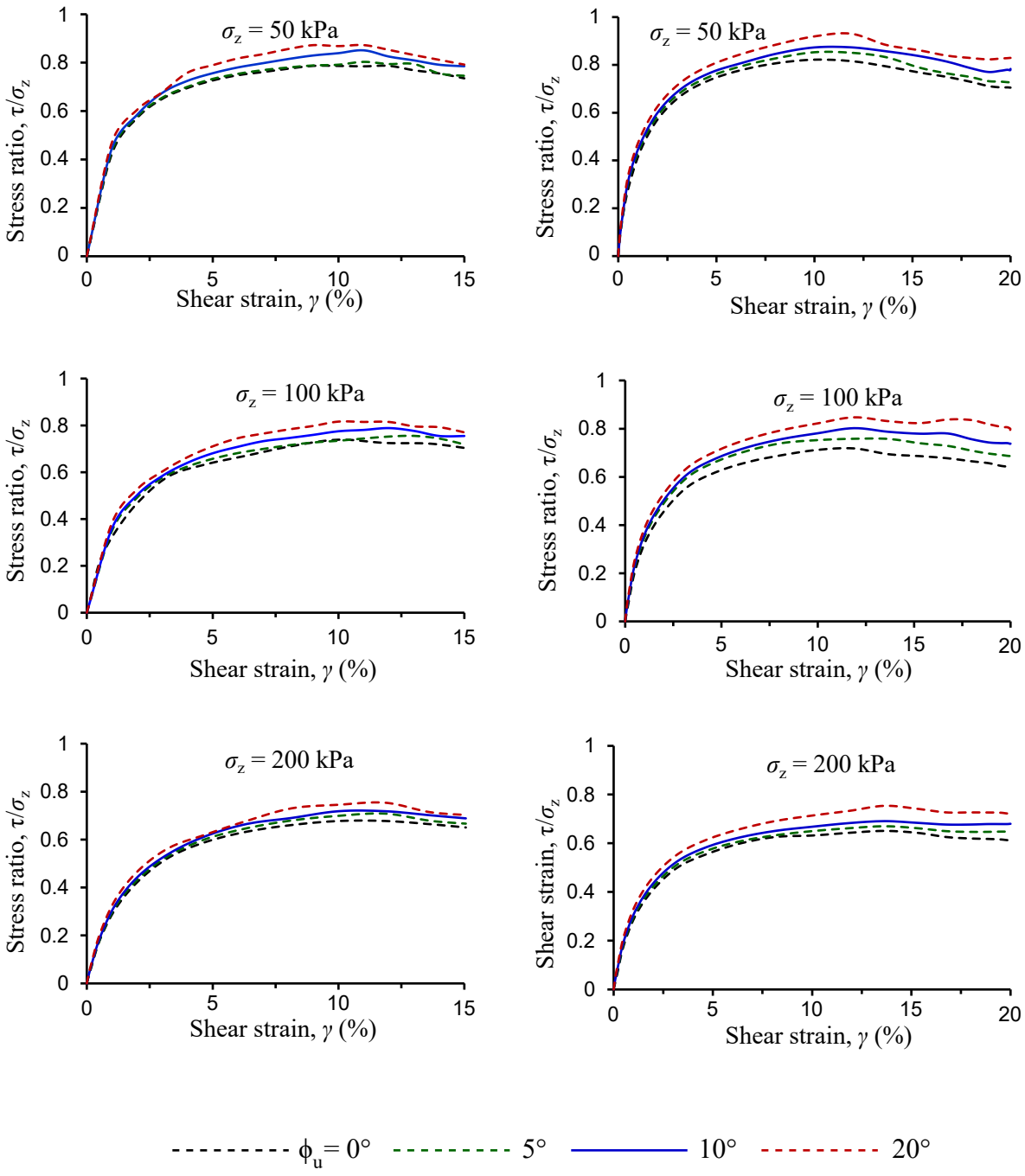

Figure 3.29: Effects of interface friction angle on stress ratio for dense sand with MMC model: stacked ring type (left column); Cambridge type (right column)

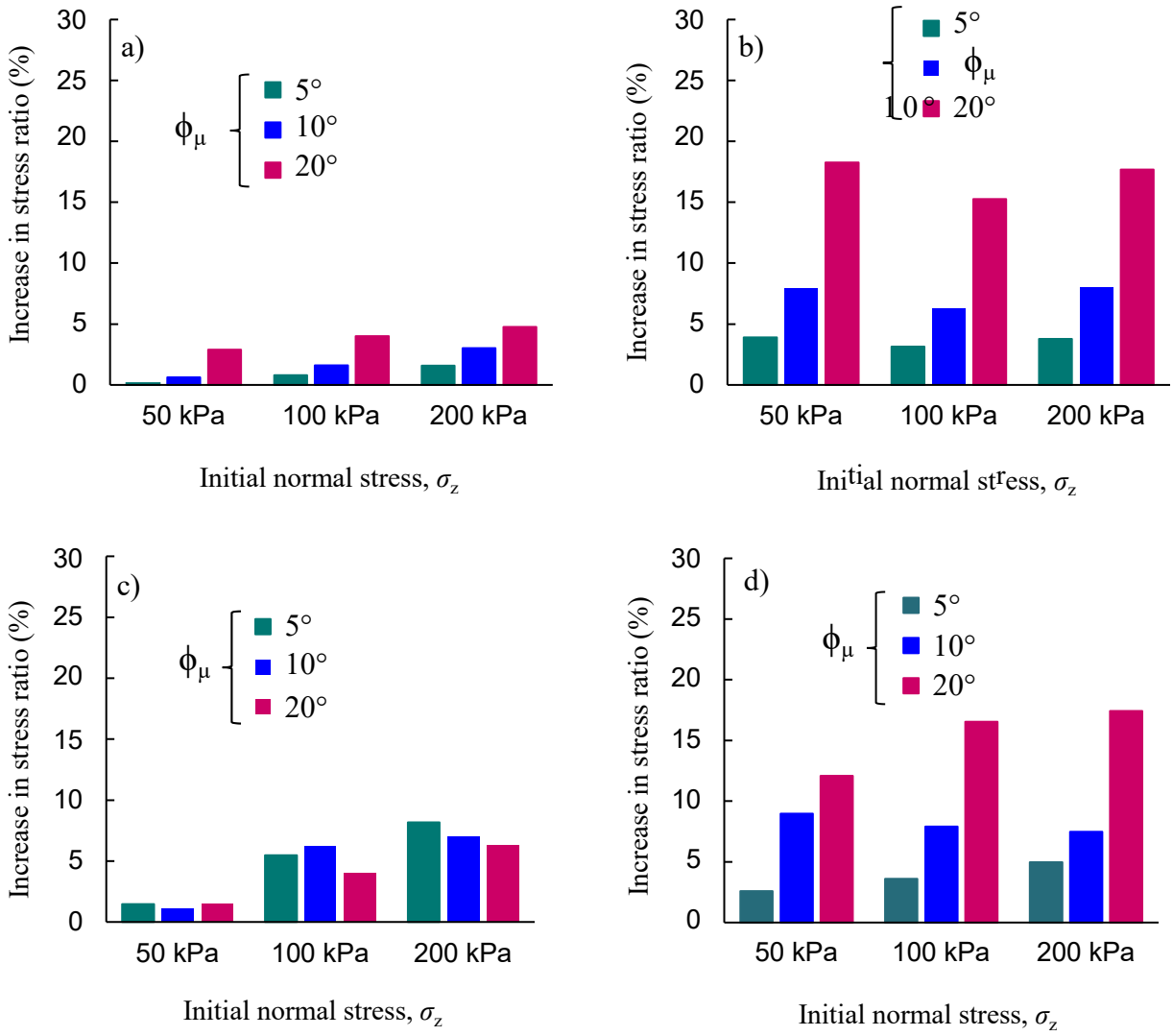

Figure 3.30: Increase in stress ratio with respect to frictionless case at γ = 15%: (a) medium sand stacked ring; (b) medium sand Cambridge; (c) dense sand stacked ring; (d) dense sand Cambridge

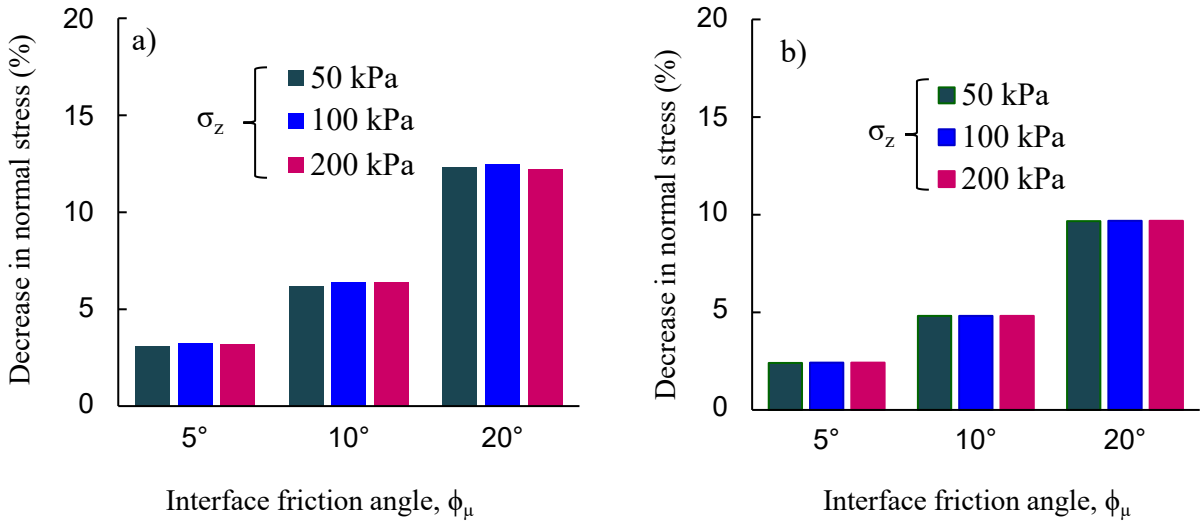

Figure 3.31: Decrease in normal stress with respect to applied stress at the top at the end of consolidation: (a) stacked ring type; (b) Cambridge type

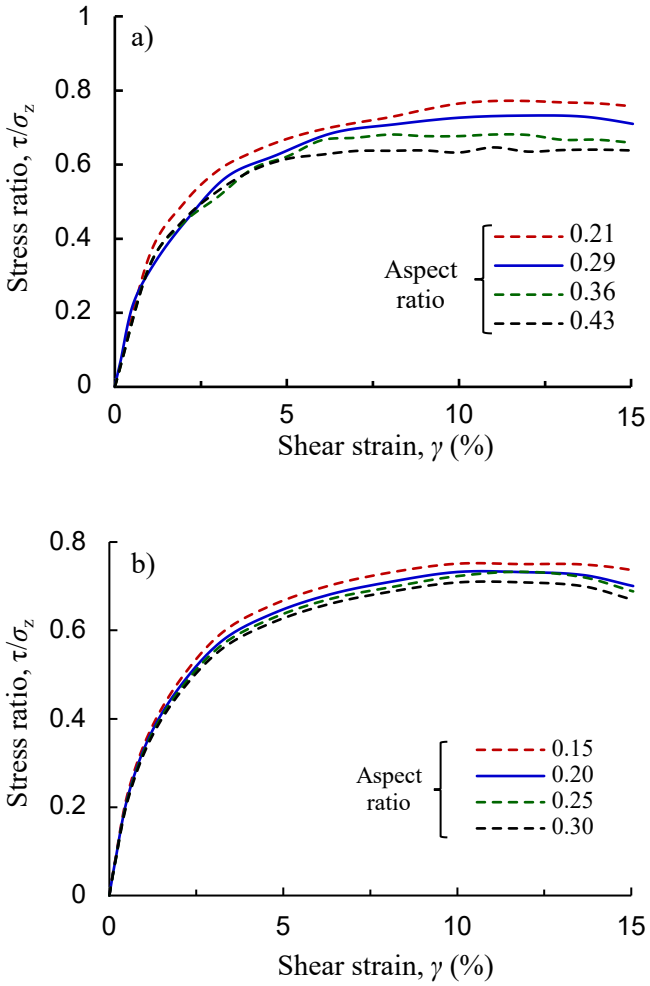

Figure 3.32: Comparison of stress ratio for different aspect ratios for dense specimens: (a) stacked ring type; (b) Cambridge type

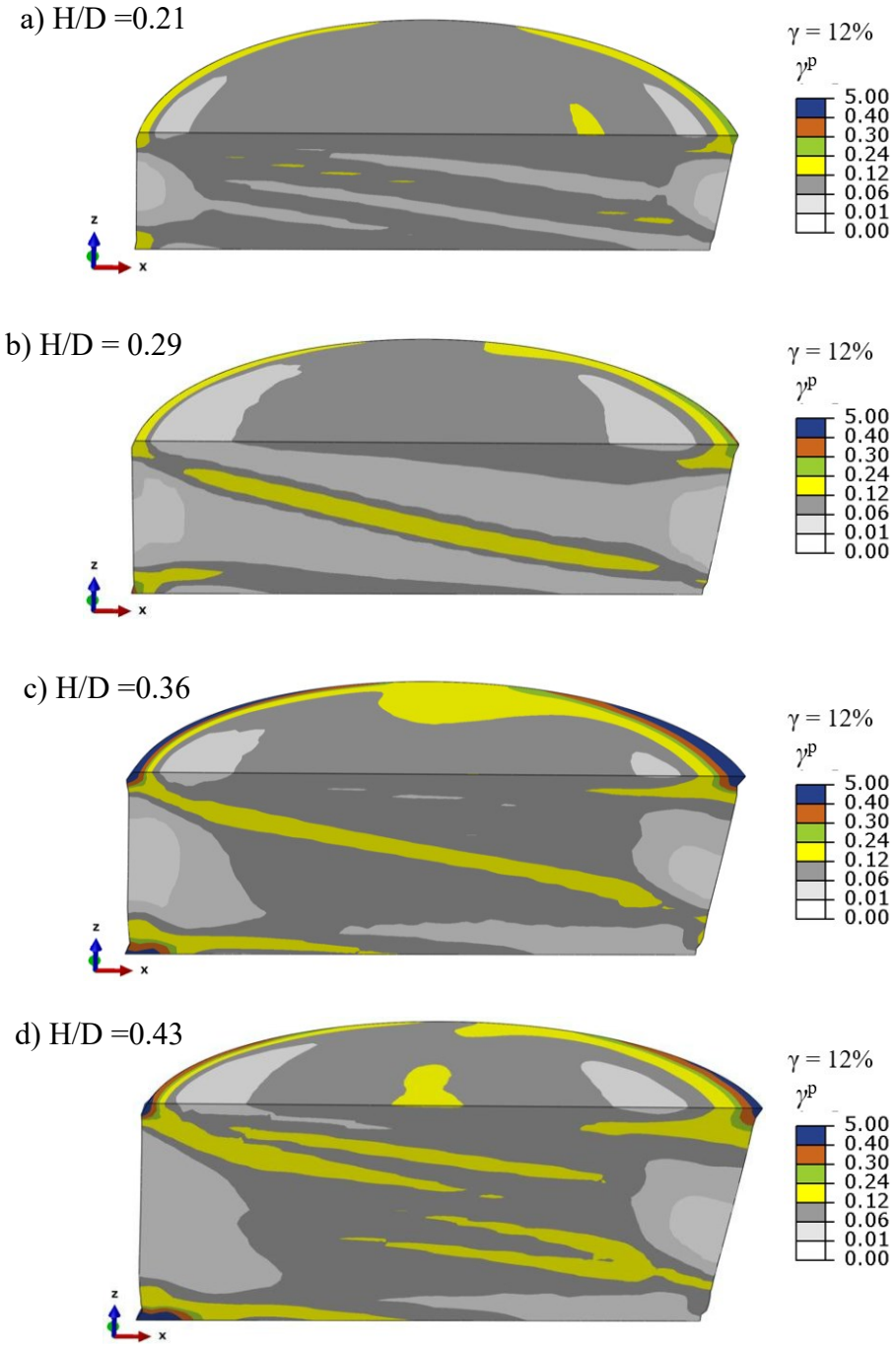

Figure 3.33: Deviatoric plastic strain at $\gamma \sim 12\%$ for different aspect ratios of stacked ring type specimen

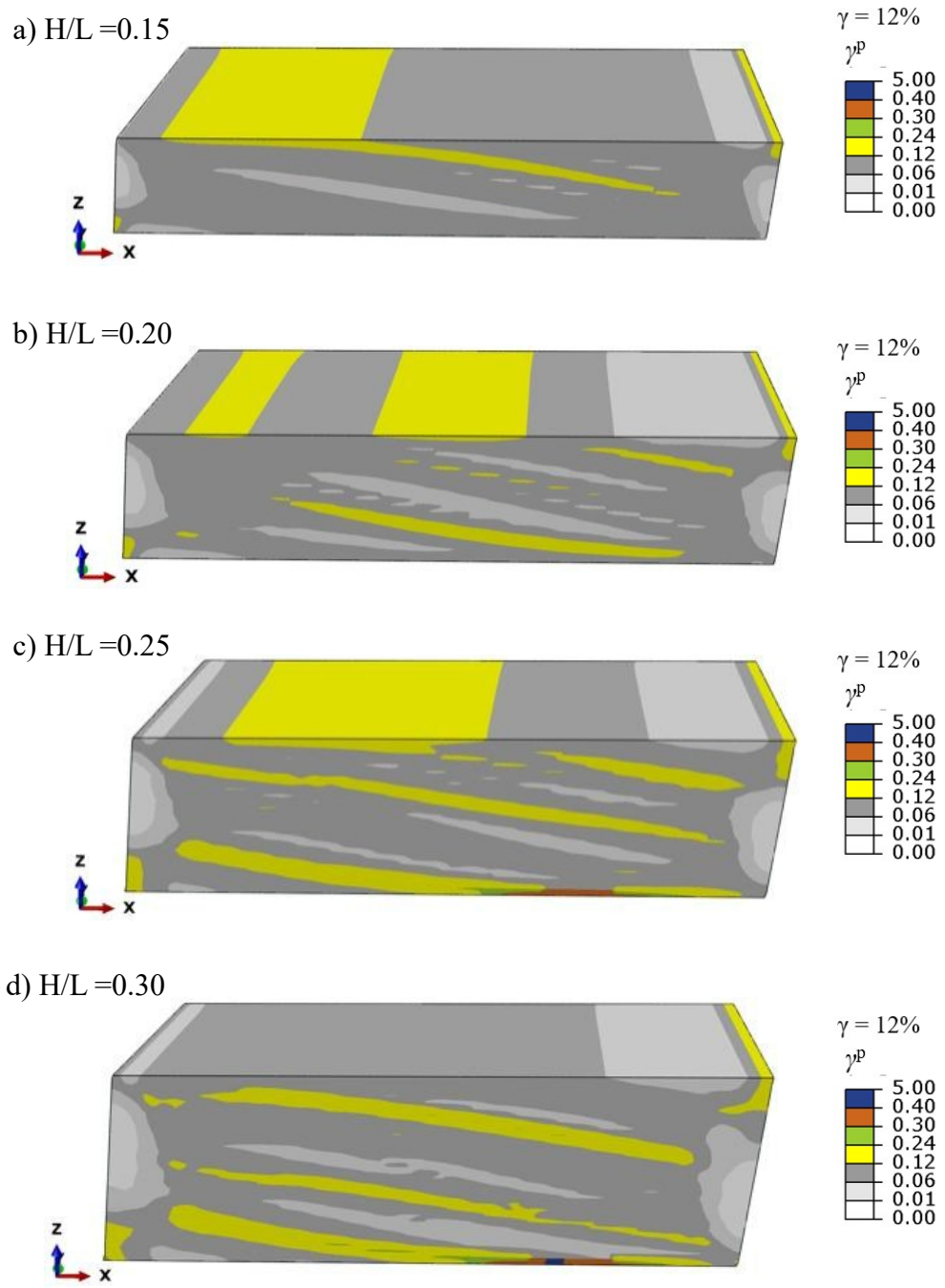

Figure 3.34: Deviatoric plastic strain at $\gamma \sim 12\%$ for different aspect ratios of Cambridge type specimen

Chapter 4: Conclusions and Recommendations for Future Research

4.1 Conclusions

Proper estimation of soil parameters is necessary for safe and economical geotechnical engineering design. The friction angle and dilation angle are the most important soil parameters for sand because they define the strength and volume change behaviour, which ultimately govern the design. While direct shear and triaxial tests are generally performed, the direct simple shear (DSS) tests better evaluate the soil behaviour because they allow for the rotation of the principal axis that occurs in many field conditions. Although the test is relatively simple compared to other simple shear tests, the interpretation of DSS test results is difficult as the normal and shear stresses on the vertical walls are unknown. Therefore, some assumptions have to be made to calculate the soil parameter (e.g., friction angle). In addition, stress and strain non-uniformities in the soil specimen might increase further uncertainties in the interpreted soil properties.

While the primary purpose of conducting a DSS test is to engage the whole soil specimen, localized plastic shear deformation occurs in the specimen, especially at a larger shear strain level, which governs the overall response. Such localized behaviour cannot be evaluated properly from laboratory experiments. Therefore, in the present study, finite element (FE) modelling techniques are developed to shear the specimen sufficiently up to a large strain level. The analysis is performed for medium and dense sands, which are modelled using the Mohr–Coulomb (MC) model and a modified Mohr–Coulomb (MMC) model, respectively. The MMC model considers the pre-peak hardening and post-peak softening behaviour of dense sand. Analyses are performed for cylindrical and cuboidal soil specimens to investigate the effects

of apparatus type on soil behaviour. Finally, a parametric study is performed to show the effects of some key parameters.

The following conclusions can be drawn from this study:

1. The developed FE method can capture the mechanics involved in DSS tests, including stress non-uniformities and strain localization.
2. The stresses measured at the horizontal boundary, together with empirical relations for the estimation of lateral or principal stresses, can be used to calculate the mobilized friction angle with reasonable accuracy.
3. The failure of soil specimen depends on normal stress. For a higher normal stress, the applied stresses at the boundary are close to the maximum shear stress point, while it is close to the maximum stress obliquity for a lower normal stress.
4. For medium dense sand, both the stacked ring and Cambridge type DSS tests give similar mobilized friction angles. However, for dense sand, the mobilized friction angle calculated from the Cambridge type DSS test is slightly greater than that obtained from the stacked ring type DSS test.
5. Increase in interface resistance between the soil and the side wall(s) decreases the resulting normal stress at the bottom of the specimen and increases the stress ratio during failure. The stress ratio increase is significant for Cambridge type tests, while it is less significant for stacked ring type apparatus, for both medium and dense sands.
6. The non-uniformity of stress distribution increases with an increase in aspect ratio of the soil specimen.

4.2 Recommendations for future research

The numerical analyses presented in this thesis show some important features that should be considered in the analysis of DSS test data and interpretation of soil parameters. However, there are some limitations that could be addressed in future studies.

i) The current study focuses only on constant stress direct simple shear tests. Further studies could be performed for constant volume DSS tests.

ii) Additional numerical studies are required to investigate the influence of normal stress level and relative density on the monotonic and cyclic behaviour of sand in DSS test.

iii) Comparison of mechanisms involved in DSS tests with other tests, such as triaxial and hollow cylinder, would help in developing/selecting appropriate soil models for analyzing three-dimensional geotechnical problems.

iv) Finally, additional experimental studies could be performed and validate further the developed FE modelling techniques.

References

Airey, DW., Budhu, M. and Wood, DM. 1985. Some aspects of the behaviour of soils in simple shear. In PK Banerjee & R Butterfield (eds), *Developments in soil mechanics and foundation engineering: Vol. 2: Stress-strain modelling of soils.* Elsevier Applied Science Publishers, London, pp. 185-213.

Al Tarhouni, M.A., Fouzder, A., Hawlader, B. and Dhar, A. 2017. Direct Simple Shear and Triaxial Compression Tests on Dense Silica Sand at Low Effective Stress. In *Proceedings of 70th Canadian Geotechnical Conference, Ottawa, ON*.

Al Tarhouni M.A. 2020. *Behaviour of sand in monotonic and cyclic simple shear loading at low-stress level.* Ph.D. Thesis, Memorial University of Newfoundland.

Al Tarhouni, M.A. and Hawlader, B.C. 2021. Monotonic and cyclic behaviour of sand in direct simple shear test conditions considering low stresses. *Soil Dynamics and Earthquake Engineering*, 150: p.106931.

Amer, M.I. 1984. *Sample size effect on dynamic properties of sand in the simple shear test (cyclic)*. Ph. D. Thesis, University of Maryland, College Park.

Asadzadeh, M. and Soroush, A. 2018. Evaluation of stress and strain non-uniformity during cyclic simple shear test using DEM: effect of the horizontal platen asperities. *Granular Matter*, 20(3):1-11.

Asadzadeh, M. and Soroush, A. 2016. Fundamental investigation of constant stress simple shear test using DEM. *Powder Technology*, 292: 129-139.

Atkinson, J.H., Lau, W.H.W. and Powell, J.J.M. 1991. Measurement of soil strength in simple shear tests. *Canadian Geotechnical Journal*, 28(2): 255-262.

Bernhardt, M. L., Biscontin, G. and O′Sullivan, C. 2016. Experimental validation study of 3D direct simple shear DEM simulations. *Soils and Foundations*, 56(3): 336-347.

Bishop, A. W. 1961. Discussion on soil properties and their measurement. Proceedings of 5th Int. Conf. on Soil mechanics and Foundation engineering, vol. III.

Bjerrum, L., 1972. Embankments on soft ground, State of the Art Report. In *Proc. Spec. Conf. on Performance of Earth and Earth-Supported Structures, Purdue Univ., ASCE,* 1: 1-54.

Bolton, M.D. 1986. The strength and dilatancy of sands. *Géotechnique*, 36(1): 65-78.

Budhu, M. 1979. *Simple Shear Deformation of Sands*. Ph.D. Thesis, University of Cambridge

Budhu, M. 1984. Non-uniformities imposed by simple shear apparatus, *Canadian Geotechnical Journal*, 21(1): 125-137.

Budhu, M. 1985. Lateral stresses observed in two simple shear apparatus, *Journal of Geotechnical Engineering*, 111(6): 698-711.

Budhu, M. and Britto, A. 1987. Numerical analysis of soils in simple shear devices, *Soils and Foundations*, 27(2): 31-41.

Budhu, M. 1988. Failure state of a sand in simple shear, *Canadian Geotechnical Journal*, 25(2): 395-400.

Chang, W.J., Chang, C.W. and Zeng, J.K. 2014. Liquefaction characteristics of gap-graded gravelly soils in K_0 condition. *Soil Dynamics and Earthquake Engineering*, 56: 74-85.

Cole, E.R.L. 1967. *The Behaviour of Soils in the Simple Shear Apparatus*. Ph. D. Thesis, University of Cambridge, Cambridge, England.

Cornforth, D.H. 1964. Some experiments on the influence of strain conditions on the strength of sand. *Géotechnique*, 14(2): 143-167.

Dabeet, A. 2014. *Discrete Element Modeling of Direct Simple Shear Response of Granular Soils and Model Validation Using Laboratory Tests*. Ph. D. Thesis, University of British Columbia. doi: http://dx.doi.org/10.14288/1.0167563.

Dabeet, A., Wijewickreme, D. and Byrne, P. 2015. Evaluation of stress strain non-uniformities in the laboratory direct simple shear test specimens using 3D discrete element analysis. *Geomechanics and Geoengineering*, 10(4): 249-260.

DeGroot, D.J., Germaine, J.T. and Ladd, C.C. 1994. Effect of nonuniform stresses on measured DSS stress–strain behavior. *Journal of Geotechnical Engineering*, 120(5): 892-912.

Doherty, J. and Fahey, M. 2011. Three-dimensional finite element analysis of the direct simple shear test. *Computers and Geotechnics*, 38(7): 917-924.

Dounias, G.T. and Potts, D.M. 1993. Numerical analysis of drained direct and simple shear tests. *Journal of Geotechnical Engineering*, 119(12): 1870-1891.

Duncan, J.M., 1969. Behavior of soils in simple shear test. In *Proc. 7th ICSMFE,* 1: 101-109

Finn, W.D.L., Bhatia, S.K. and Pickering, D.J. 1982. The cyclic simple shear test. *In Soil MechanicsTransient and Cyclic Loads.* John Wiley & Sons Ltd: 583–607.

Finn, W.D. 1985. Aspects of constant volume cyclic simple shear, *Advances in the Art of Testing soils under cyclic conditions, ASCE*: 74-98.

Frydman, S. and Talesnick, M. 1991. Simple shear of isotropic elasto-plastic soil. *International Journal for Numerical and Analytical Methods in Geomechanics*, 15(4): 251-270.

Fu, P. and Dafalias, Y.F. 2011. Fabric evolution within shear bands of granular materials and its relation to critical state theory. *International Journal for numerical and analytical methods in geomechanics*, 35(18): 1918-1948.

Grimstad, G., Andresen, L. and Jostad, H.P. 2012. NGI-ADP: Anisotropic shear strength model for clay. *International journal for numerical and analytical methods in geomechanics*, 36(4): 483-497.

Grognet, M.F. 2011. *The boundary conditions in direct simple shear tests: Developments for peat testing at low normal stress*. M.Sc. Thesis, Delft University of Technology.

Guo, J., Bernhardt-Barry, M.L. and Biscontin, G. Evaluation of boundary effects in simple shear tests using discrete element modelling. In *Geo-Congress* 2022: 599-607.

Guo, P.J. and Stolle, D.F. 2005. On the failure of granular materials with fabric effects. *Soils and foundations*, 45(4): 1-12.

Hardin, B.O. and Black, W.L. 1966. Sand stiffness under various triaxial stress. *Journal of the Soil Mechanics and Foundations Division, ASCE*, 92(SM2): 27-42.

Hsu, S.T. and Liao, H.J. 1998. Uplift behaviour of cylindrical anchors in sand. *Canadian Geotechnical Journal*, 35(1): 70-80.

Janbu, N. 1963. Soil compressibility as determined by oedometer and triaxial tests. Proceedings, European Conference on Soil Mechanics and Foundations Engineering, Wiesbaden, Germany, Vol. 1:19-25

Lade, P.V. and Nelson, R.B. 1984. Incrementalization procedure for elasto-plastic constitutive model with multiple, intersecting yield surfaces. *International Journal for Numerical and Analytical Methods in Geomechanics*, 8(4): 311-323.

Lings, M.L. and Dietz, M.S. 2004. An improved direct shear apparatus for sand. *Géotechnique*, 54(4): 245-256.

Liu, X., Li, S., Sun, L. and Li, T. 2022. Mechanical behavior and particle crushing of Carbonate sand in simple shear tests. *International Journal of Geomechanics*, 22(7): p.06022011.

Loukidis, D. and Salgado, R. 2011. Effect of relative density and stress level on the bearing capacity of footings on sand. *Géotechnique*, *61*(2): 107-119.

Lucks, A.S., Christian, J.T., Brandow, G.E. and Höeg, K. 1972. Stress conditions in NGI simple shear test, *Journal of the Soil Mechanics and Foundations Division*, 98(1): 155-160.

Ochiai, H., Yamanouchi, T. and Tanabashi, Y. 1983. On the rotation of principal stress axes in the simple shear test and its utilizations, *Advances in the Mechanics and the Flow of Granular Materials*, 2: 871-883.

Oda, M. 1975 a. On the relation $\tau/\sigma_N = \kappa \cdot \tan\psi$ in the simple shear test. *Soils and Foundations*, 15(4): 35-41.

Oda, M. 1975 b. On stress-dilatancy relation of sand in simple shear test. *Soils and Foundations*, 15(2): 17-29.

Oda, M. and Konishi, J. 1974. Rotation of principal stresses in granular material during simple shear. *Soils and Foundations*, 14(4): 39-53.

Potts, D.M., Dounias, G.T. and Vaughan, P.R. 1987. Finite element analysis of the Direct Shear Box test. *Géotechnique*, 37(1): 11-23.

Prevost, J.H. and Høeg, K. 1976. Reanalysis of simple shear soil testing. *Canadian Geotechnical Journal*, 13(4): 418-429.

Randolph, M.F. and Wroth, C.P. 1981. Application of the failure state in undrained simple shear to the shaft capacity of driven piles. *Géotechnique*, 31(1): 143-157.

Roscoe, K.H. 1953. An apparatus for the application of simple shear to soil samples. *In Proc. 3rd ICSMFE*, London, England, 1: 86-191.

Roscoe, K.H.; Bassett, R.H.; Cole, E.R.L. 1 967. Principal Axes Observed During Simple Shear of a Sand. *In Proceedings of the Geotechnical Conference on Shear Strength Properties of Natural Soils and Rocks*, Oslo, Norway, 19–22 September. 213–237.

Rousé, P.C. 2018. Relation between the critical state friction angle of sands and low vertical stresses in the direct shear test. *Soils and foundations*, 58(5):1282–1287

Roy, K., Hawlader, B.C., Kenny, S. and Moore, I. 2016. Finite element modeling of lateral pipeline−soil interactions in dense sand. *Canadian Geotechnical Journal*, 53(3), 490–504.

Roy, K., Hawlader, B.C., Kenny, S. and Moore, I. 2018a. Upward pipe–soil interaction for shallowly buried pipelines in dense sand. *J. Geotech. Geoenviron. Eng*, 144(11), p.04018078.

Roy, K., Hawlader, B.C., Kenny, S. and Moore, I. 2018b. Lateral resistance of pipes and strip anchors buried in dense sand. *Canadian Geotechnical Journal*, 55(12), 1812–1823.

Roy, K., Hawlader, B.C, Kenny, S. and Moore, I. 2018c. Uplift failure mechanisms of pipes buried in dense sand. *International Journal of Geomechanics*, 18(8): p.04018087.

Saada, A.S. and Townsend, F.C. 1981. State of the art: laboratory strength testing of soils. *Laboratory shear strength of soil, ASTM STP*, 740: 7-77.

Saada, A.S., Fries, G. and Ker, C.C. 1983. Stress induced in short cylinders subjected to axial deformation and lateral pressures. *Soils and Foundations*, 23(1): 114-118.

Shen, C.K., Sadigh, K. and Herrmann, L.R. 1978. An analysis of NGI simple shear apparatus for cyclic soil testing. *Dynamic Geotechnical Testing, ASTM STP*, 654: 148-162.

Shibuya, S. and Hight, D. W. 1987. On the stress path in simple shear. *Géotechnique*, 37(4): 511-515.

Stroud, M.A. 1971. *The behaviour of sand at low stress levels in the simple-shear apparatus*. Ph.D. Thesis, University of Cambridge.

Toyota, H., Nakamura, K. and Kazama, M. 2004. Shear and liquefaction characteristics of sandy soils in triaxial tests. *Soils and foundations*, 44(2): 117-126.

Vaid, Y.P., Byrne, P.M. and Hughes, J.M. 1981. Dilation angle and liquefaction potential. *Journal of the Geotechnical Engineering Division*, 107(7): 1003-1008.

Vucetic, M. and Lacasse, S. 1982. Specimen size effect in simple shear test. *Journal of the Geotechnical Engineering Division*, 108(12): 1567-1585.

Wai, M.H.D. 2019. *Effect of imperfect direct simple shear test boundary conditions on monotonic and cyclic measurements.* Ph.D. Thesis, University of Toronto (Canada).

Wang, B., Popescu, R. and Prevost, J.H. 2004. Effects of boundary conditions and partial drainage on cyclic simple shear test results—a numerical study. *International journal for numerical and analytical methods in geomechanics*, 28(10): 1057-1082.

Wai, D., Manmatharajan, M.V. and Ghafghazi, M. 2022. Effects of Imperfect Simple Shear Test Boundary Conditions on Monotonic and Cyclic Measurements in Sand. *Journal of Geotechnical and Geoenvironmental Engineering*, 148(1): p.04021-164.

Wijewickreme, D., Dabeet, A. and Byrne, P. 2013. Some observations on the state of stress in the direct simple shear test using 3D discrete element analysis. *Geotechnical Testing Journal*, 36(2): 292-299.

Wood, D.M. and Budhu, M. 1980. The behaviour of Leighton Buzzard sand in cyclic simple shear tests. In *International Symposium on Soils under Cyclic and Transient Loading*: 9-21. AA Balkema Publishers.

Wu, Z. 2017. *Mechanical Modelling of Sand Considering Simple Shear Condition and Its Application to Pile Foundation.* Ph.D. Thesis, École centrale de Nantes.

Zhang, L. 2003. *The behaviour of granular material in pure shear, direct shear and simple shear.* Ph.D. Thesis, Aston University.

APPENDIX A

Numerical Investigation of Stress and Strain Nonuniformities in Direct Simple Shear Sample and Its Effects on Overall Stress–Strain Behaviour

This paper has been published and presented in 75th Canadian Geotechnical Conference (GeoCalgary 2022), Conference, Calgary, Alberta, Canada, paper ID-328. Most of the research work presented in this paper was conducted by the first author. He also prepared the draft manuscript. The other authors supervised the research and reviewed the manuscript.

Numerical Investigation of Stress and Strain Nonuniformities in Direct Simple Shear Sample and Its Effects on Overall Stress–Strain Behaviour

Sudipta Bhowmick & Bipul Hawlader
Department of Civil Engineering, Memorial University of Newfoundland, St. John's, Newfoundland and Labrador, Canada

GeoCalgary 2022 October 2-5
Reflection on Resources

ABSTRACT
The stress state in many geotechnical problems is similar to the simple shear conditions. While direct shear and triaxial tests are commonly performed for practical engineering and research activities, the direct simple shear (DSS) test facilities are available in some advanced laboratories. One of the limitations of the DSS test is that only the vertical normal and horizontal shear stresses are measured in most cases. The unknown shear stress on the vertical boundary makes the interpretation of the test results difficult. In addition, stress and strain nonuniformities might occur in the sample. In the present study, three-dimensional finite element (FE) modelling of stacked-ring type DSS samples is performed for different soil conditions to investigate the possible nonuniformities and their effects on the interpreted strength parameters. The FE simulated results are compared with the laboratory test results on sand. The applicability and limitations of DSS tests are highlighted.

RÉSUMÉ
L'état de contrainte dans de nombreux problèmes géotechniques est similaire aux conditions de cisaillement simples. Alors que les tests de cisaillement direct et triaxiaux sont couramment effectués pour les activités pratiques d'ingénierie et de recherche, les installations de test de cisaillement simple direct (DSS) sont disponibles dans certains laboratoires avancés. L'une des limites du test DSS est que seules les contraintes de cisaillement normales verticales et horizontales sont mesurées dans la plupart des cas. La contrainte de cisaillement inconnue sur la limite verticale rend difficile l'interprétation des résultats des essais. De plus, des non-uniformités de contrainte et de déformation peuvent se produire dans l'échantillon. Dans la présente étude, une modélisation tridimensionnelle par éléments finis (EF) d'un échantillon DSS de type anneau empilé est réalisée pour différentes conditions de sol afin d'étudier les non-uniformités possibles et leurs effets sur les paramètres de résistance interprétés. Les résultats simulés par EF sont comparés aux résultats des essais en laboratoire sur sable. L'applicabilité et les limites des tests DSS sont mises en évidence.

1 INTRODUCTION

In geotechnical laboratories, several devices are used to determine the shear strength parameters of soil, including commonly used direct shear (DS) and triaxial (TX) tests apparatus. Advanced systems, such as direct simple shear (DSS), plane strain, and hollow cylinder torsional shear test apparatus, were also developed to apply complex loadings that better represent the field behaviour. The simple shear condition is a loading condition that better represents many field conditions, such as slope failure along a riverbank or embankment, pipeline–soil and pile–soil interactions.

For simple shear loading, direct simple shear device and hollow cylinder torsional apparatus (HCA) are generally used. While a better measurement and control of the stresses can be performed in the HCA, the sample preparation is relatively difficult and time consuming. On the other hand, sample preparation and DSS testing are relatively simple (Bernhardt et al. 2016). Over the last few decades, a variety of DSS devices were developed (e.g., NGI type and Cambridge type). Among them, the NGI-type is the commonly used DSS apparatus that uses the cylindrical specimen with a wire-reinforced membrane to provide the lateral confinement. In recent years, stacked rings instead of a wire-reinforced membrane are used.

Several researchers discussed the advantages and disadvantages of these DSS devices (Frydman and Talesnick 1991; Shibuya and Hight 1987). One of the major advantages of DSS is that it allows the rotation of the principal stresses during shearing, which cannot be done in a triaxial test. One of the main limitations of DSS testing is the missing information on the shear and normal stresses on the vertical plane in a typical DSS apparatus, which makes the interpretation of test results difficult. However, many researchers agreed that the core part of the soil specimen is in simple shear condition, and the nonuniformity occurs mainly near the boundary. Unfortunately, no consensus has been reached and a varying degree of nonuniformity was reported.

Measurement of stress and strain nonuniformities within the sample is difficult, if not impossible. Therefore, numerical simulations could be an alternative to understand further insights into the mechanisms and overall response. Some studies used Discrete Element Methods (DEM) to simulate DSS tests (Asadzadeh and Soroush 2016; Bernhardt et al. 2016; Dabeet et al. 2015; Guo et al. 2022). While it provides some valuable information, one of the limitations of DEM is the defining some input parameters, such as interparticle frictional resistance. Finite element methods have also been used to simulate DSS tests (Doherty and Fahey 2011, Potts et al.

1987; Wai et al. 2021; Wu 2017). Wai et al. (2021) simulated monotonic DSS tests only for limited strain (< 4%), and therefore the behaviour of soil for a wider range of strains was not investigated.

The objective of the present study is to understand the behaviour of soil elements in a DSS soil specimen and the effects of nonuniformity on the overall response by conducting FE simulations.

2 FINITE ELEMENT MODELING

Three-dimensional FE analysis is performed using Abaqus/Explicit FE software (Dassault Systemes 2019). A circular soil specimen of diameter D = 70 mm, height H = 20 mm is sheared up to 20% shear strain. Taking advantage of symmetry, only half of the specimen is modelled. Figure 1 shows the typical FE mesh used in the present study. A structured mesh is created by zoning the soil. An adaptive mesh domain with Lagrangian type boundary regions is used to improve the aspect ratio of the elements.

The top cap and bottom pedestal are modelled by 2-mm thick rigid plates. Twenty-two rigid stacked rings of an internal diameter of 70 mm, a width of 2 mm and a thickness of 1 mm (each) are used to provide lateral restraint. The diameter of the top plate is 70 mm, which is the same as the internal diameter of the stacked rings and the diameter of the soil sample such that the top plate can move vertically during loading. The diameter of the bottom plate is 74 mm (i.e., same as the outer diameter of the stacked ring). Mesh convergence analysis has been performed for this study. The detailed analysis shown in this paper has an approximate element size of 0.5 mm, and the total number of elements for the analysis was 80949. Analysis has also been performed with finer mesh density, but no significant difference was found in those analysis results.

The soil in the specimen is discretized by Lagrangian eight-node linear brick elements having reduced integration and hourglass control. The interface between the soil and the inner surface of the stacked rings is frictionless. Abaqus general contact algorithm is used to model this frictionless contact behaviour. To prevent sliding, rigid frictional interface conditions are used for the interfaces between soil and the top and bottom plates. Also, the top and bottom plates are not allowed to rotate during loading.

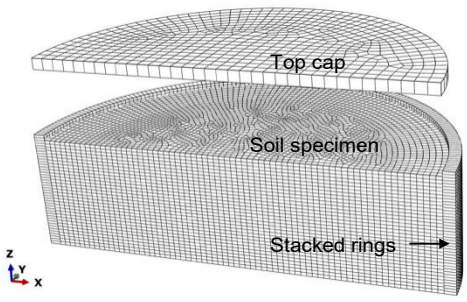

Figure 1. Typical finite element mesh prior to loading

Each simulation is performed in two steps. In the first step, the specimen is consolidated under K_0 condition by applying vertical load on the top plate. As the simulations are performed for dry sand, the term consolidation in this paper represents vertical one-dimensional compression without modelling pore pressure dissipation. In the shearing stage, keeping the top plate fixed to horizontal movements, the bottom plate is displaced leftward along the x-direction (Fig. 1) at a rate of 0.004 m/s without rotation and vertical displacement. The vertical displacement of the top plate provides the volume change of the specimen. The method of simulation described above represents the conditions similar to those used in laboratory tests by Al Tarhouni and Hawlader (2021).

Simulations are performed for constant normal stress (σ_z') conditions. That means, a given σ_z' is applied in the consolidation stage, and σ_z' remains constant in the shearing stage. Analyses are performed for medium dense dry sand. The parameters used in numerical simulations are listed in Table 1. The soil is modelled as linear elastic perfectly plastic material using the Mohr–Coulomb model. The authors understand that some level of strain-softening would occur in medium dense sand; however, it has not been modelled in the present study. In other words, the simulations are performed for the constant angle of internal friction (ϕ') and dilation angle (ψ).

Table 1. Dimensions and geotechnical parameters used in FE analysis

Parameters	Values
Diameter of soil specimen, D (mm)	70
Height of soil specimen, H (mm)	20
Young's modulus of soil, E (MPa)	10
Poisson's ratio of soil, ν_{soil}	0.3
Angle of internal friction of soil, ϕ' (°)	38
Dilation angle of soil, ψ (°)	8
Unit weight of soil, γ_{soil} (kN/m^3)	16.9

3 RESULTS

3.1 Stress–strain behaviour

Figure 2(a) shows the simulated stress–strain behaviour for σ_z' = 50, 100, and 200 kPa. Figure 2(b) shows the variation of stress ratio R (= τ_{zx}/σ_z') with shearing. A similar stress–strain behaviour was found from DSS tests on silica sand for similar test conditions (Al Tarhouni and Hawlader 2021).

Young's modulus (E) of sand increases with confining pressure (Hardin and Black 1966). However, a stress-independent constant value of E is used in this study. Figure 2(a) shows that, at the early stage of shearing, τ_{zx} increases linearly with shear strain, which is almost independent of confining pressure. However, when the simulation results are plotted in terms of stress ratio (Fig. 2(b)), it shows that R increases at a slower rate for higher σ_z'. Note that all the elements do not reach the same stress ratio for a given applied shear strain (γ) at the

boundary, rather the failure occurs progressively, which could cause different level of nonuniformity for varying σ_z'. Therefore, R vs γ curves are not the same for all σ_z', although the same value of ϕ' and ψ are used.

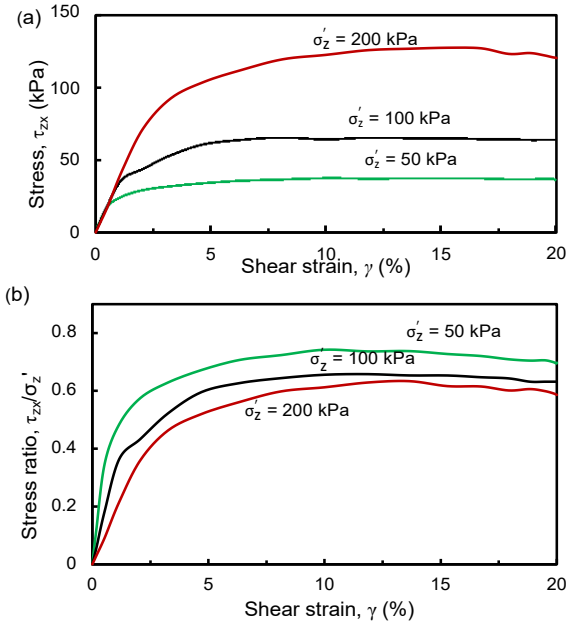

Figure 2. Finite element simulation results: (a) stress-strain response; (b) variation of stress ratio

4 ESTIMATION OF STRESSES TO CONSTRUCT MOHR'S CIRCLE

Based on the measurements in a typical DSS tests, the following stress and strain components can be calculated: vertical normal stress (σ_z'), shear stress (τ_{zx}), axial strain (ε_z) and shear strain (γ_{zx}). The location of σ_z' and τ_{zx} is shown in Fig. 3.

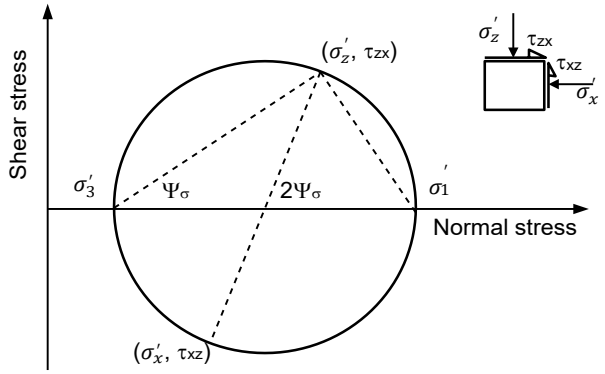

Figure 3. Estimation of stresses from DSS test results

Unfortunately, these two stresses are not sufficient to construct a Mohr's circle and determination of shear strength parameters. Several studies are available to address these issues. In the following sections, two approaches are discussed and compared with FE simulation results. Firstly, the estimation of principal stresses (σ_1' & σ_3') (Oda 1975), and secondly, the estimation of lateral stress (σ_x') (Frydman and Talesnick 1991).

4.1 Estimation of principal stresses

The rotation of principal stress direction with shearing in a simple shear test was examined in several studies, and the following relationship has been proposed (e.g., Ochiai et al. 1983; Oda and Konishi 1974; Oda 1975a, b).

$$R = k \tan\Psi_\sigma \quad (1)$$

$$k = \sin\phi_{cv}' \quad (2)$$

Where Ψ_σ is the inclination of the major principal stress to the vertical, ϕ_{cv}' is the angle of internal friction at constant volume (i.e., critical state), and k is a material property. The value of k is constant irrespective of applied normal stress, initial void ratio, stress path, and initial fabric (Cole 1967).

Several approaches have been proposed to estimate the value of the parameter k. Airey et al. (1985) and Borin (1973) suggested that k is slightly greater than $\tan\phi_{cv}'$. For Leighton Buzzard sand, Ochiai et al. (1983) and Oda (1975a) independently found that Eq. (2) could be used to estimate the value of k, based on the assumption that the principal axes of stress and strain increments coincide at the critical state (Cole 1967).

Ochiai et al. (1983) carried out a series of simple shear experiments and proposed the following empirical equation for Ψ_σ as a function of stress ratio R.

$$\Psi_\sigma = 1.82R - 0.75\,R^2 \ \text{(in rad.)} \quad (3)$$

Now for a given R (known in DSS tests), the value Ψ_σ can be calculated using Eq. (3), which is then used to calculate $\tan\Psi_\sigma$ and plotted against R in Fig. 4. The slope of this R vs $\tan\Psi_\sigma$ line gives the value of k in Eq. (1). Figure 4 also shows the plot of R vs $\tan\Psi_\sigma$ (Eq. (1)) if $k = \sin\phi_{cv}$ (i.e., Eq. (2) is used with ϕ_{cv}= 32° (typical value of critical state friction angle). There is no significant difference between these two lines. In the following sections, $k = \sin\phi_{cv}$ is used.

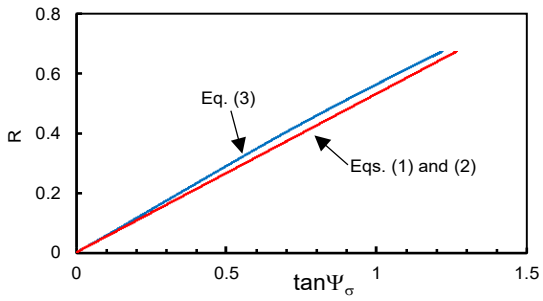

Figure 4. Variation of k with shear stress increase and rotation of principal stress

4.2 Estimation of lateral stress

Lateral stress is not measured in typical DSS tests. However, some modification was done in some studies to measure lateral stress (e.g., Budhu 1984, 1985; Kang and Kang 2015).

Frydman and Talesnick (1991) showed that the lateral stress (σ_x') of a simple shear element can be estimated from the following equation.

$$\sigma_x' = [1 - k + R^2/k]\,\sigma_z' \quad (4)$$

The applicability of Eq. (4) is evaluated using the present FE simulation results. For each time increment, the vertical and lateral reaction forces acting on the rigid top plate is obtained from the simulation results. Dividing these forces by the cross-sectional area of the specimen (A), the normal (σ_z') and shear (τ_{zx}) stresses acting on the plane for that shear strain level (γ) is obtained, which are then used to calculate R (= τ_{zx}/σ'). Now inserting R and k (= $\sin\phi_{cv}$), the value of σ_x' is calculated using Eq. (4).

As will be shown in later sections, stress nonuniformity occurs mainly near the boundaries. Therefore, to compare with FE simulation results, the average of lateral stresses σ_x' for all the soil elements in a central core (6 mm thick and 36 mm diameter in the middle of the specimen) is calculated.

The empirical parameter in Eq. 4 has been derived from a wide range of laboratory tests (Ochiai et al. 1983). Fig. 5 shows the comparison of calculated lateral stress using Eq. (4) and average lateral stress in the soil elements in the central core. No significant difference is found between the calculated σ_x', which implies that Eq. (4) could be used for a reasonable estimation of σ_x'.

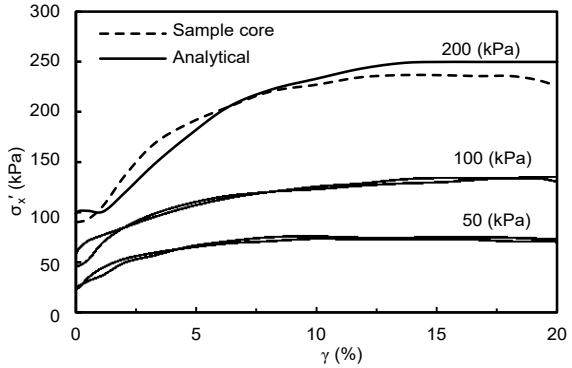

Figure 5. Estimation of lateral stress in DSS tests

4.3 Mobilized friction angle

The above discussion suggests that Mohr's circle could be constructed for the DSS test results by estimating principal stresses or lateral stress (Fig. 3). Now, using the values of σ_z' and τ_{zx} at the shear strain level of 15% (when the stress–strain curve becomes almost horizontal) and principal /lateral stresses, the Mohr's circle is constructed. Now drawing a tangent to this circle, the angle of internal friction is calculated for different normal stress levels. Table 2 shows that the calculated friction angle is lower (0.9°–3.2°) than the angle of internal friction given as the input parameter (38°), and the difference increases with an increase in normal stress. One potential reason behind this is the stress nonuniformity, which is discussed further in the following sections.

Table 2. Friction angle based on estimated values of non-measured stresses

	σ_z' = 50 kPa	σ_z' = 100 kPa	σ_z' = 200 kPa
Based on principal stresses	37.1°	35.9°	35.3°
Based on lateral stress	36.8°	35.6°	34.8°

5 STRESS NONUNIFORMITIES

Stress nonuniformity is one of the limitations of the DSS test. Nonuniformity occurs not only near the cylindrical vertical face (Wai et al. 2022; Wu 2017) but also near the top and bottom surfaces of the specimen (DeGroot et al. 1994; Wai et al. 2022; Wu 2017). The nonuniformity of stresses coupled with unknown normal and shear stresses on the cylindrical surface cause the interpretation of the test results to be challenging; for example, a Mohr's circle cannot be drawn as in the triaxial test. Several studies have assessed the degree of nonuniformity and its effects on the boundary stress (Asadzadeh and Soroush 2016; Bernhardt et al. 2016; DeGroot et al. 1994; Wai et al. 2022; Wijewickreme et al. 2013; Wu 2017). In the following sections, the nonuniformities of stresses are investigated using the simulation results for σ_z' = 100 kPa.

To show the variation of stresses, five paths are created (Fig. 6). Paths 1 and 2 are along the x-axis and 1.0-mm inside the soil from the top and bottom plates, respectively. Paths 4 and 5 are along the z-axis and again 1.0-mm inside the soil from the left and right vertical surfaces, respectively. Finally, path 3 is a circular line at a radial distance of 25-mm and 1.0-mm inside the soil from the top.

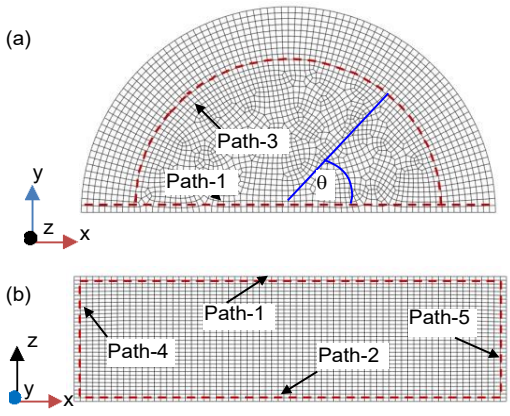

Figure 6. Paths to show stress distribution: (a) top view, (b) side view.

5.1 Distribution of shear stresses along the paths

Figure 7 shows that the distribution of shear stress (τ_{zx}) along the paths 1 and 2 is not uniform. The shear stress drops to a small value in the upper right and lower-left corners of the soil sample (see points c and a in the inset of Fig. 7). However, τ_{zx} in the middle two-thirds is almost uniform throughout the test. Modelling the soil as an elastic material, Roscoe (1953) also showed a similar pattern of shear stress distribution along the horizontal boundaries.

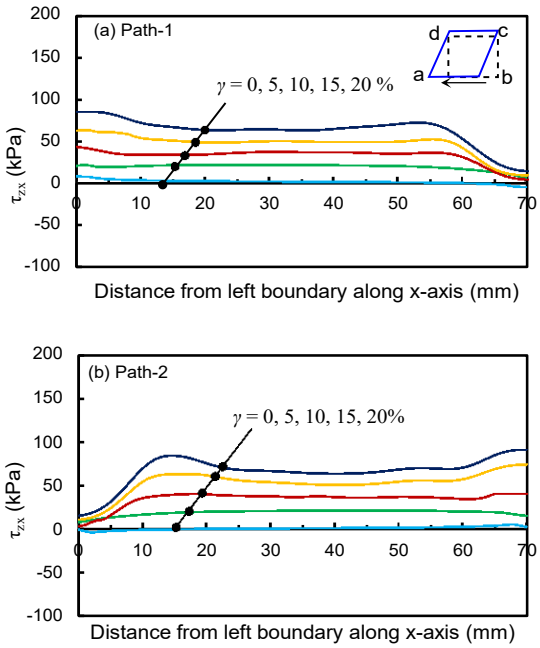

Figure 7. Distribution of shear stress for varying shear strains under σ_z' = 100 kPa: (a) along path-1 and (b) along path-2

The distribution of shear stress (τ_{xz}) along the Paths 4 and 5 is shown in Fig. 8. Shear stress concentration occurs at the top left and bottom right corners of the soil sample (near points d and b of the inset). Note that higher shear stress also generated in these corners, as shown in Fig. 7. However, τ_{xz} is relatively smaller in the other two corners. At the lower strain level (γ = 0–5%), the shear stress distribution along these paths is almost uniform. With increase in γ (e.g., γ = 15%) shear stress nonuniformity increases.

5.2 Distribution of vertical normal stresses

Figure 9 shows the vertical normal stress (σ_z') distribution along path-1 and path-2. As no wall friction is considered at the vertical boundary, the normal stress distribution at the end of consolidation (i.e., beginning of the shearing, γ = 0) is uniform. With shearing, σ_z' becomes nonuniform, although the total force applied from the top plate is kept the same. σ_z' is considerably higher than 100 kPa within ~5 mm in the top left (point d in the inset) and bottom right corners (point b). On the other hand, σ_z' is considerably lower than 100 kPa in the soil elements near the top right and bottom left corners.

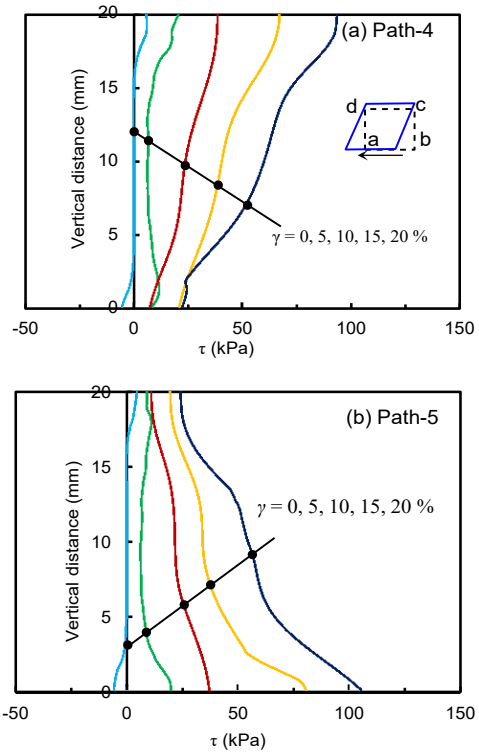

Figure 8. Distribution of shear stress for varying shear strain level under σ_z' = 100 kPa: (a) along path-4 and (b) along path-5

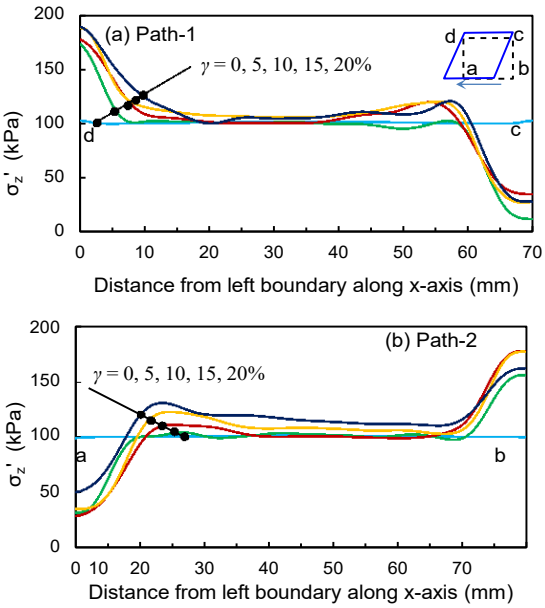

Figure 9. Distribution of vertical normal stress for varying shear strain level: (a) along path-1 and (b) along path-2

A similar trend has also been shown in previous studies (e.g., Budhu and Britto 1987; Finn 1978; Lucks et al. 1972; Wai et al. 2022; Wu 2017). However, Figs. 9(a) and 9 (b) show that the vertical stress remains almost constant at the targeted value (100 kPa) in the middle two-thirds of the specimen for the whole range of shear strain levels simulated in this study.

Figure 10 shows the vertical normal stress distribution along the radial path-3, as shown in Fig. 6. In this figure, the radial distance from the origin represents the $\sigma_z^{'}$ at a point on path 3 at angle θ to the horizontal (see Fig. 6). Again, $\sigma_z^{'}$ is uniform at the beginning of shearing (symmetric in Fig. 10). With increase in shear strain, stress nonuniformity develops (non-symmetric curves). The left half of the soil specimen experiences higher $\sigma_z^{'}$ than the right half for these soil elements near the top cap. An opposite pattern is found for the soil elements near the bottom pedestal.

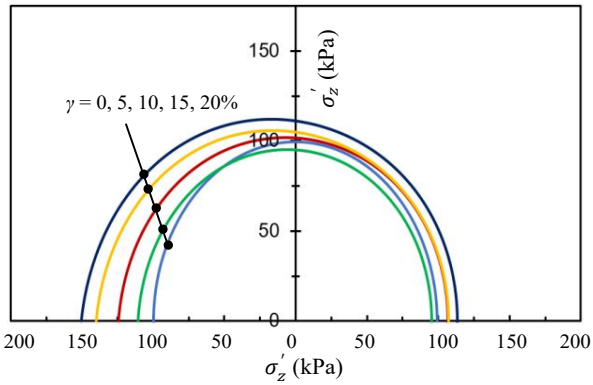

Figure 10. Distribution of vertical normal stress for varying shear strain levels along path-3

5.3 Plastic shear strains

Figure 11 shows the development of maximum plastic shear strain (ε_d^p) with loading. After a certain level of shearing, plastic shear strain accumulation occurs locally and failure planes form. To show the plastic shear strains and failure planes, the front view (left column of Fig. 11) and rare view (right column of Fig. 11) are shown. The plastic shear strain is small and almost homogeneous throughout the specimen during the early stage of shearing, especially in the central area. At γ = 2%–3%, a shear band (zone of large plastic shear strain) develops in the middle of the soil specimen. As the simulation progressed, this diagonal shear band extents towards the boundary and separates the specimen into two parts (Figs. 11(a) & 11(b)). A similar pattern of the rupture zone on the cylindrical soil sample is also reported by Budhu (1984) using the radiographic technique. In addition, considerably large plastic shear strains develop in the soil elements near the top and bottom plates could affect the stress distribution, such as lateral stress on the rings and stress nonuniformity.

6 DISCUSSION AND CONCLUSIONS

Direct simple shear test is one of the advanced methods of geotechnical testing as the test conditions are similar to many field conditions. However, stress nonuniformity and estimation of shear strength parameters (e.g., angle of internal friction) are some of the issues of DSS tests pointed out in several studies. Finite element analysis can provide some insights into the response, which can also explain the usefulness of the test results.

The present study simulates DSS tests on dry sand using a relatively simple elastic-plastic model. Comparing the FE simulation results, it is shown that the existing empirical relations could be used to estimate unknown lateral stress and principal stresses, which could be used to develop the Mohr's circle. The calculated angle of internal friction based on the developed Mohr's circle is slightly lower than the input value of the friction angle given for the Mohr–Coulomb model.

Nonuniformities developed near the boundaries, especially near the vertical surfaces because of the lack of complementary shear stress development at the soil–ring interface. Large plastic shear strains develop with shearing and shear bands form, which separates the soil specimens into blocks, especially at large shear strains. The formation of shear bands could affect stress development and nonuniformities at large strains.

Analyses presented in the paper do not consider the variation of density and strain-softening behaviour. Moreover, all the simulations are performed for constant normal stress conditions. Further studies are required, including the investigation of the above-mentioned issues.

7 ACKNOWLEDGEMENTS

The work presented in this paper has been supported by the Natural Sciences and Engineering Research Council of Canada (NSERC) and Equinor Research Chair grants.

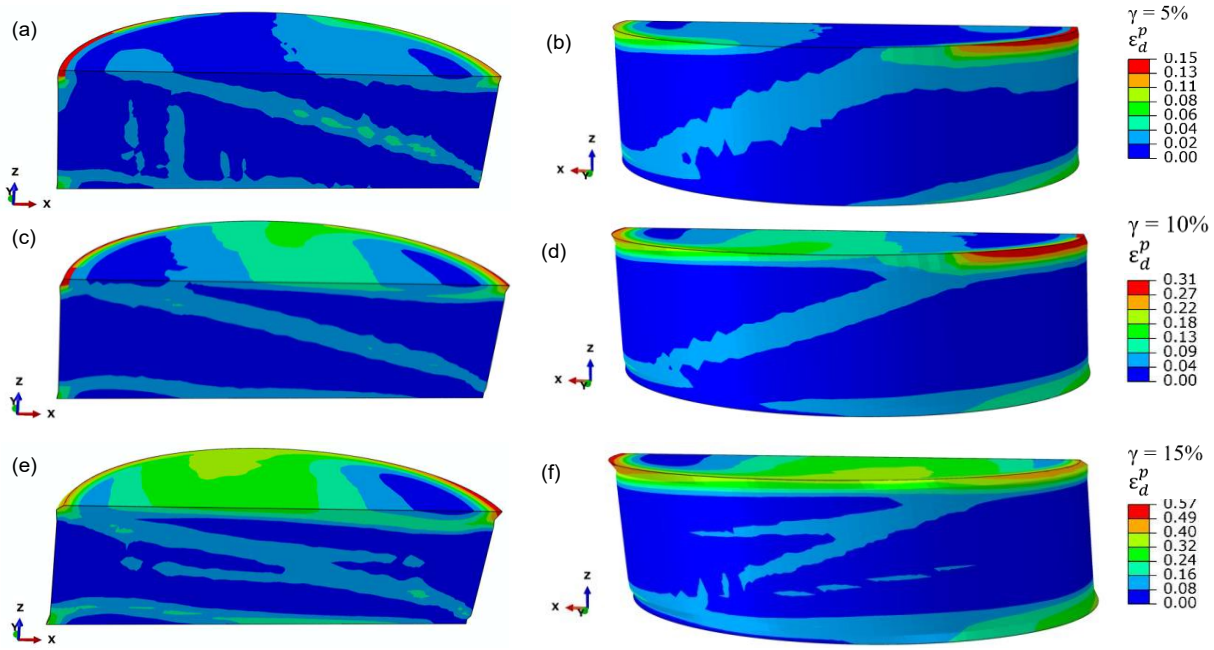

Figure 11. Maximum plastic strains for 100 kPa vertical normal stress: left column front view and right column rare view

8 REFERENCES

ABAQUS (2019), "ABAQUS Documentation", Dassault Systèmes, RI, USA.

Asadzadeh, M. and Soroush, A., 2016. Fundamental investigation of constant stress simple shear test using DEM. *Powder Technology*, 292: 129-139.

Airey, D.W., Budhu, M. and Wood, D.M. 1985. 'Some aspects of the behaviour of soils in simple shear', in Banerjee, P.K. and Butterfield, R. (cds), Developments in Soil Mechanics and Foundation Engineering-2 Stress-Strain Modelling in Soils, Elsevier, Amsterdam: 185-213.

Al Tarhouni, M.A. and Hawlader, B. 2021. Monotonic and Cyclic Behaviour of Sand in Direct Simple Shear Test Conditions Considering Low Stresses, *Soil Dynamics and Earthquake Engineering*, 150: p.106931.

Bernhardt, M. L., Biscontin, G. and O'Sullivan, C. 2016. Experimental validation study of 3D direct simple shear DEM simulations, *Soils and Foundations*, 56(3): 336-347.

Borin, D.L. 1973. *The behaviour of saturated kaolin in the simple shear apparatus.* Ph.D. Thesis, University of Cambridge, Cambridge, England.

Budhu, M. 1984. Nonuniformities Imposed by Simple Shear Apparatus, *Canadian Geotechnical Journal*, 21(1): 125-137.

Budhu, M. 1985. Lateral Stresses Observed in Two Simple Shear Apparatus, *Journal of Geotechnical Engineering*, 111(6): 698-711.

Budhu, M. and Britto, A. 1987. Numerical Analysis of Soils in Simple Shear Devices, *Soils and Foundations*, 27(2): 31-41.

Budhu, M. 1988. Failure State of a Sand in Simple Shear, *Canadian Geotechnical Journal*, *25*(2): 395-400.

Cole, E.R.L. 1967. *The Behaviour of Soils in the Simple Shear Apparatus*. Ph. D. Thesis, University of Cambridge, Cambridge, England.

Dabeet, A., Wijewickreme, D. and Byrne, P. 2015. Evaluation of stress strain non-uniformities in the laboratory direct simple shear test specimens using 3D discrete element analysis, *Geomechanics and Geoengineering*, 10(4): 249-260.

DeGroot, D.J., Germaine, J.T. and Ladd, C.C. 1994. Effect of Nonuniform Stresses on Measured DSS Stress–Strain Behavior, *Journal of Geotechnical Engineering*, 120(5): 892-912.

Doherty, J. and Fahey, M. 2011. Three-Dimensional Finite Element Analysis of the Direct Simple Shear Test, *Computers and Geotechnics*, 38(7): 917-924.

Finn, W.D. 1985. Aspects of constant volume cyclic simple shear, In *Advances in the art of testing soils under cyclic conditions,* ASCE: 74-98.

Frydman, S. and Talesnick, M. 1991. Simple Shear of Isotropic Elasto-Plastic Soil, *International Journal for Numerical and Analytical Methods in Geomechanics*, 15(4) : 251-270.

Guo, J., Bernhardt-Barry, M.L. and Biscontin, G. Evaluation of Boundary Effects in Simple Shear Tests Using Discrete Element Modelling. In *Geo-Congress 2022*: 599-607.

Hardin, B.O., and Black, W.L. 1966. Sand stiffness under various triaxial stress. Journal of the Soil Mechanics and Foundations Division, ASCE, 92(SM2): 27–42.

Kang X, Kang G. (2015) Modified monotonic simple shear tests on silica sand. Journal of Marine Georesources & Geotechnology, 33: 122–126.

Lucks, A.S., Christian, J.T., Brandow, G.E. and Höeg, K. 1972. Stress Conditions in NGI Simple Shear Test, *Journal of the Soil Mechanics and Foundations Division*, 98(1): 155-160.

Ochiai, H., Yamanouchi, T. and Tanabashi, Y. 1983. On the Rotation of Principal Stress Axes in the Simple Shear Test and Its Utilizations, *Advances in the Mechanics and the Flow of Granular Materials*, 2: 871-883.

Oda, M. 1975 a. On the Relation $\tau/\sigma_N = \kappa \cdot \tan\psi$ in the Simple Shear Test, *Soils and Foundations*, 15(4): 35-41.

Oda, M. 1975 b. On Stress-dilatancy Relation of Sand in Simple Shear Test. *Soils and Foundations*, 15(2): 17-29.

Oda, M. and Konishi, J. 1974. Rotation of principal stresses in granular material during simple shear, *Soils and Foundations*, 14(4): 39-53.

Potts, D.M., Dounias, G.T. and Vaughan, P.R. 1987. Finite element analysis of the Direct Shear Box Test. *Géotechnique*, 37(1): 11-23.

Pradhan, T.B., Tatsuoka, F. and Horii, N. 1988. Simple shear testing on sand in a torsional shear apparatus, *Soils and Foundations*, *28*(2): 95-112.

Roscoe, K.H. 1953. An Apparatus for the Application of Simple Shear to Soil Samples. *In Proc. 3rd ICSMFE*, London, England, 1: 86-191.

Shibuya, S. and Hight, D. W. 1987. On the Stress Path in Simple Shear, *Géotechnique*, 37(4): 511–515.

Wai, D., Manmatharajan, M.V. and Ghafghazi, M. 2022. Effects of Imperfect Simple Shear Test Boundary Conditions on Monotonic and Cyclic Measurements in Sand, *Journal of Geotechnical and Geoenvironmental Engineering*, 148(1): p.04021164.

Wijewickreme, D., Dabeet, A. and Byrne, P. 2013. Some Observations on the State of Stress in the Direct Simple Shear Test Using 3D Discrete Element Analysis, *Geotechnical Testing Journal*, 36(2): 292-299.

Wu, Z. 2017. *Mechanical Modelling of Sand Considering Simple Shear Condition and Its Application to Pile Foundation.* Ph.D. Thesis, École centrale de Nantes.